E-ISSN: 2147-1959

MIRT

Molecular Imaging and Radionuclide Therapy

October 2021 Volume 30 Issue 3 www.tsnm.org

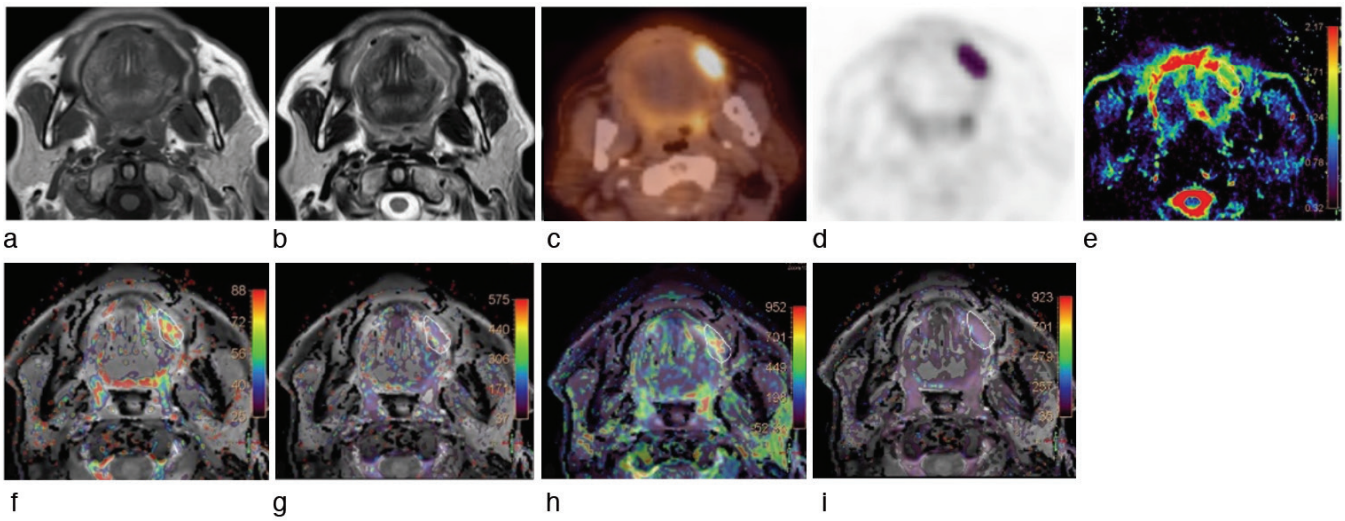

"Official Journal of the Turkish Society of Nuclear Medicine"

galenos yayinevi

TURKISH SOCIETY OF NUCLEAR MEDICINE 1975

MIRT

Molecular Imaging and Radionuclide Therapy

MIRT

Molecular Imaging and Radionuclide Therapy

Turkish Society of Nuclear Medicine
Cinnah Caddesi Pilot Sokak No: 10/12 Çankaya 06650 Ankara, Turkey **Phone:** +90 312 441 00 45 **Fax:** +90 312 441 12 95 **Web:** www.tsnm.org **E-mail:** dernekmerkezi@tsnm.org
"Formerly Turkish Journal of Nuclear Medicine"

Reviewing the articles' conformity to the publishing standards of the Journal, typesetting, reviewing and editing the manuscripts and abstracts in English, creating links to source data, and publishing process are realized by Galenos.

Galenos Publishing House
Owner and Publisher
Derya Mor
Erkan Mor

Publication Coordinator
Burak Sever

Web Coordinators
Fuat Hocalar
Turgay Akpınar

Graphics Department
Ayda Alaca
Çiğdem Birinci
Gülşah Özgül

Finance Coordinator
Sevinç Çakmak

Project Coordinators
Aysel Balta
Duygu Yıldırm
Gamze Aksoy
Gülay Akın
Hatice Sever
Melike Eren
Meltem Acar
Özlem Çelik Çekil
Pınar Akpınar
Rabia Palazoğlu

Research&Development
Melisa Yiğitoğlu
Nihan Karamanlı

Digital Marketing Specialist
Seher Altundemir

Publisher Contact
Address: Molla Gürani Mah. Kaçamak Sk. No: 21/1
34093 İstanbul, Turkey
Phone: +90 (212) 621 99 25 **Fax:** +90 (212) 621 99 27
E-mail: info@galenos.com.tr/yayin@galenos.com.tr
Web: www.galenos.com.tr
Publisher Certificate Number: 14521

Online Publication Date: October 2021
ISSN: 2146-1414 **E-ISSN:** 2147-1959
International scientific journal published quarterly.

MIRT

Molecular Imaging and Radionuclide Therapy

ABOUT US

Molecular Imaging and Radionuclide Therapy (formerly Turkish Journal of Nuclear Medicine) is the official publication of Turkish Society of Nuclear Medicine.

Focus and Scope

Molecular Imaging and Radionuclide Therapy (Mol Imaging Radionucl Ther, MIRT) is a double-blind peer-review journal published in English language. It publishes original research articles, invited reviews, editorials, short communications, letters, consensus statements, guidelines and case reports with a literature review on the topic, in the field of molecular imaging, multimodality imaging, nuclear medicine, radionuclide therapy, radiopharmacy, medical physics, dosimetry and radiobiology. MIRT is published three times a year (February, June, October). Audience: Nuclear medicine physicians, medical physicists, radiopharmaceutical scientists, radiobiologists.

The editorial policies are based on the "Recommendations for the Conduct, Reporting, Editing, and Publication of Scholarly Work in Medical Journals (ICMJE Recommendations)" by the International Committee of Medical Journal Editors (2016, archived at http://www.icmje.org/) rules.

Molecular Imaging and Radionuclide Therapy is indexed in **Pubmed, Pubmed Central (PMC), Emerging Sources Citation Index (ESCI), TUBITAK-ULAKBIM, DOAJ, Scopus, Gale/Cengage Learning, EBSCO databases, Embase, ProQuest Health & Medical Complete, CINAHL, Index Copernicus, J-Gate, IdealOnline, ROOT INDEXING, Türkiye Atıf Dizini-Turkiye Citation Index, Turk Medline, EuroPub, Hinari, GOALI, ARDI, OARE** and **AGORA.**

Open Access Policy

This journal provides immediate open access to its content on the principle that making research freely available to the public supports a greater global exchange of knowledge.

Open Access Policy is based on rules of Budapest Open Access Initiative (BOAI) (http://www.budapestopenaccessinitiative.org/). By "open access" to [peer-reviewed research literature], we mean its free availability on the public internet, permitting any users to read, download, copy, distribute, print, search, or link to the full texts of these articles, crawl them for indexing, pass them as data to software, or use them for any other lawful purpose, without financial, legal, or technical barriers other than those inseparable from gaining access to the internet itself. The only constraint on reproduction and distribution, and the only role for copyright in this domain, should be to give authors control over the integrity of their work and the right to be properly acknowledged and cited.

Subscription Information

Manuscripts can only be submitted electronically through the Journal Agent website (http://www.journalagent.com/mirt/?plng=eng) after creating an account. This system allows online submission and review.

All published volumes in full text can be reached free of charge through the website http://mirt.tsnmjournals.org

Copyright Statement

Turkish Society of Nuclear Medicine holds the international copyright of all the content published in the journal.

Republication and reproduction of images or tables in any published material should be done with proper citation of source providing authors names; article title; journal title; year (volume) and page of publication; copyright year of the article.

The author(s) hereby affirms that the manuscript submitted is original, that all statement asserted as facts are based on author(s) careful investigation and research for accuracy, that the manuscript does not, in whole or part, infringe any copyright, that it has not been published in total or in part and is not being submitted or considered for publication in total or in part elsewhere.

Completed Copyright Statement form should be submitted to the online article system.

By signing this form,

1. Each author acknowledge that he/she participated in the work in a substantive way and is prepared to take public responsibility for the work.

2. Each author further affirms that he or she has read and understands the "Ethical Guidelines for Publication of Research".

3. The author(s), in consideration of the acceptance of the manuscript for publication, does hereby assign and transfer to the Molecular Imaging and Radionuclide Therapy all of the rights and interest in and the copyright of the work in its current form and in any form subsequently revised for publication and/or electronic dissemination.

Instructions for Authors

Instructions for authors are published in the journal and on the website http://mirt.tsnmjournals.org

Material Disclaimer

Scientific and legal responsibilities pertaining to the papers belong to the authors. Contents of the manuscripts and accuracy of references are also the author's responsibility. The Turkish Society of Nuclear Medicine, the Editor, the Editorial Board or the publisher do not accept any responsibility for opinions expressed in articles.

Financial expenses of the journal are covered by Turkish Society of Nuclear Medicine.

Correspondence Address

Editor in Chief Prof. Murat Fani Bozkurt, MD, FEBNM Hacettepe University, Medical School, Department of Nuclear Medicine, Ankara, Turkey

E-mail: fanibozkurt@gmail.com

Web page: http://mirt.tsnmjournals.org/

Publisher Corresponding Address

Galenos Yayınevi Tic. Ltd. Şti.
Address: Molla Gürani Mah. Kaçamak Sk. No: 21/1 34093 Fındıkzade, İstanbul, Turkey
Phone: +90 212 621 99 25
Fax: +90 212 621 99 27
E-mail: info@galenos.com.tr

MIRT

Molecular Imaging and Radionuclide Therapy

INSTRUCTIONS TO AUTHORS

Molecular Imaging and Radionuclide Therapy (Mol Imaging Radionucl Ther, MIRT) publishes original research articles, short communications, invited reviews, editorials, case reports with a literature review on the topic, interesting images, consensus statements, guidelines, letters in the field of molecular imaging, multimodality imaging, nuclear medicine, radionuclide therapy, radiopharmacy, medical physics, dosimetry and radiobiology. MIRT is published by the Turkish Society of Nuclear Medicine three times a year (February, June, October).

Molecular Imaging and Radionuclide Therapy does not charge any article submission or processing fees.

GENERAL INFORMATION

MIRT commits to rigorous peer review, and stipulates freedom from commercial influence, and promotion of the highest ethical and scientific standards in published articles. Neither the Editor(s) nor the publisher guarantees, warrants or endorses any product or service advertised in this publication. All articles are subject to review by the editors and peer reviewers. If the article is accepted for publication, it may be subjected to editorial revisions to aid clarity and understanding without changing the data presented.

Manuscripts must be written in English and must meet the requirements of the journal. The journal is in compliance with the uniform requirements for manuscripts submitted to biomedical journals published by the International Committee of Medical Journal Editors (NEJM 1997; 336:309-315, updated 2016). Manuscripts that do not meet these requirements will be returned to the author for necessary revision before the review. Authors of manuscripts requiring modifications have a maximum of two months to resubmit the revised text. Manuscripts returned after this deadline will be treated as new submissions.

It is the authors' responsibility to prepare a manuscript that meets ethical criteria. The Journal adheres to the principles set forth in the Helsinki Declaration October 2013 (https://www.wma.net/policies-post/wma-declaration-of-helsinki-ethical-principles-for-medical-research-involving-human-subjects/) and holds that all reported research involving "Human beings" conducted in accordance with such principles.

Reports describing data obtained from research conducted in human participants must contain a statement in the MATERIALS AND METHODS section indicating approval by the ethical review board (including the approval number) and affirmation that INFORMED CONSENT was obtained from each participant.

All manuscripts reporting experiments using animals must include a statement in the MATERIALS AND METHODS section giving assurance that all animals have received humane care in compliance with the Guide for the Care and Use of Laboratory Animals (www.nap.edu) and indicating approval by the ethical review board.

If the study should have ethical approval, authors asked to provide ethical approval in order to proceed the review process. If they provide approval, review of the manuscript will continue.

In case report(s) and interesting image(s) a statement regarding the informed consent of the patients should be included in the manuscript and the identity of the patient(s) should be hidden.

Subjects must be identified only by number or letter, not by initials or names. Photographs of patients' faces should be included only if scientifically relevant. Authors must obtain written consent from the patient for use of such photographs. In cases of image media usage that potentially expose patients' identity requires obtaining permission for publication from the patients or their parents/guardians.

If the proposed publication concerns any commercial product, the author must include in the cover letter a statement indicating that the author(s) has (have) no financial or other interest with the product or explaining the nature of any relations (including consultancies) between the author(s) and editor the manufacturer or distributor of the product.

All submissions will be screened by Crossref Smilarity Check powered by "iThenticate". Manuscripts with an overall similarity index of greater than 25%, or duplication rate at or higher than 5% with a single source will be returned back to authors.

MANUSCRIPT CATEGORIES

1. Original Articles

2. Short Communications are short descriptions of focused studies with important, but very straightforward results.

3. Reviews address important topics in the field. Authors considering the submission of uninvited reviews should contact the editor in advance to determine if the topic that they propose is of current potential interest to the Journal. Reviews will be considered for publication only if they are written by authors who have at least three published manuscripts in the international peer reviewed journals and these studies should be cited in the review. Otherwise only invited reviews will be considered for peer review from qualified experts in the area.

4. Editorials are usually written by invitation of the editor by the editors on current topics or by the reviewers involved in the evaluation of a submitted manuscript and published concurrently with that manuscript.

5. Case Report and Literature Reviews are descriptions of a case or small number of cases revealing a previously undocumented disease process, a unique unreported manifestation or treatment of a known disease process, unique unreported complications of treatment regimens or novel and important insights into a condition's pathogenesis, presentation, and/or management. The journal's policy is to accept case reports only if it is accompanied by a review of the literature on the related topic. They should include an adequate number of images and figures.

6. Interesting Image

One of the regular parts of Molecular Imaging and Radionuclide Therapy is a section devoted to interesting images. Interesting image(s) should describe case(s) which are unique and include interesting findings adding insights into the interpretation of patient images, a condition's pathogenesis, presentation, and/or management.

7. Consensus Statements or Guidelines may be submitted by professional societies. All such submissions will be subjected to peer review, must be modifiable in response to criticisms, and will be published only if they meet the Journal's usual editorial standards.

8. Letters to the Editor may be submitted in response to work that has been published in the Journal. Letters should be short commentaries related to specific points of agreement or disagreement with the published work.

Note on Prior Publication

Articles are accepted for publication on the condition that they are original, are not under consideration by another journal, or have not been previously published. Direct quotations, tables, or illustrations that have appeared in

MIRT
Molecular Imaging and Radionuclide Therapy

copyrighted material must be accompanied by written permission for their use from the copyright owner and authors. Materials previously published in whole or in part shall not be considered for publication. At the time of submission, authors must report that the manuscript has not been published elsewhere. Abstracts or posters displayed at scientific meetings need not be reported.

MANUSCRIPT SUBMISSION PROCEDURES

MIRT only accepts electronic manuscript submission at the web site http://www.journalagent.com/mirt/. After logging on to the website Click the 'online manuscript submission' icon. All corresponding authors should be provided with a password and a username after entering the information required. If you already have an account from a previous submission, enter your username and password to submit a new or revised manuscript. If you have forgotten your username and/or password, please send an e-mail to the editorial office for assistance. After logging on to the article submission system please read carefully the directions of the system to give all needed information and attach the manuscript, tables and figures and additional documents.

All Submissions Must Include:

1. Completed Copyright Assignment & Disclosure of Potential Conflict of Interest Form; This form should be downloaded from the website (provided in the author section), filled in thoroughly and uploaded to the website during the submission.
2. All manuscripts describing data obtained from research conducted in human participants must be accompanied with an approval document by the ethical review board.
3. All manuscripts reporting experiments using animals must include approval document by the animal ethical review board.
4. All submissions must include the authorship contribution form which is signed by all authors.

Authors must complete all online submission forms. If you are unable to successfully upload the files please contact the editorial office by e-mail.

MANUSCRIPT PREPARATION

General Format

The Journal requires that all submissions be submitted according to these guidelines:

- Text should be double spaced with 2.5 cm margins on both sides using 12-point type in Times Roman font.
- All tables and figures must be placed after the text and must be labeled.
- Each section (abstract, text, references, tables, figures) should start on a separate page.
- Manuscripts should be prepared as a word document (*.doc) or rich text format (*.rtf).
- Please make the tables using the table function in Word.
- Abbreviations should be defined in parenthesis where the word is first mentioned and used consistently thereafter.
- Results should be expressed in metric units. Statistical analysis should be done accurately and with precision. Please consult a statistician if necessary.
- Authors' names and institutions should not be included in the manuscript text and should be written only in the title page.

Title Page

The title page should be a separate form from the main text and should include the following:

- Full title (in English and in Turkish). Turkish title will be provided by the editorial office for the authors who are not Turkish speakers.
- Authors' names and institutions.
- Short title of not more than 40 characters for page headings.
- At least three and maximum eight keywords. (in English and in Turkish). Do not use abbreviations in the keywords. Turkish keywords will be provided by the editorial office for the authors who are not Turkish speakers. If you are not a native Turkish speaker, please reenter your English keywords to the area provided for the Turkish keywords. English keywords should be provided from http://www.nlm.nih.gov/mesh (Medical Subject Headings) while Turkish keywords should be provided from http://www.bilimterimleri.com.
- Word count (excluding abstract, figure legends and references).
- Corresponding author's e-mail and address, telephone and fax numbers.
- Name and address of person to whom reprint requests should be addressed.

Original Articles

Authors are required to state in their manuscripts that ethical approval from an appropriate committee and informed consents of the patients were obtained.

Original Articles should be submitted with a structured abstract of no more than 250 words. All information reported in the abstract must appear in the manuscript. The abstract should not include references. Please use complete sentences for all sections of the abstract. Structured abstract should include background, objective, methods, results and conclusions. Turkish abstract will be provided by the editorial office for the authors who are not Turkish speakers. If you are not a native Turkish speaker, please reenter your English abstract to the area provided for the Turkish abstract.

- Introduction
- Materials and Methods
- Results
- Discussion
- Study Limitations
- Conclusion

May be given for contributors who are not listed as authors, or for grant support of the research.

References should be cited in numerical order (in parentheses) in the text and listed in the same numerical order at the end of the manuscript on a separate page or pages. The author is responsible for the accuracy of references. Examples of the reference style are given below. Further examples will be found in the articles describing the Uniform Requirements for Manuscripts Submitted to Biomedical Journals (Ann Intern Med.1988; 208:258-265, Br Med J. 1988; 296:401-405). The titles of journals should be abbreviated according to the style used in the Index Medicus. Journal Articles and Abstracts: Surnames and initials of author's name, title of the article, journal name, date, volume number, and pages. All authors should be listed regardless of number. The citation of unpublished papers, observations or personal communications is not permitted. Citing an abstract is not recommended. Books: Surnames and initials of author's names, chapter title, editor's name, book title, edition, city, publisher, date and pages.

MIRT
Molecular Imaging and Radionuclide Therapy

INSTRUCTIONS TO AUTHORS

Sample References

Journal Article: Sayit E, Söylev M, Capa G, Durak I, Ada E, Yilmaz M. The role of technetium-99m-HMPAO-labeled WBC scintigraphy in the diagnosis of orbital cellulitis. Ann Nucl Med 2001;15:41-44.

Erselcan T, Hasbek Z, Tandogan I, Gumus C, Akkurt I. Modification of Diet in Renal Disease equation in the risk stratification of contrast induced acute kidney injury in hospital inpatients. Nefrologia 2009 doi: 10.3265/Nefrologia.2009.29.5.5449.en.full.

Article in a journal published ahead of print: Ludbrook J. Musculovenous pumps in the human lower limb. Am Heart J 2009;00:1-6. (accessed 20 February 2009).

Lang TF, Duryea J. Peripheral Bone Mineral Assessment of the Axial Skeleton: Technical Aspects. In: Orwoll ES, Bliziotes M (eds). Osteoporosis: Pathophsiology and Clinical Management. New Jersey, Humana Pres Inc, 2003;83-104.

Books: Greenspan A. Orthopaedic Radiology a Pratical Approach. 3th ed. Philadelphia, Lippincott Williams Wilkins 2000, 295-330.

Website: Smith JR. 'Choosing Your Reference Style', Online Referencing 2(3), http://orj.sagepub.com (2003, accessed October 2008).

- Tables

Tables must be constructed as simply as possible. Each table must have a concise heading and should be submitted on a separate page. Tables must not simply duplicate the text or figures. Number all tables in the order of their citation in the text. Include a title for each table (a brief phrase, preferably no longer than 10 to 15 words). Include all tables in a single file following the manuscript.

– Figure Legends

Figure legends should be submitted on a separate page and should be clear and informative.

– Figures

Number all figures (graphs, charts, photographs, and illustrations) in the order of their citation in the text. At submission, the following file formats are acceptable: AI, EMF, EPS, JPG, PDF, PPT, PSD, TIF. Figures may be embedded at the end of the manuscript text file or loaded as separate files for submission. All images MUST be at or above intended display size, with the following image resolutions: Line Art 800 dpi, Combination (Line Art + Halftone) 600 dpi, Halftone 300 dpi. Image files also must be cropped as close to the actual image as possible.

Short Communications:

Short communications should be submitted with a structured abstract of no more than 200 words. These manuscripts should be no longer than 2000 words, and include no more than two figures and tables and 20 references. Other rules which the authors are required to prepare and submit their manuscripts are the same as described above for the original articles.

Invited Review Articles:

- Title page (see above)
- Abstract: Maximum 250 words; without structural divisions; in English and in Turkish . Turkish abstract will be provided by the editorial office for the authors who are not Turkish speakers. If you are not a native Turkish speaker, please reenter your English abstract to the area provided for the Turkish abstract.
- Text
- Conclusion
- Acknowledgements (if any)
- References

Editorial:

- Title page (see above)
- Abstract: Maximum 250 words; without structural divisions; in English and in Turkish. Turkish abstract will be provided by the editorial office for the authors who are not Turkish speakers. If you are not a native Turkish speaker, please re enter your English abstract to the area provided for the Turkish abstract.
- Text
- References

Case Report and Literature Review

- Title page (see above)
- Abstract: Approximately 100-150 words; without structural divisions; in English and in Turkish. Turkish abstract will be provided by the editorial office for the authors who are not Turkish speakers. If you are not a native Turkish speaker, please re-enter your English abstract to the area provided for the Turkish abstract.
- Introduction
- Case report
- Literature Review and Discussion
- References

Interesting Image:

No manuscript text is required. Interesting Image submissions must include the following:

Title Page: (see Original article section)

Abstract: Approximately 100-150 words; without structural divisions; in English and in Turkish. Turkish abstract will be provided by the editorial office for the authors who are not Turkish speakers. If you are not a native Turkish speaker, please re-enter your English abstract to the area provided for the Turkish abstract.

Image(s): The number of images is left to the discretion of the author. (See Original article section)

Figure Legend: Reference citations should appear in the legends, not in the abstract. Since there is no manuscript text, the legends for illustrations should be prepared in considerable detail but should be no more than 500 words total. The case should be presented and discussed in the Figure legend section.

References: Maximum eight references (see original article section).

Letters to the Editor:

- Title page (see above)
- Short comment to a published work, no longer than 500 words, no figures or tables.
- References no more than five.

Consensus Statements or Guidelines: These manuscripts should typically be no longer than 4000 words and include no more than six figures and tables and 120 references.

Proofs and Reprints

Proofs and a reprint orders are sent to the corresponding author. The author should designate by footnote on the title page of the manuscript the name and

MIRT
Molecular Imaging and Radionuclide Therapy

address of the person to whom reprint requests should be directed. The manuscript when published will become the property of the journal.

Archiving

The editorial office will retain all manuscripts and related documentation (correspondence, reviews, etc.) for 12 months following the date of publication or rejection.

Submission Preparation Checklist

As part of the submission process, authors are required to check off their submission's compliance with all of the following items, and submissions may be returned to authors that do not adhere to these guidelines.

1. The submission has not been previously published, nor is it before another journal for consideration (or an explanation has been provided in Comments to the Editor).
2. The submission file is in Microsoft Word, RTF, or WordPerfect document file format. The text is double-spaced; uses a 12-point font; employs italics, rather than underlining (except with URL addresses); and the location for all illustrations, figures, and tables should be marked within the text at the appropriate points.
3. Where available, URLs for the references will be provided.
4. All authors should be listed in the references, regardless of the number.
5. The text adheres to the stylistic and bibliographic requirements outlined in the Author Guidelines, which is found in About the Journal.
6. English keywords should be provided from http://www.nlm.nih.gov/mesh(Medical Subject Headings), while Turkish keywords should be provided fromhttp://www.bilimterimleri.com
7. The title page should be a separate document from the main text and should be uploaded separately.
8. The "Affirmation of Originality and Assignment of Copyright/The Disclosure Form for Potential Conflicts of Interest Form" and Authorship Contribution Form should be downloaded from the website, filled thoroughly and uploaded during the submission of the manuscript.

TO AUTHORS

Copyright Notice

The author(s) hereby affirms that the manuscript submitted is original, that all statement asserted as facts are based on author(s) careful investigation and research for accuracy, that the manuscript does not, in whole or part, infringe any copyright, that it has not been published in total or in part and is not being submitted or considered for publication in total or in part elsewhere. Completed Copyright Assignment & Affirmation of Originality Form will be uploaded during submission. By signing this form;

1. Each author acknowledges that he/she participated in the work in a substantive way and is prepared to take public responsibility for the work.
2. Each author further affirms that he or she has read and understands the "Ethical Guidelines for Publication of Research".
3. The author(s), in consideration of the acceptance of the manuscript for publication, does hereby assign and transfer to the Molecular Imaging and Radionuclide Therapy all of the rights and interest in and the copyright of the work in its current form and in any form subsequently revised for publication and/or electronic dissemination.

Privacy Statement

The names and email addresses entered in this journal site will be used exclusively for the stated purposes of this journal and will not be made available for any other purpose or to any other party.

Peer Review Process

1. The manuscript is assigned to an editor, who reviews the manuscript and makes an initial decision based on manuscript quality and editorial priorities.
2. For those manuscripts sent for external peer review, the editor assigns at least two reviewers to the manuscript.
3. The reviewers review the manuscript.
4. The editor makes a final decision based on editorial priorities, manuscript quality, and reviewer recommendations.
5. The decision letter is sent to the author.

Contact Address

All correspondence should be directed to the Editorial Office:
Cinnah Caddesi Pilot Sokak No:10/12 06650 Çankaya / Ankara, Turkey
Phone: +90 312 441 00 45
Fax: +90 312 441 12 97
E-mail: info@tsnmjournals.org

MIRT
Molecular Imaging and Radionuclide Therapy

CONTENTS

Original Articles

129 Evaluation of the Histopathological Features of Early-stage Invasive Ductal Breast Carcinoma by ^{18}Fluoride-fluorodeoxyglucose Positron Emission Tomography/Computed Tomography

^{18}Flor-florodeoksiglukoz Pozitron Emisyon Tomografi/Bilgisayarlı Tomografi ile Erken Evre İnvaziv Duktal Meme Karsinomunun Histopatolojik Özelliklerinin Değerlendirilmesi

Mustafa Erol, Hasan Önner, Meryem İlkay Eren Karanis; Konya, Turkey

137 The Use of ^{18}F-FDG PET/CT in Patients with Recurrent Differentiated Thyroid Cancer

Rekürren Diferansiye Tiroid Kanserinde ^{18}F-FDG PET/BT'nin Katkısı

Özgül Ekmekçioğlu; İstanbul, Turkey

144 Is SUV Corrected for Lean Body Mass Superior to SUV of Body Weight in ^{68}Ga-PSMA PET/CT?

^{68}Ga PSMA PET/BT'de Yağsız Vücut Kütlesine Göre Düzeltilmiş SUV Vücut Ağırlığına Göre Hesaplanan SUV'den Daha mı Üstün?

Ayşegül Aksu, Gamze Çapa Kaya; İstanbul, İzmir, Turkey

150 The Relationship Between HER-2 Expression Levels and ^{18}F-FDG PET/CT Parameters in Gastric Cancer

Mide Kanseri Hastalarında HER-2 Ekspresyon Düzeyleri ve ^{18}F-FDG PET/BT Parametreleri Arasındaki İlişki

Seyit Ahmet Ertürk, Zekiye Hasbek, Hatice Özer; Tokat, Sivas, Turkey

158 Prognostic Prediction of BRCA Mutations by ^{18}F-FDG PET/CT SUV_{max} in Breast Cancer

Meme Kanserlerinde BRCA Mutasyonlarının ^{18}F-FDG PET/BT SUV_{max} Değeri ile Prognostik Tahmini

Semra Özdemir, Fatma Sılan, Mehmet Yılmaz Akgün, Nilgün Aracı, İsmail Çırpan, Fulya Koç Öztürk, Öztürk Özdemir; Çanakkale, Turkey

169 The Comparison of Quantitative Evaluation Results of the MPS SPECT/CT and Coronary Angiography: Determining the Most Valuable Quantitative Evaluation Score

MPS SPECT/BT Kantitatif Değerlendirme Sonuçlarının Koroner Anjiyografi Sonuçları ile Karşılaştırılması: En Değerli Kantitatif Değerlendirme Skorunun Belirlenmesi

Nazlı Pınar Karahan Şen, Recep Bekis, Bihter Şentürk, Bahri Akdeniz; İzmir, Turkey

177 Relationships Between DCE-MRI, DWI, and ^{18}F-FDG PET/CT Parameters with Tumor Grade and Stage in Patients with Head and Neck Squamous Cell Carcinoma

Baş Boyun Yassı Hücreli Kanser Hastalarında Tümör Derecesi ve Evre ile DK-MRG, DAG ve ^{18}F-FDG PET/BT Parametrelerinin İlişkisi

Hande Melike Bülbül, Ogün Bülbül, Sülen Sarıoğlu, Özhan Özdoğan, Ersoy Doğan, Nuri Karabay; Rize, İzmir, Turkey

Interesting Images

187 The Role of a Bone SPECT/CT Scan in the Follow-up of a Solitary Bone Lesion in a Patient with Langerhans' Cell Histiocytosis

Langerhans Hücreli Histiyositoz Tanılı Hastada Soliter Kemik Lezyonunun Takibinde Kemik Sintigrafi ve SPECT/BT'nin Rolü

Selin Kesim, Halil Turgut Turoğlu, Sabahat İnanır, Salih Özgüven, Tanju Yusuf Erdil; İstanbul, Turkey

MIRT
Molecular Imaging and Radionuclide Therapy

CONTENTS

190 ^{18}F-Sodium Fluoride (NaF) Uptake in Calcified Bladder Carcinoma: Double Density Sign
Kalsifiye Mesane Karsinomunda ^{18}F-Sodyum Florür (NaF) Tutulumu: Çift Yoğunluk İşareti
Sharjeel Usmani, Najeeb Ahmed; Shuwaikh, Kuwait, Cottingham, United Kingdom

193 Radium-223 Treatment in mCRPC Patient with Polycythemia Vera
Polisitemi Vera Tanılı mCRPC Hastasında Radyum-223 Tedavisi
Cristina de Angelis, Viviana Frantellizzi, Mariano Pontico, Maria Silvia de Feo, Julia Lazri, Giuseppe de Vincentis; Rome, Italy

197 PET/CT for Early Detection of COVID-19 Pneumonia: Diffuse Fluorodeoxyglucose Uptake in the Lungs without any Additional Changes in a Patient with Breast Cancer
PET/BT'de COVID-19 Erken Bulgusu: Meme Kanserli Hastada Sekel BT Bulguları Zemininde Diffüz Artmış Akciğer Tutulumu
Büşra Özdemir, Burak Günay, Derya Karabulut, Gülay Durmuş Altun; Edirne, Turkey

201 A Case with ^{68}Ga-FAPI Positive and ^{18}F-FDG Negative Breast Cancer
^{68}Ga-FAPI Pozitif, ^{18}F-FDG Negatif Meme Kanseri Olgusu
Halil Kömek, Cihan Gündoğan, Hülya Etem, Canan Can; Diyarbakır, Turkey

Index

2021 Referee Index / *2021 Hakem Dizini*

2021 Author Index / *2021 Yazar Dizini*

2021 Subject Index / *2021 Konu Dizini*

Original Article
Mol Imaging Radionucl Ther 2021;30:129-136 DOI:10.4274/mirt.galenos.2021.25582

Evaluation of the Histopathological Features of Early-stage Invasive Ductal Breast Carcinoma by ^{18}Fluoride-fluorodeoxyglucose Positron Emission Tomography/Computed Tomography

^{18}Flor-florodeoksiglukoz Pozitron Emisyon Tomografi/Bilgisayarlı Tomografi ile Erken Evre İnvaziv Duktal Meme Karsinomunun Histopatolojik Özelliklerinin Değerlendirilmesi

Mustafa Erol[1], Hasan Önner[1], Meryem İlkay Eren Karanis[2]

[1]*University of Health Sciences Turkey, Konya City Hospital, Clinic of Nuclear Medicine, Konya, Turkey*
[2]*University of Health Sciences Turkey, Konya City Hospital, Clinic of Pathology, Konya, Turkey*

Abstract

Objectives: This study investigates the relationship between ^{18}fluoride-fluorodeoxyglucose (^{18}F-FDG) positron emission tomography/computed tomography (PET/CT) parameters and histopathological features in patients with early-stage invasive ductal breast carcinoma (IDBC).

Methods: Patients with early-stage IDBC who underwent ^{18}F-FDG PET/CT scan for staging were included in this retrospective study. The status of estrogen receptor (ER), progesterone receptor (PR), and human epidermal growth factor receptor-2, Ki-67 proliferative index, and grades of tumors were recorded. The conventional metabolic parameters [maximum standard uptake value (SUV_{max}) and average standard uptake value] and volume-based parameters [metabolic tumor volume (MTV) and total lesion glycolysis] of the primary tumor were obtained from the ^{18}F-FDG PET/CT images. The associations and correlations between the ^{18}F-FDG PET/CT parameters and histopathological features were assessed.

Results: One hundred forty-three patients were included. ^{18}F-FDG PET/CT parameters, other than MTV, were significantly associated with the ER and PR status and Ki-67 index, while T-staging was significantly associated with all ^{18}F-FDG PET/CT parameters. In the axillary lymph node (ALN) involvement, no significant difference was found in the ^{18}F-FDG PET/CT parameters. In terms of the pathological stage, a significant difference was found in all ^{18}F-FDG PET/CT parameters. ^{18}F-FDG PET/CT parameters, other than MTV, were significantly higher in non-luminal breast tumors than luminal tumors and in high-grade tumors than low-grade ones. Triple-negative tumors had the highest ^{18}F-FDG PET/CT parameter, but the difference was insignificant for MTV. The SUV_{max} had the strongest correlation with Ki-67 proliferative index.

Conclusion: Tumors with aggressive histopathological features had higher ^{18}F-FDG PET/CT parameter values. This study suggests that ^{18}F-FDG PET/CT may provide prognostic information in patients with early-stage IDBC.

Keywords: Breast cancer, metabolic tumor volume, total lesion glycolysis, ^{18}fluoride-fluorodeoxyglucose, positron emission tomography/computed tomography

Öz

Amaç: Bu çalışmada, erken evre invaziv duktal meme karsinomunun histopatolojik özellikleri ile ^{18}florür-florodeoksiglukoz (^{18}F-FDG) pozitron emisyon tomografi/bilgisayarlı tomografi (PET/BT) parametreleri arasındaki ilişki incelenmiştir.

Yöntem: Bu retrospektif çalışmaya evreleme için ^{18}F-FDG PET/BT taraması yapılan erken evre invaziv duktal meme karsinomlu hastalar dahil edildi. Primer tümörün östrojen reseptör (ER), progesteron reseptör (PR) durumları ile insan epidermal büyüme faktörü reseptörü-2 ekspresyon durumu, Ki-67 proliferasyon indeksi ve histolojik dereceleri kaydedildi. Primer tümörün geleneksel metabolik parametreleri [maksimum standart alım değeri

Address for Correspondence: Mustafa Erol MD, University of Health Sciences Turkey, Konya City Hospital, Clinic of Nuclear Medicine, Konya, Turkey
Phone: +90 531 797 26 11 **E-mail:** mustafaerol82@hotmail.com ORCID ID: orcid.org/0000-0003-3121-5330
Received: 25.12.2020 **Accepted:** 06.04.2021

(SUV_{maks}), ortalama standart alım değeri] ve hacim bazlı parametreler [metabolik tümör hacmi (MTV) ve toplam lezyon glikoliz] ^{18}F-FDG PET/BT görüntülerinden elde edildi. ^{18}F-FDG PET/BT parametreleri ile histopatolojik özellikler arasındaki ilişki ve korelasyon değerlendirildi.

Bulgular: Çalışmaya toplam 143 hasta dahil edildi. MTV dışındaki ^{18}F-FDG PET/BT parametreleri, ER-PR durumu ve Ki-67 indeksi grubu ile anlamlı şekilde farklıydı. Öte yandan, T-evreleme ile tüm ^{18}F-FDG PET/BT parametreleri arasında ileri düzeyde farklılık bulundu. Aksiller lenf nodu tutulumu durumunda ^{18}F-FDG PET/BT parametreleri arasında anlamlı bir fark bulunmadı. Patolojik evre açısından tüm ^{18}F-FDG PET/BT parametrelerinde anlamlı farklılık vardı. MTV dışındaki ^{18}F-FDG PET/BT parametreleri non-luminal tümörlerinde luminal tümörlere göre ve yüksek grade tümörlerde düşük grade tümörlere göre anlamlı olarak daha yüksekti. Üçlü negatif tümörler en yüksek ^{18}F-FDG PET/BT parametrelerine sahipti, ancak MTV için fark anlamlı değildi. Ki-67 proliferasyon indeksi ile en güçlü korelasyon SUV_{maks} değerinde görüldü.

Sonuç: Agresif histopatolojik özellikleri olan tümörlerin ^{18}F-FDG PET/BT parametreleri daha yüksekti. Bu sonuçlar, ^{18}F-FDG PET/BT'nin erken evre invaziv duktal meme karsinomunda prognostik bilgi sağlayabileceğini düşündürmektedir.

Anahtar kelimeler: Meme kanseri, metabolik tümör hacmi, toplam lezyon glikolizi, ^{18}florür-florodeoksiglukoz, pozitron emisyon tomografisi/bilgisayarlı tomografi

Introduction

Breast cancer (BC) is the most widely diagnosed form of cancer and the second cause of cancer-related death in women (1). The most common pathological subtype is invasive ductal breast carcinoma (IDBC), which is associated with different prognostic behaviors concerning molecular subtypes (2). The size and grade of tumors, hormonal receptor status, human epidermal growth factor receptor-2 (HER-2) expression, Ki-67 proliferative index, axillary lymph node (ALN) involvement, and distant metastasis are important for the prognosis and treatment of IDBC (3,4).

^{18}Fluoride-fluorodeoxyglucose (^{18}F-FDG) positron emission tomography/computed tomography (PET/CT) has been widely used for the staging, restaging, assessment of treatment response, and prediction of prognosis in BC (5). Several studies have previously evaluated the relationship between the maximum standard uptake value (SUV_{max}) and clinicopathological factors in BC (6,7,8,9,10,11), while the metabolic tumor volume (MTV) or total lesion glycolysis (TLG), called volume-based PET parameters, shows the total tumor burden and tumor metabolism. The prognostic value of these parameters was significantly associated with BC subtypes and prognosis in many studies (12,13,14,15,16,17).

This study aimed to evaluate the relationship between the ^{18}F-FDG PET/CT parameters [SUV_{max}, average standard uptake value (SUV_{avg}), MTV, and TLG] and histopathological features (pathologic T size, pathological stage, ALN involvement, hormone receptor expressions, HER-2 receptor expression, Ki-67 proliferative index, and molecular subtypes) in IDBC.

Materials and Methods

The Local Ethics Committee of KTO Karatay University Faculty of Medicine approved this study under the decision number: 2020/10. Written informed consent was obtained from all patients. The data of patients with histopathologically documented and surgically excised IDBC, who underwent a preoperative ^{18}F-FDG PET/CT between July 2013 and December 2019, were analyzed. Patients with the following features were excluded from the study: Multifocal or multicentric tumors; bilateral breast tumors; chest wall, surrounding muscle, or skin tissue involvement; distant metastasis; missing clinical data; those with a history of any therapeutic intervention before surgery (e.g., chemotherapy, radiotherapy, and hormone therapy). Moreover, in this study, the largest diameter of the evaluated lesions required to be larger than 10 mm to decrease the partial volume effect.

Imaging and Analysis of ^{18}F-FDG PET/CT

Before the ^{18}F-FDG injection, the patients were fasted for at least six hours to ensure that the blood glucose levels were below 150 mg/dL. The scan was performed 60 min after the intravenous injection. The region of interest (ROI) around the primary tumor was drawn by manual adjustment to exclude structures showing physiological ^{18}F-FDG uptake around the tumor. The tumor was completely covered in three planes. SUV_{max} was obtained by manually drawing the ROI from the slice with the highest uptake of ^{18}F-FDG in the primary tumor. MTV was obtained using a 42% threshold of SUV_{max}. TLG was calculated by multiplying SUV_{avg} by MTV.

Histopathological Analysis and Molecular Subtypes

Patients included in this study underwent surgery or ALN dissection. The pathological data of the tumors, such as size, grade, pathological stage, and other prognostic parameters, were obtained from the records. The tumor has been graded according to the Bloom-Richardson grading system updated by Elston and Ellis (18). The pathological prognostic staging was performed according to the eighth edition of

the American Joint Committee on Cancer's Staging Manual (19). The status of the estrogen receptor (ER), progesterone receptor (PR), and HER-2 expression and the Ki-67 proliferative index were evaluated immunohistochemically. The fluorescence *in situ* hybridization method was used to confirm the presence of HER-2 expression, when the scores were 2+ (20). The molecular subtypes of the ER, PR, and HER-2 expression status were determined. The proliferative index was considered high when the Ki-67 was ≥14% and low when it was <14%. The subjects were classified according to the molecular subtypes as recommended in the 12th International Breast Conference (2). The molecular subtypes were divided into two groups: Luminal (luminal A, luminal B HER-2-negative, and luminal B HER-2-positive subtypes) and non-luminal [HER-2-positive and triple-negative (TN) subtypes].

Statistical Analysis

The statistical analyses were performed using IBM SPSS Statistics for Windows (ver. 21, IBM Corp., Armonk, NY). The normality of the distribution of the continuous data was evaluated. The continuous data were expressed as medians or mean ± standard deviations, where appropriate. The categorical data were shown as frequencies and percentages. For comparing continuous data, non-parametric tests were used. The relationship between the continuous data was evaluated using a Spearman correlation test. A p value less than 0.05 was considered statistically significant.

Results

One hundred forty-three female patients with IDBC and a mean age of 52.43±11.79 years (range: 29-81 years) were included. Table 1 shows the characteristics of the patients. Table 2 shows the relationship between the histopathological features and ^{18}F-FDG PET/CT parameters.

Fifty-nine (41.3%) tumors were stage T1c, and 84 (58.7%) tumors were stage T2. The median values of all ^{18}F-FDG PET/CT parameters were higher in the T2 group than the T1c group (p<0.001 for all comparisons).

All ^{18}F-FDG PET/CT parameters were almost similar across ALN states. The SUV_{max}, SUV_{avg}, and TLG were higher in high-grade tumors (p<0.001 for all comparisons). Moreover, high-grade tumors had higher MTV, but the difference was insignificant.

The SUV_{max}, TLG, and SUV_{avg} were higher in hormone-receptor-negative tumors compared with the positive ones. The MTV was also higher in hormone-receptor-negative tumors compared with the positive ones, but the differences were insignificant. HER-2-positive tumors had higher SUV_{avg} and SUV_{max} than the negative ones (p=0.046 and p=0.04, respectively). The TLG and MTV were higher in HER-2-positive tumors compared with the negative ones, but the differences were insignificant.

Figure 1 shows the transaxial slice of PET/CT images of a patient with IDBC (histologic grade 3; ER-positive, PR-positive, and HER-2-positive).

Luminal A was found in 33 patients (23.1%); luminal B HER-2-negative, 61 patients (42.7%); luminal B HER-

Table 1. Patients' characteristics

Characteristics	n
Number of patients	143
Age, mean	52.43±11.79
Pathological tumor stage	
T1c	59 (41.3%)
T2	84 (58.7%)
Grade of tumor	
I	17 (11.9%)
II	77 (53.8%)
III	49 (34.3%)
Axillary lymph node status	
Positive	78 (54.5%)
Negative	65 (45.5%)
ER status	
Positive	122 (85.3%)
Negative	21 (14.7%)
PR status	
Positive	114 (79.7%)
Negative	29 (20.3%)
HER-2 status	
Positive	38 (26.6%)
Negative	105 (73.4%)
Ki-67 index	
≥14	101 (70.6%)
<14	42 (29.4%)
Molecular subtypes	
Luminal A	33 (23.1%)
Luminal B HER-2-negative	61 (42.7%)
Luminal B HER-2-positive	28 (19.6%)
HER-2-positive	10 (7.0%)
TN	11 (7.7%)
Pathological N (pN)	
N0	65 (45.5%)
Nmi	3 (2.1%)
N1	54 (37.7%)
N2	13 (9.1%)
N3	8 (5.6%)
Pathological stage	
I	34 (23.7%)
II	88 (61.6%)
III	21 (14.7%)

ER: Estrogen receptor, PR: Progesterone receptor, HER-2: Human epidermal growth factor receptor-2; Nmi: Nodal micrometastasis, TN: Triple-negative

2-positive, 28 patients (19.6%); HER-2-positive, 10 patients (7.0%); TN, 11 patients (7.7%). The SUV_{max}, SUV_{avg}, and TLG were different among the five molecular subtypes (p<0.001, p<0.001, and p=0.010, respectively).

Table 2. Associations between the histopathological features and ^{18}F-FDG PET/CT parameters

	SUV_{max} median	SUV_{avg} median	MTV median	TLG median
Pathological tumor stage				
T1c	6.02	3.87	1.59	5.77
T2	10.58	6.52	3.48	22.15
p value	<0.001	<0.001	<0.001	<0.001
Axillary lymph node status				
Positive	7.99	5.00	2.72	12.04
Negative	8.17	4.94	2.06	10.81
p value	0.913	0.955	0.627	0.504
Pathological stage				
I	6.45	4.13	1.44	6.05
II	9.13	5.92	2.95	18.46
III	9.13	5.62	3.11	17.18
p value	0.013	0.028	<0.001	<0.001
Grade of tumor				
I	5.98	3.72	1.95	6.25
II	6.78	4.34	2.41	10.34
III	13.02	8.07	2.87	20.06
p value	<0.001	<0.001	0.294	<0.001
ER status				
Positive	6.88	4.47	2.24	10.15
Negative	17.07	10.55	3.75	28.84
p value	<0.001	<0.001	0.269	0.001
PR status				
Positive	6.88	4.47	2.28	10.67
Negative	13.02	8.07	2.87	18.31
p value	0.001	0.001	0.819	0.049
HER-2 status				
Positive	11.55	7.05	2.49	12.04
Negative	7.11	4.57	2.41	10.53
p value	0.04	0.046	0.773	0.340
Ki-67 index				
≥14	10.4	6.36	2.75	15.27
<14	6.05	3.66	2.06	6.83
p value	<0.001	<0.001	0.410	0.002
Molecular subtypes				
Luminal A	6.36	3.83	2.25	6.89
Luminal B HER-2-negative	7.05	4.54	2.32	11.95
Luminal B HER-2-positive	11.04	6.32	2.09	11.57
HER-2-positive	13.19	8.16	3.05	18.78
TN	21.29	13.24	5.22	50.21
p value	<0.001	<0.001	0.855	0.010
Molecular group				
Luminal	6.89	4.47	3.75	10.16
Non-luminal	17.07	10.55	3.75	28.85
p value	<0.001	<0.001	0.269	0.001

SUV_{max}: Maximum standard uptake value, SUV_{avg}: Average standard uptake value, MTV: Metabolic tumor volume, TLG: Total lesion glycolysis, ER: Estrogen receptor, PR: Progesterone receptor, HER-2: Human epidermal growth factor receptor-2, TN: Triple-negative

Although MTV varied among the molecular subtypes, the difference was insignificant. All ^{18}F-FDG PET/CT parameters were the highest in TN groups in terms of the molecular subtypes. In the post-hoc analysis, the luminal A group had a significantly lower SUV_{max} (p=0.026 and p<0.001, respectively) and SUV_{avg} (p=0.016 and p<0.001, respectively) than the HER-2-positive and TN groups. The luminal B HER-2-negative group had a significantly lower SUV_{max} (p=0.006) and SUV_{avg} (p=0.007) than the TN group. TLG was significantly lower in the luminal A group compared with the TN group (p=0.015).

Among the ^{18}F-FDG PET/CT parameters, TLG had the strongest correlation with the tumor's diameter (r=0.679; p<0.001). Moreover, SUV_{avg} had a modest correlation with Ki-67 (r=0.472; p<0.001). The group with Ki-67 ≥14% had a significantly higher SUV_{avg}, SUV_{max}, and TLG compared with that with Ki-67 <14% (p<0.001, p<0.001, and p=0.002, respectively). The MTV was higher in the group with Ki-67 ≥14% compared with that with Ki-67 <14%, but the difference was statistically insignificant.

There was a difference in the volumetric parameters (MTV and TLG) in the pathological stage (p<0.001 for both comparisons). Other PET parameters also varied significantly (SUV_{max} and SUV_{avg}; p=0.013 and p=0.028, respectively). In the post-hoc analysis, stage-I and stage-II tumors showed differences in terms of SUV_{max} (p=0.01), SUV_{avg} (p=0.026), MTV (p<0.001), and TLG (p<0.001), and stage-I and stage-III tumors showed differences in terms of MTV (p=0.008) and TLG (p=0.001).

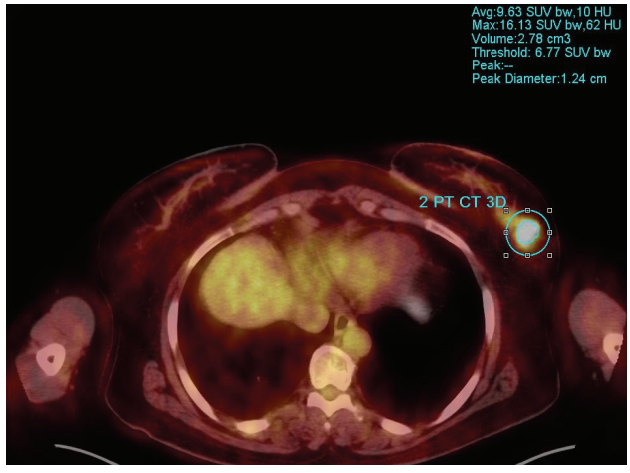

Figure 1. A 55-year-old patient with invasive ductal breast carcinoma (histologic grade 3; ER-positive, 90%; PR-positive, 40%; HER-2-positive). Intense ^{18}F-FDG uptake was seen in the primary tumor (SUV_{max}: 16.13, SUV_{avg}: 9.63, MTV: 2.78, and TLG: 26.73)
ER: Estrogen receptor, PR: Progesterone receptor, HER-2: Human epidermal growth factor receptor-2, ^{18}F-FDG: ^{18}Fluoride-fluorodeoxyglucose, MTV: Metabolic tumor volume, TLG: Total lesion glycolysis, SUV_{max}: Maximum standardized uptake value, SUV_{avg}: Average standard uptake value

Table 3 shows the comparison of the area-under-the-curve (AUC) values of ^{18}F-FDG PET/CT parameters for the histopathological. The AUC values were similar in all tested features except for MTV. Of note, the AUC of SUV_{avg} was the largest for ER and PR status, Ki-67 index, and molecular group. Considering the HER-2 status, TLG had the largest AUC.

Discussion

IDBC is a heterogeneous group of tumors (21). Several studies have reported a correlation between the parameters of ^{18}F-FDG PET/CT and the histopathological features of BC (12,22,23,24). However, most of them evaluated different histological subtypes of BC and reported highly variable results. This study showed that tumors with aggressive histopathological features are associated with high ^{18}F-FDG PET/CT parameters in IDBC.

Table 3. Comparison of the AUC values of the ^{18}F-FDG PET/CT parameters for predicting prognostic factors

	AUC	95% confidence interval	p value
ER negativity			
SUV_{max}	0.795	0.72-0.86	<0.001
SUV_{avg}	0.799	0.72-0.86	<0.001
MTV	0.576	0.49-0.66	0.386
TLG	0.724	0.64-0.80	<0.001
PR negativity			
SUV_{max}	0.701	0.62-0.77	<0.001
SUV_{avg}	0.703	0.62-0.78	<0.001
MTV	0.514	0.43-0.60	0.849
TLG	0.619	0.53-0.70	0.054
HER-2 positivity			
SUVmax	0.612	0.58-0.69	0.041
SUVavg	0.610	0.52-0.69	0.046
MTV	0.484	0.40-0.60	0.779
TLG	0.619	0.47-0.64	0.347
High Ki-67 index			
SUV_{max}	0.702	0.62-0.78	<0.001
SUV_{avg}	0.710	0.63-0.79	<0.001
MTV	0.544	0.46-0.63	0.391
TLG	0.669	0.58-0.74	<0.001
Non-luminal group			
SUV_{max}	0.780	0.72-0.86	<0.001
SUV_{avg}	0.799	0.72-0.86	<0.001
MTV	0.576	0.49-0.68	0.386
TLG	0.724	0.64-0.80	<0.001

AUC: Area-under-the-curve, ER: Estrogen receptor, PR: Progesterone receptor, SUV_{max}: Maximum standard uptake value, SUV_{avg}: Average standard uptake value, MTV: Metabolic tumor volume, TLG: Total lesion glycolysis

An independent prognostic factor for BC is the tumor's size. Moreover, poor histopathological differentiation and larger tumor size are related to an increased metastasis risk in BC (25). While some studies reported the correlation between the tumor's size and ^{18}F-FDG PET/CT parameters (9,23,26,27,28), others did not report such an association (8,10,29). In this study, the T-stage groups were associated with all ^{18}F-FDG PET/CT parameters. Our patient population was predominantly composed of individuals with pathological T2-stage tumors, and there were no T3 tumors in this series.

Studies showed that the negative ER status was associated with higher ^{18}F-FDG PET/CT parameters (12,24,26). In line with these studies, we found significantly higher ^{18}F-FDG PET/CT parameters in ER-negative patients than ER-positive patients, but the difference was statistically insignificant for MTV. According to the studies by Kajáry et al. (12) and Groheux et al. (24), a negative PR status was associated with higher SUV_{max}, MTV, and TLG. Conversely, according to the study by Kaida et al. (23), there was no association between PR status and any volumetric parameters (MTV and TLG). In the present study, there was a significant association between the ER or PR status and the ^{18}F-FDG PET/CT parameters, except for MTV. Some studies (12,30) have reported significant associations between HER-2 status and ^{18}F-FDG PET/CT parameters, but others did not report such an association (24,29). All ^{18}F-FDG PET/CT parameters were higher in HER-2-positive tumors than the negative ones, but significant associations were observed only for SUV_{max} and SUV_{avg} in the present study. A higher histological grade is associated with aggressive behavior (24). Several studies have demonstrated a significant relationship between the histological grade and ^{18}F-FDG PET/CT parameters (9,10,12,26,31,32,33). Similarly, in the present study, there was a significant association between tumor's grade and all ^{18}F-FDG PET/CT parameters, except for MTV. Several studies have demonstrated a positive correlation between the Ki-67 index levels and ^{18}F-FDG PET/CT parameters (9,26,29,32). Similarly, in our study, a positive correlation was observed between the Ki-67 levels and SUV_{max}, SUV_{avg}, and TLG. When the patients were grouped for their Ki-67 levels, the higher-level group had a significantly higher SUV_{max}, SUV_{avg}, and TLG. Our results showed that, among the ^{18}F-FDG PET/CT parameters, SUV_{max} had the strongest correlation with Ki-67.

Studies have reported that molecular subtypes are associated with a variable prognosis, for example, the worst for TN and HER-2-positive and the best for luminal A (12,26,34). Concerning the molecular subtypes, Kajáry et al. (12), Groheux et al. (24), and Önner et al. (26) reported significant associations with SUV_{max}, SUV_{avg}, and TLG. Similarly, in our study, there was a significant relationship between the molecular subtypes and ^{18}F-FDG PET/CT parameters, except for MTV. In the luminal A subtype, cellular proliferation genes are expressed at low levels. Conversely, the *HER-2* gene promotes both cancer growth and progression, and the rates of recurrence and mortality are higher in the HER-2-positive subtype (35). TN BC is the most aggressive subtype and is associated with a worse prognosis (36). In this study, the lowest SUV_{max}, SUV_{avg}, and TLG were observed in the luminal A group, while the highest was in the TN group. In this line, Önner et al. (26) and Kajáry et al. (12) observed the lowest SUV_{max}, SUV_{avg}, MTV, and TLG in the luminal A group and the highest SUV_{max}, MTV, and TLG in the TN group. In this study, SUV_{max}, SUV_{avg}, and TLG were significantly higher in the non-luminal group. Regarding MTV, the median values of MTV were similar in both groups. Similarly, previous studies reported that ^{18}F-FDG parameters were significantly higher in the non-luminal groups (12,24,26).

We performed receiver operating characteristic analyses to find which ^{18}F-FDG PET/CT parameters reflected the pathological features better. The AUC values of SUV_{max}, SUV_{avg}, and TLG were high in all pathological variables (ER, PR, and HER-2 status, Ki-67 index, and molecular subtypes). The largest AUC value was seen for SUV_{avg} in terms of the ER and PR status, Ki-67 index, and molecular groups and for TLG in terms of the HER-2 status. This was incompatible with some recent studies (12,23). We think that these differences are due to different SUV_{max} threshold values used in MTV calculation. Kaida et al. (23) used a threshold of 50% of peak SUV within the lesions for calculating MTV and reported that TLG reflected the tumor metabolism with histopathological features better than SUV_{max} or MTV. However, in another study using 2.5 as the SUV_{max} threshold value in MTV calculation, a high AUC value could not be achieved with MTV. There is a lack of consensus on methods for calculating the volumetric parameters in the literature (12,23,24,26,37,38). In solid tumors such as BC, some authors recommend using 42% of tumor SUV_{max} as a threshold to represent the glycolytic activity (37,38). So, we used 42% as the threshold for the present study.

Study Limitations

The limitations of this study include being retrospective and having low patients in the groups. Moreover, we cannot predict the findings of this study in patients with advanced IDBC.

Conclusion

The findings of this study showed that tumors with aggressive histopathological features are associated with high ^{18}F-FDG PET/CT parameters, and therefore, ^{18}F-FDG PET/CT imaging can be used as an aid in predicting the prognosis in early-stage IDBC.

Ethics

Ethics Committee Approval: The Local Ethics Committee of KTO Karatay University Faculty of Medicine approved this study under the decision number: 2020/10.

Informed Consent: Written informed consent was obtained from all patients.

Peer-review: Externally peer-reviewed.

Authorship Contributions

Surgical and Medical Practices: M.İ.E.K., Concept: M.E., H.Ö., Design: M.E., H.Ö., Data Collection or Processing: M.E., H.Ö., M.İ.E.K., Analysis or Interpretation: M.E., Literature Search: M.E., Writing: M.E.

Conflict of Interest: No conflict of interest was declared by the authors.

Financial Disclosure: The authors declared that this study has received no financial support.

References

1. Siegel RL, Miller KD, Jemal A. Cancer statistics, 2019. CA Cancer J Clin 2019;69:7-34.
2. Goldhirsch A, Wood WC, Coates AS, Gelber RD, Thürlimann B, Senn HJ; Panel members. Strategies for subtypes–dealing with the diversity of breast cancer: highlights of the St. Gallen International Expert Consensus on the Primary Therapy of Early Breast Cancer 2011. Ann Oncol 2011;22:1736-1747.
3. Banerjee M, George J, Song EY, Roy A, Hryniuk W. Tree-based model for breast cancer prognostication. J Clin Oncol 2004;22:2567-2575.
4. Kwast AB, Voogd AC, Menke-Pluijmers MB, Linn SC, Sonke GS, Kiemeney LA, Siesling S. Prognostic factors for survival in metastatic breast cancer by hormone receptor status. Breast Cancer Res Treat 2014;145:503-511.
5. Caresia Aroztegui AP, García Vicente AM, Alvarez Ruiz S, Delgado Bolton RC, Orcajo Rincon J, Garcia Garzon JR, de Arcocha Torres M, Garcia-Velloso MJ; Oncology Task Force of the Spanish Society of Nuclear Medicine and Molecular Imaging. 18F-FDG PET/CT in breast cancer: Evidence-based recommendations in initial staging. Tumour Biol 2017;39:1010428317728285.
6. Song BI, Hong CM, Lee HJ, Kang S, Jeong SY, Kim HW, Chae YS, Park JY, Lee SW, Ahn BC, Lee J. Prognostic Value of Primary Tumor Uptake on F-18 FDG PET/CT in Patients with Invasive Ductal Breast Cancer. Nucl Med Mol Imaging 2011;45:117-124.

7. Kumar R, Chauhan A, Zhuang H, Chandra P, Schnall M, Alavi A. Clinicopathologic factors associated with false negative FDG-PET in primary breast cancer. Breast Cancer Res Treat 2006;98:267-274.
8. Avril N, Menzel M, Dose J, Schelling M, Weber W, Jänicke F, Nathrath W, Schwaiger M. Glucose metabolism of breast cancer assessed by 18F-FDG PET: histologic and immunohistochemical tissue analysis. J Nucl Med 2001;42:9-16.
9. Gil-Rendo A, Martínez-Regueira F, Zornoza G, García-Velloso MJ, Beorlegui C, Rodriguez-Spiteri N. Association between [18F]fluorodeoxyglucose uptake and prognostic parameters in breast cancer. Br J Surg 2009;96:166-170.
10. Groheux D, Giacchetti S, Moretti JL, Porcher R, Espié M, Lehmann-Che J, de Roquancourt A, Hamy AS, Cuvier C, Vercellino L, Hindié E. Correlation of high 18F-FDG uptake to clinical, pathological and biological prognostic factors in breast cancer. Eur J Nucl Med Mol Imaging 2011;38:426-435.
11. Koo HR, Park JS, Kang KW, Cho N, Chang JM, Bae MS, Kim WH, Lee SH, Kim MY, Kim JY, Seo M, Moon WK. 18F-FDG uptake in breast cancer correlates with immunohistochemically defined subtypes. Eur Radiol 2014;24:610-618.
12. Kajáry K, T kés T, Dank M, Kulka J, Szakáll S Jr, Lengyel Z. Correlation of the value of 18F-FDG uptake, described by SUVmax, SUVavg, metabolic tumour volume and total lesion glycolysis, to clinicopathological prognostic factors and biological subtypes in breast cancer. Nucl Med Commun 2015;36:28-37.
13. Chen S, Ibrahim NK, Yan Y, Wong ST, Wang H, Wong FC. Risk stratification in patients with advanced-stage breast cancer by pretreatment [(18) F] FDG PET/CT. Cancer 2015;121:3965-3974.
14. Hyun SH, Choi JY, Kim K, Kim J, Shim YM, Um SW, Kim H, Lee KH, Kim BT. Volume-based parameters of (18)F-fluorodeoxyglucose positron emission tomography/computed tomography improve outcome prediction in early-stage non-small cell lung cancer after surgical resection. Ann Surg 2013;257:364-370.
15. Son SH, Lee SW, Jeong SY, Song BI, Chae YS, Ahn BC, Lee J. Whole-Body Metabolic Tumor Volume, as Determined by (18)F-FDG PET/CT, as a Prognostic Factor of Outcome for Patients With Breast Cancer Who Have Distant Metastasis. AJR Am J Roentgenol 2015;205:878-885.
16. Ulaner GA, Eaton A, Morris PG, Lilienstein J, Jhaveri K, Patil S, Fazio M, Larson S, Hudis CA, Jochelson MS. Prognostic value of quantitative fluorodeoxyglucose measurements in newly diagnosed metastatic breast cancer. Cancer Med 2013;2:725-733.
17. Kim J, Yoo SW, Kang SR, Cho SG, Oh JR, Chong A, Min JJ, Bom HS, Yoon JH, Song HC. Prognostic Significance of Metabolic Tumor Volume Measured by (18)F-FDG PET/CT in Operable Primary Breast Cancer. Nucl Med Mol Imaging 2012;46:278-285.
18. Elston CW, Ellis IO. Pathological prognostic factors in breast cancer. I. The value of histological grade in breast cancer: experience from a large study with long-term follow-up. Histopathology 1991;19:403-410.
19. Edge SB, Byrd DR, Carducci MA, Compton CC, Fritz A, Greene F. AJCC cancer staging manual: Springer New York; 2010.
20. Wolff AC, Hammond ME, Hicks DG, Dowsett M, McShane LM, Allison KH, Allred DC, Bartlett JM, Bilous M, Fitzgibbons P, Hanna W, Jenkins RB, Mangu PB, Paik S, Perez EA, Press MF, Spears PA, Vance GH, Viale G, Hayes DF; American Society of Clinical Oncology; College of American Pathologists. Recommendations for human epidermal growth factor receptor 2 testing in breast cancer: American Society of Clinical Oncology/College of American Pathologists clinical practice guideline update. Arch Pathol Lab Med 2014;138:241-256.
21. Parker JS, Mullins M, Cheang MC, Leung S, Voduc D, Vickery T, Davies S, Fauron C, He X, Hu Z, Quackenbush JF, Stijleman IJ, Palazzo J, Marron JS, Nobel AB, Mardis E, Nielsen TO, Ellis MJ, Perou CM, Bernard PS. Supervised risk predictor of breast cancer based on intrinsic subtypes. J Clin Oncol 2009;27:1160-1167.
22. Kitajima K, Fukushima K, Miyoshi Y, Nishimukai A, Hirota S, Igarashi Y, Katsuura T, Maruyama K, Hirota S. Association between ^{18}F-FDG uptake and molecular subtype of breast cancer. Eur J Nucl Med Mol Imaging 2015;42:1371-1377.
23. Kaida H, Toh U, Hayakawa M, Hattori S, Fujii T, Kurata S, Kawahara A, Hirose Y, Kage M, Ishibashi M. The relationship between 18F-FDG metabolic volumetric parameters and clinicopathological factors of breast cancer. Nucl Med Commun 2013;34:562-570.
24. Groheux D, Majdoub M, Tixier F, Le Rest CC, Martineau A, Merlet P, Espié M, de Roquancourt A, Hindié E, Hatt M, Visvikis D. Do clinical, histological or immunohistochemical primary tumour characteristics translate into different (18)F-FDG PET/CT volumetric and heterogeneity features in stage II/III breast cancer? Eur J Nucl Med Mol Imaging 2015;42:1682-1691.
25. Robinson BD, Sica GL, Liu YF, Rohan TE, Gertler FB, Condeelis JS, Jones JG. Tumor microenvironment of metastasis in human breast carcinoma: a potential prognostic marker linked to hematogenous dissemination. Clin Cancer Res 2009;15:2433-2441.
26. Önner H, Canaz F, Dinçer M, Işiksoy S, Sivrikoz İA, Entok E, Erkasap S. Which of the fluorine-18 fluorodeoxyglucose positron emission tomography/computerized tomography parameters are better associated with prognostic factors in breast cancer? Medicine (Baltimore) 2019;98:e15925.
27. Ekmekcioglu O, Aliyev A, Yilmaz S, Arslan E, Kaya R, Kocael P, Erkan ME, Halac M, Sonmezoglu K. Correlation of 18F-fluorodeoxyglucose uptake with histopathological prognostic factors in breast carcinoma. Nucl Med Commun 2013;34:1055-1067.
28. Ueda S, Tsuda H, Asakawa H, Shigekawa T, Fukatsu K, Kondo N, Yamamoto M, Hama Y, Tamura K, Ishida J, Abe Y, Mochizuki H. Clinicopathological and prognostic relevance of uptake level using 18F-fluorodeoxyglucose positron emission tomography/computed tomography fusion imaging (18F-FDG PET/CT) in primary breast cancer. Jpn J Clin Oncol 2008;38:250-258.
29. Buck A, Schirrmeister H, Kühn T, Shen C, Kalker T, Kotzerke J, Dankerl A, Glatting G, Reske S, Mattfeldt T. FDG uptake in breast cancer: correlation with biological and clinical prognostic parameters. Eur J Nucl Med Mol Imaging 2002;29:1317-1323.
30. Sanli Y, Kuyumcu S, Ozkan ZG, Işik G, Karanlik H, Guzelbey B, Turkmen C, Ozel S, Yavuz E, Mudun A. Increased FDG uptake in breast cancer is associated with prognostic factors. Ann Nucl Med 2012;26:345-350.
31. Berriolo-Riedinger A, Touzery C, Riedinger JM, Toubeau M, Coudert B, Arnould L, Boichot C, Cochet A, Fumoleau P, Brunotte F. [18F]FDG-PET predicts complete pathological response of breast cancer to neoadjuvant chemotherapy. Eur J Nucl Med Mol Imaging 2007;34:1915-1924.
32. Shimoda W, Hayashi M, Murakami K, Oyama T, Sunagawa M. The relationship between FDG uptake in PET scans and biological behavior in breast cancer. Breast Cancer 2007;14:260-268.
33. Ikenaga N, Otomo N, Toyofuku A, Ueda Y, Toyoda K, Hayashi T, Nishikawa K, Tanaka M. Standardized uptake values for breast carcinomas assessed by fluorodeoxyglucose-positron emission tomography correlate with prognostic factors. Am Surg 2007;73:1151-1157.
34. Sorlie T, Tibshirani R, Parker J, Hastie T, Marron JS, Nobel A, Deng S, Johnsen H, Pesich R, Geisler S, Demeter J, Perou CM, Lønning PE, Brown PO, Børresen-Dale AL, Botstein D. Repeated observation of breast tumor subtypes in independent gene expression data sets. Proc Natl Acad Sci U S A 2003;100:8418-8423.
35. Gianni L, Dafni U, Gelber RD, Azambuja E, Muehlbauer S, Goldhirsch A, Untch M, Smith I, Baselga J, Jackisch C, Cameron D, Mano M, Pedrini JL, Veronesi A, Mendiola C, Pluzanska A, Semiglazov V, Vrdoljak E, Eckart MJ, Shen Z, Skiadopoulos G, Procter M, Pritchard KI, Piccart-Gebhart MJ, Bell R; Herceptin Adjuvant (HERA) Trial Study Team. Treatment with trastuzumab for 1 year after adjuvant chemotherapy in patients with HER2-positive early breast cancer: a 4-year follow-up of a randomised controlled trial. Lancet Oncol 2011;12:236-244.

36. Caudle AS, Yu TK, Tucker SL, Bedrosian I, Litton JK, Gonzalez-Angulo AM, Hoffman K, Meric-Bernstam F, Hunt KK, Buchholz TA, Mittendorf EA. Local-regional control according to surrogate markers of breast cancer subtypes and response to neoadjuvant chemotherapy in breast cancer patients undergoing breast conserving therapy. Breast Cancer Res 2012;14:R83.
37. Hatt M, Cheze-Le Rest C, Aboagye EO, Kenny LM, Rosso L, Turkheimer FE, Albarghach NM, Metges JP, Pradier O, Visvikis D. Reproducibility of 18F-FDG and 3'-deoxy-3'-18F-fluorothymidine PET tumor volume measurements. J Nucl Med 2010;51:1368-1376.
38. Marinelli B, Espinet-Col C, Ulaner GA, McArthur HL, Gonen M, Jochelson M, Weber WA. Prognostic value of FDG PET/CT-based metabolic tumor volumes in metastatic triple negative breast cancer patients. Am J Nucl Med Mol Imaging 2016;6:120-127.

Original Article
Mol Imaging Radionucl Ther 2021;30:137-143 DOI:10.4274/mirt.galenos.2021.02360

The Use of ^{18}F-FDG PET/CT in Patients with Recurrent Differentiated Thyroid Cancer

Rekürren Diferansiye Tiroid Kanserinde ^{18}F-FDG PET/BT'nin Katkısı

Özgül Ekmekçioğlu

University of Health Sciences Turkey, Şişli Hamidiye Etfal Training and Research Hospital, Clinic of Nuclear Medicine, İstanbul, Turkey

Abstract

Objectives: ^{18}Fluorine-fluorodeoxyglucose (^{18}F-FDG) positron emission tomography/computed tomography (PET/CT) is used to monitor the recurrence in thyroid cancer patients when there is suspicion of metastases. De-differentiated lesions become ^{18}F-FDG avid with a more aggressive clinical course. The aim of this study was to investigate the use of ^{18}F-FDG PET/CT in differentiated thyroid cancer.

Methods: Forty-six patients, either with a negative radioiodine scan or clinical progression and suspicions for metastases with differentiated thyroid cancer that were referred to our department for ^{18}F-FDG PET/CT scan and evaluated retrospectively. PET/CT findings were correlated with clinical and histopathological findings, serum thyroglobulin (Tg), and anti-Tg levels.

Results: Twenty-six patients (56.2%) were positive for recurrence in ^{18}F-FDG PET/CT images. Positive ^{18}F-FDG PET/CT findings were significantly correlated with the disease stage and Tg levels. Maximum standardized uptake value did not correlate with other findings or patients' profiles. The cut-off value for Tg was at 52.5 ng/mL having 73.08% sensitivity, 75% specificity, 79.17% positive predictive value, and 68.18% negative predictive value for ^{18}F-FDG PET/CT imaging.

Conclusion: ^{18}F-FDG PET/CT is useful for detecting recurrence in differentiated thyroid cancer. Increased Tg levels and stage of the disease were significantly correlated with ^{18}F-FDG positivity. ^{18}F-FDG positivity may also provide information about the de-differentiation process that may support the treatment plan.

Keywords: Thyroid cancer, ^{18}F-FDG PET/CT, SUV_{max}

Öz

Amaç: ^{18}Flor-florodeoksiglukoz (^{18}F-FDG) pozitron emisyon tomografi/bilgisayarlı tomografi (PET/BT) metastaz şüphesi bulunan tiroid kanseri hastalarında rekürrensi araştırmak için kullanılır. Özellikle de-diferansiye olan lezyonlar ^{18}F-FDG tutulumu göstermekte olup hastalığın klinik seyri daha agresif olarak izlenir. Bu çalışmada ^{18}F-FDG PET/BT'nin diferansiye tiroid kanserindeki katkısını araştırmayı amaçladık.

Yöntem: İyot-131 (I-131) tüm vücut tarama sintigrafisi negatif olarak saptanan ve/veya metastaz şüphesi uyandıran klinik olarak progrese diferansiye tiroid kanseri tanılı bölümümüzde ^{18}F-FDG PET/BT çekimi yapılan 46 hasta retrospektif olarak incelendi. ^{18}F-FDG PET/BT bulguları ile klinik ve histopatolojik özellikleri ile serum tiroglobulin (Tg) ve anti-Tg değerleri karşılaştırıldı.

Bulgular: Grupta bulunan 26 hastada (%56,2) ^{18}F-FDG PET/BT görüntülemesinde pozitif olarak değerlendirilen bulgular saptandı. Hastalık evresi ve Tg düzeyleri ile ^{18}F-FDG PET/BT pozitifliği arasında pozitif bir korelasyon bulundu. Lezyonların maksimum standart tutulum değeri (SUV_{maks}) ile anlamlı bir ilişki saptanmadı. Tg cut-off değeri 52,5 ng/mL olarak hesaplandı. Bu değer bazında ^{18}F-FDG PET/BT görüntüleme için %73,08 duyarlılık, %75 özgüllük, %79,17 pozitif prediktif değer ve %68,18 negatif prediktif değerler elde edildi.

Sonuç: ^{18}F-FDG PET/BT diferansiye tiroid kanserinde rekürrensi saptamada faydalı bir yöntem olarak değerlendirildi. Hastalığın evresi ve Tg değerleri ile PET görüntülemede elde edilen pozitif bulguları arasında anlamlı olarak korelasyon saptandı. Pozitif PET bulguları ile tümör dediferansiasyonu hakkında bilgi edinilmesi açısından tedavi planına katkısı bulunabileceği sonucuna varıldı.

Anahtar kelimeler: Tiroid kanseri, ^{18}F-FDG PET/BT, SUV_{maks}

Address for Correspondence: Özgül Ekmekçioğlu MD, University of Health Sciences Turkey, Şişli Hamidiye Etfal Training and Research Hospital, Clinic of Nuclear Medicine, İstanbul, Turkey
Phone: +90 212 373 52 14 **E-mail:** ozgulek@gmail.com ORCID ID: orcid.org/0000-0002-3313-8087
Received: 02.02.2021 **Accepted:** 24.04.2021

Introduction

Differentiated thyroid cancers are slowly growing tumors with a good prognosis and relatively low mortality rates (1,2). The American Thyroid Association (ATA) defines the thyroglobulin (Tg) level of 0.2 ng/mL as acceptable after the ablation and/or radioiodine treatment. Routine follow-up is conducted by measuring serum Tg and anti-Tg levels, with a neck ultrasound (3). Whole-body scintigraphy with radioiodine is advisable when Tg serum levels are at the rise or on the occasion or suspicion of metastases. Residual disease or recurrence has been mostly detected in the thyroid bed or cervical lymph nodes (4). However, in the case of suspicion of residual disease or recurrence that could not be detected with the ultrasound, conventional imaging techniques are applied. Positron emission tomography/computed tomography (PET/CT) is helpful in restaging patients with increased Tg levels and a negative iodine whole-body scan (5,6). ATA guidelines suggest a serum Tg cut-off at 10 ng/mL to benefit from PET/CT imaging in metastatic cancers.

Whole-body iodine-131 (I-131) scan has high sensitivity and specificity for the detection of differentiated thyroid cancer. It is routinely used in searching for metastases or recurrence, as recommended in the ATA guidelines (7). However, spatial resolution might not be efficient in the case of small lesions (<1 cm). Additionally, thyroid cells may de-differentiate which leads to aggressive malignancy and loss of the iodine uptake during the follow-up. ^{18}Fluoride-fluorodeoxyglucose (^{18}F-FDG) PET/CT is useful for the detection of metastases, especially when cancer cells de-differentiate. While the iodine transport decrease in thyroid cancer cells, glucose metabolism increases and becomes more FDG avid; this is called the "flip-flop phenomenon" and serves as a sign of de-differentiation (8,9,10). Imaging techniques other than whole-body radioiodine scan are necessary in these cases. While ^{18}F-FDG avidity represents the aggressiveness of tumor cells, CT depicts metastatic lesions with negative ^{18}F-FDG uptake. This may benefit the tumors, where some of the metastases have a lower level of differentiation.

Maximum standardized uptake values (SUV_{max}) may provide a direction of the therapy, since the higher the values, the worse the prognosis (10). Recent studies have also emphasized the importance of ^{18}F-FDG PET/CT in patients with suspicions of recurrence and prior radioiodine treatment (11,12). Furthermore, ^{18}F-FDG PET/CT scan has an impact on disease management and prognosis (6). Nevertheless, PET/CT in routine imaging of thyroid cancer patients is not part of the recent guidelines' recommendations.

This study aimed to evaluate the use of ^{18}F-FDG PET/CT scans in differentiated thyroid cancer, in patients with suspicions of recurrence or metastases in our hospital. Moreover, we assessed the relation of SUV_{max} levels with clinical and pathological findings of the patients.

Materials and Methods

Patients with intermediate or high-risk differentiated thyroid cancer, who were referred to our department for radioiodine treatment between 2017 and 2020, have been analyzed retrospectively. Patients were either operated in our hospital or were following-up from the other clinics. A group of patients were referred to our department without previous routine follow-up. All patients had undergone thyroidectomy, with or without the central and lateral lymph node dissection, and radioiodine treatment. The I-131 treatment dosage was between 3700 (100 mCi) and 7400 MBq (200 mCi) by following the ATA guidelines' recommendations and risk assessment of the patient.

Six months after the treatment, when the thyroid stimulating hormone serum levels measurement had reached >30 ng/mL, Tg and anti-Tg levels were measured. Patients with suspicion or already discovered metastases with increasing levels of either Tg or anti-Tg after the radioiodine treatment were included in the study. Serum stimulated Tg and anti-Tg levels were measured. The risk stratification and suspicion for a recurrence or metastases are defined by the ATA guidelines. All the patients signed informed consent forms. University of Health Sciences Turkey, Şişli Hamidiye Etfal Training and Research Hospital Clinical Research Ethics Committee approved (number: 3112, date: 02.02.2021).

Imaging Techniques

Ultrasound for residual disease or abnormal lymph node on the neck region was performed. Whole-body scan was performed 48-72 hours after administering the 185 MBq (5 mci) I-131 for the patients with increasing levels of either Tg or anti-Tg. A Mediso dual-head camera was used for whole-body scintigraphy and single photon emission computed tomography/CT images when detailed images are required. Finally, ^{18}F-FDG PET/CT scan was performed on the patients with either a negative I-131 scan or clinical signs of disease progression after the iodine treatment. Patients with already known metastases and increased levels of either Tg or anti-Tg were also included and screened with ^{18}F-FDG PET/CT scan.

FDG PET/CT protocol had the following parameters: 45-60 mins after receiving approximately 111-370 Mbq (3-10 mci) of ^{18}F-FDG with patient having an empty

bladder, underwent a head to mid-thigh whole-body CT scan (130 kV, 50-80 mAs, thickness slice of 3 mm) and followed by a PET scan (GE Healthcare, Wisconsin, USA). Neither oral nor intravenous contrast was used in any of the patients. A region of interest was drawn around the metastases to measure the SUV_{max}. Lesions with an abnormal anatomical shape and higher SUV_{max} levels than the background were accepted as PET-positive for recurrence or metastases. Biopsy confirmation was not achieved in all the patients.

Statistical Analysis

All data were analyzed on SPSS software for Windows (v17.0; IBM, Armonk, NY, USA). Individual and aggregate data were summarized using descriptive statistics including the mean, standard deviations, medians (min-max), frequency distributions, and percentages. The normality of the data distribution was verified by the histogram graphs and the Kolmogorov-Smirnov test. For the variables that were not normally distributed, the Mann-Whitney U and Kruskal-Wallis tests were applied to compare between groups. The correlation was analyzed with Spearman's Rho tests. Receiver operating characteristic (ROC) analysis was used to determine the cut-off levels of Tg and anti-Tg. P values of <0.05 were considered statistically significant.

Results

Forty-six patients with a mean age of 47.65±15.82 were included in our study (Table 1). Seventeen of the patients were male. The patients were categorized according to the type of cancer. Papillary thyroid cancer (PTC) corresponded to 76.09% (n=35), follicular thyroid cancer (FTC) to 6.52% (n=3), and mixed type of differentiated thyroid cancer to 17.39% (n=8). Two of the PTC patients had tall cell variant and one had an oncocytic variant. Two of the mixed type patients had tall cell variant tumors. According to the classification of the American Joint Committee of Cancer and the TNM guidelines, 27 patients were stage-I, nine patients were stage-II, and four patients were stage-IV (13). Twenty-six patients (56.2%) had at least one lesion with a SUV_{max} >2.5, were grouped as recurrent or metastatic disease, and consequently accepted as PET-positive group. In the PET-positive group, 12 patients had local recurrence findings, and 14 patients had lesions positive for metastatic lymph nodes in the cervical region. Furthermore, five patients had lesions in the mediastinum, five had lung lesions, and three had bone lesions compatible with the metastases (Figure 1).

The mean Tg levels were 240.36±372.75 ng/mL (range between 0.04 and 11.000 ng/mL), and the mean anti-Tg levels were 37.87±237.37 ng/mL (range between 0.9 and 1.611 ng/mL). Tg and anti-Tg levels of all patients were categorized into two groups as PET-positive and negative. Tg levels were detected significantly higher in PET-positive patients (101.3 ng/mL) than in PET-negative patients (19.4 ng/mL; p=0.001, Table 2). The cut-off value of Tg levels for PET-positive patients was at 52.5 ng/mL, as calculated by the ROC analysis (Figure 2). With this cut-off value for Tg, 73.08% sensitivity, 75% specificity, 79.17% positive predictive value, and 68.18% negative predictive value were achieved in the PET-positive patients. Eight of the total number of patients had increased anti-Tg levels, of which two had ^{18}F-FDG-positive lesions. However, there was either no significant relation or no meaningful cut-off value for the anti-Tg levels, probably due to the smaller sample size.

The comparison between PET-positive disease and the TNM stage of the patients showed significant differences between stage-I and stage-II or stage-IV patients. Stages-II and-IV disease had significantly higher ^{18}F-FDG positivity in PET/CT images (p=0.049, Table 3).

Table 1. Patient characteristics

Clinicopathologic features	**n**
Age (mean ± SD)	47.65±15.82
Sex	
Male	17
Female	29
Tumor type	
Papillary thyroid cancer	
- Classic type	35
- Mixed type	8
Folicular carcinoma	3
PET/CT findings	
^{18}F-FDG-positive	26
^{18}F-FDG negative	20
Previous treatment dose of I-131	
3.7 GBq (100 mCi)	13
5.6 GBq (150 mCi)	23
7.4 GBq (200 mCi)	10
Serum thyroglobulin level (ng/mL) (mean ± SD)	240.36±372.75
Serum anti-thyroglobulin level (ng/mL) (mean ± SD)	37.87±237.37
Serum thyroid stimulating hormone (mIU/mL) (mean ± SD)	71.3±14.11
Size of primary tumor (cm) (mean ± SD)	2.83±1.87
Localization of recurrence/metastases	
Local	12
Neck	14
Mediastinum	5
Lung	5
Bone	3

SD: Standard deviation, PET/CT: Positron emission tomography/computed tomography, ^{18}F-FDG: ^{18}Fluoride-fluorodeoxyglucose, I-131: Iodine-131

Table 2. Mean and median values of ^{18}F-FDG PET/CT positive and negative patients

	^{18}F-FDG PET		p
	Positive	Negative	
	Mean ± SD	Mean ± SD	
Age	51.35±16.35	42.85±14.08	0.063
Serum Tg level (ng/mL)	339.55±417.29	111.41±262.65	**0.001**
Serum anti-Tg level (ng/mL)	65.91±315.49	1.43±2.20	0.375
Size of primary tumor (cm)	2.97±1.93	2.63±1.83	0.519

SD: Standard deviation, PET/CT: Positron emission tomography/computed tomography, ^{18}F-FDG: ^{18}Fluoride-fluorodeoxyglucose, Tg: Thyroglobulin

Gender, age, and tumor type did not exhibit a significant effect on PET/CT positivity. SUV_{max} data also correlated with the clinical and pathological findings of the patients. The mean SUV_{max} value for the recurrent or metastatic lesions in PET/CT scan was 7.65±5.99 (2.5-25.3). The highest SUV_{max} was 25.3 in one patient with FTC. However, it did not have any correlation with the prognostic factors or patients' characteristics.

Discussion

^{18}F-FDG PET/CT scan is useful in staging and following-up most of the cancer types, yet the evidence of the benefits in thyroid cancer is limited. Even the cost-effectiveness relationship of PET/CT imaging in differentiated thyroid

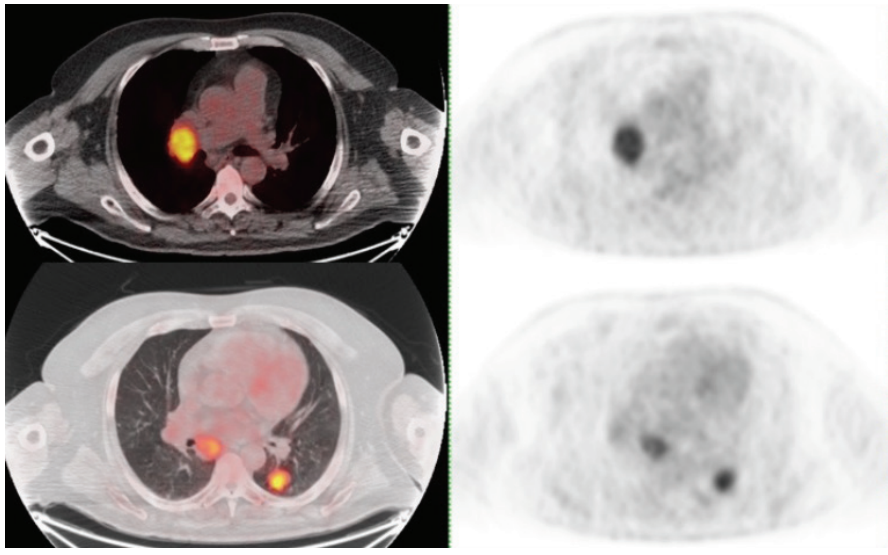

Figure 1. A 56-year-old man with classic type papillary thyroid cancer, previously received 200 mCi I-131 treatment. He was referred for clinical progression. Lesions with high ^{18}F-FDG uptake were found in the mediastinum and lung parenchyma (Tg: 1.853 ng/mL, anti-Tg: 0.9 ng/mL)
I-131: Iodine-131, ^{18}F-FDG: ^{18}Fluoride-fluorodeoxyglucose, Tg: Thyroglobulin

Table 3. Detailed data of ^{18}F-FDG PET/CT positive and negative patients' group

		^{18}F-FDG PET				p
		Positive		Negative		
		n	%	n	%	
Sex	Male	10	(58.82)	7	(41.18)	0.809
	Female	16	(55.17)	13	(44.83)	
Tumor type	Classic type	21	(60.02)	14	(39.98)	0.125
	Folicular C	3	(100)	0	(0)	
	Mixed type	2	(25.00)	6	(75.00)	
Stage	1	12	(44.44)	15	(55.56)	**0.049**
	2	8	(88.89)	1	(11.11)	
	4	3	(75.00)	1	(25.00)	

^{18}F-FDG: ^{18}Fluoride-fluorodeoxyglucose, PET/CT: Positron emission tomography/computed tomography

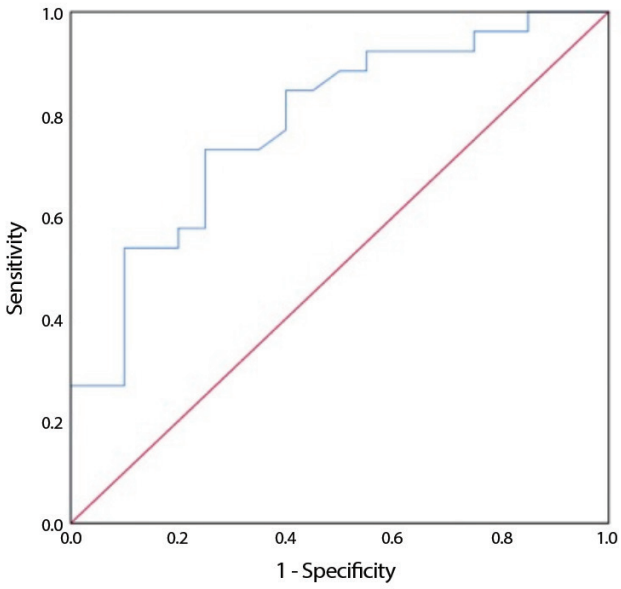

Figure 2. ROC curve of Tg serum levels
ROC: Receiver operating characteristic, Tg: Thyroglobulin

cancer is still being discussed. ^{18}F-FDG uptake represents de-differentiation, and the "flip-flop" phenomenon serves as a sign of worse prognosis (10).

The results from our study indicate that the TNM stage of the disease may lead to specific follow-up for patients who could benefit from the PET/CT. ^{18}F-FDG positivity is significantly higher in patients with stage-II and -IV, consistent with the aggressive potentiality of the disease. The other prognostic factors like age, gender, type, or size of the tumor did not have a significant relation to PET positivity.

The group of ^{18}F-FDG-positive lesions in PET/CT scan had a significantly higher median of Tg levels than the ^{18}F-FDG negative group (101.3 ng/mL vs. 19.4 ng/mL; p=0.001). The cut-off Tg value in the present study was higher than that indicated by the guidelines and that of other studies (7,14,15,16). We believe it resulted from the low number of patients participating in our study, and/or the high mean of Tg levels (240.36±372.75; median: 59.65). Some of the patients that presented to our department were not routinely followed up, so they had already developed metastatic pathologies before they underwent the PET/CT scan.

SUV_{max} values significantly did not correlate with the other clinical findings or characteristics of the patients. Nevertheless, SUV_{max} values provide important information about the de-differentiation degree. Other groups have reported a correlation between high SUV_{max} and worse prognosis in PTC patients (17). As a result of de-differentiation of tumor cells, the glucose transporter-1 increases and affects the increase in ^{18}F-FDG uptake (18). Robbins et al. (19) demonstrated that SUV_{max} affected positively both the prognosis and the survival of the patients. ^{18}F-FDG-positive lesions indicate higher aggressiveness correlated with the value of the SUV_{max} (20). Furthermore, another study has demonstrated that a SUV_{max} >10 is related to shorter locoregional disease-free survival (21). The two patients with aggressive variant (tall cell) PTC in our study had ^{18}F-FDG-positive metastatic lesions. They had Tg levels of 1.522 ng/mL, 35 ng/mL, and SUV_{max} values of 12.9, 5.8, respectively. Both patients had local recurrence while one of them, with the highest Tg and SUV_{max} levels, additionally presented with lung metastases. These findings are compatible with the literature, but further correlations are necessary with more patients in aggressive differentiated thyroid cancers. More observational studies for detecting or staging thyroid cancers with ^{18}F-FDG PET/CT in the initial phases of the disease also provide valuable information for the treatment decision (22). Furthermore, the challenge of treatment for the patients with simultaneous iodine positivity and ^{18}F-FDG positivity should be taken into consideration (23). We also had a patient with both iodine-positive and negative metastases. Intense ^{18}F-FDG uptake was detected in de-differentiated metastatic lesions, as seen in PET/CT images (Figure 3). Therapy management is a challenge in such cases and the treatment decision, including tyrosine kinase as an option, should be made in accordance with oncology.

Study Limitations

This study had some limitations. ^{18}F-FDG negative patients could not be discussed in detail, due to the lack of follow-up data. Some of the initial clinical data were not available because of the referrals from different hospitals for the radioiodine treatment. Hence, the correlations with other conventional imaging techniques were not applicable.

Conclusion

^{18}F-FDG PET/CT may be useful in detecting recurrence for differentiated thyroid cancer patients. Tg levels and the initial stage of the disease are significantly correlated with FDG positivity. It may also provide information about the de-differentiation process which supports the treatment plan.

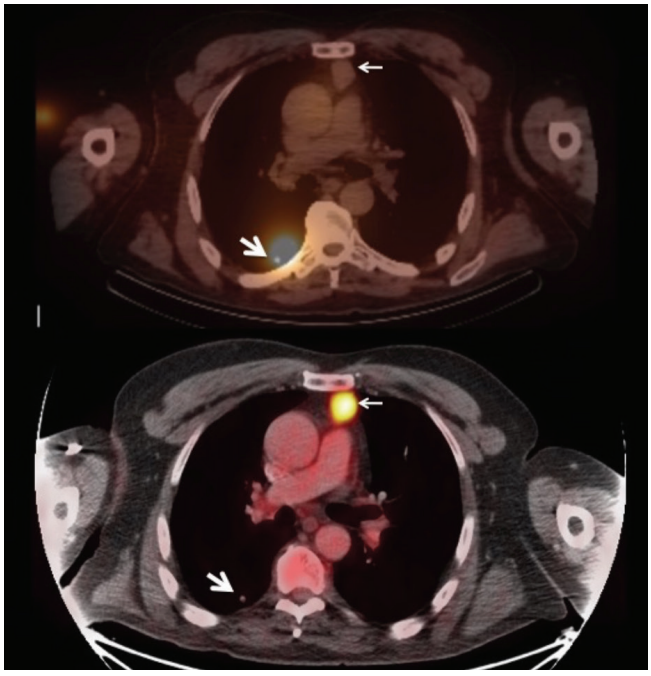

Figure 3. A 64-year-old woman with mixed type of differentiated thyroid cancer (classic and follicular type) had increased Tg levels (167 ng/mL) after radioiodine treatment. The upper row demonstrates SPECT/CT image of positive I-131 for metastatic lung lesion in the posterior part of the upper right lobe, whereas no uptake in the lymph node of the anterior mediastinum. The lower row shows intense ^{18}F-FDG uptake in the same mediastinal lymph node in PET/CT images, later histopathologically proven as metastases

Tg: Thyroglobulin, SPECT: Single photon emission computed tomography, CT: Computed tomography, I-131: Iodine-131, PET: Positron emission tomography, ^{18}F-FDG: ^{18}Fluoride-fluorodeoxyglucose

Ethics

Ethics Committee Approval: University of Health Sciences Turkey, Şişli Hamidiye Etfal Training and Research Hospital Clinical Research Ethics Committee approved (number: 3112, date: 02.02.2021).

Informed Consent: All the patients signed informed consent forms.

Peer-review: Externally and internally peer-reviewed.

Financial Disclosure: The author declared that this study has received no financial support.

References

1. Siegel RL, Miller KD, Jemal A. Cancer statistics, 2019. CA Cancer J Clin 2019;69:7-34.
2. Sherman SI. Thyroid carcinoma. Lancet 2003;361:501-511.
3. American Thyroid Association (ATA) Guidelines Taskforce on Thyroid Nodules and Differentiated Thyroid Cancer, Cooper DS, Doherty GM, Haugen BR, Kloos RT, Lee SL, Mandel SJ, Mazzaferri EL, McIver B, Pacini F, Schlumberger M, Sherman SI, Steward DL, Tuttle RM. Revised American Thyroid Association management guidelines for patients with thyroid nodules and differentiated thyroid cancer. Thyroid 2009;19:1167-1214.
4. Mazzaferri EL, Jhiang SM. Long-term impact of initial surgical and medical therapy on papillary and follicular thyroid cancer. Am J Med 1994;97:418-428.
5. Wang W, Macapinlac H, Larson SM, Yeh SD, Akhurst T, Finn RD, Rosai J, Robbins RJ. [18F]-2-fluoro-2-deoxy-D-glucose positron emission tomography localizes residual thyroid cancer in patients with negative diagnostic (131)I whole body scans and elevated serum thyroglobulin levels. J Clin Endocrinol Metab 1999;84:2291-2302.
6. Larg MI, Barbus E, Gabora K, Pestean C, Cheptea M, Piciu D. 18F-FDG PET/CT in Differentiated Thyroid Carcinoma. Acta Endocrinol (Buchar) 2019;15:203-208.
7. Haugen BR, Alexander EK, Bible KC, Doherty GM, Mandel SJ, Nikiforov YE, Pacini F, Randolph GW, Sawka AM, Schlumberger M, Schuff KG, Sherman SI, Sosa JA, Steward DL, Tuttle RM, Wartofsky L. 2015 American Thyroid Association Management Guidelines for Adult Patients with Thyroid Nodules and Differentiated Thyroid Cancer: The American Thyroid Association Guidelines Task Force on Thyroid Nodules and Differentiated Thyroid Cancer. Thyroid 2016;26:1-133.
8. Gild ML, Topliss DJ, Learoyd D, Parnis F, Tie J, Hughes B, Walsh JP, McLeod DSA, Clifton-Bligh RJ, Robinson BG. Clinical guidance for radioiodine refractory differentiated thyroid cancer. Clin Endocrinol (Oxf) 2018;88:529-537.
9. Cooray SD, Topliss DJ. The management of metastatic radioiodine-refractory differentiated thyroid cancer requires an integrated approach including both directed and systemic therapies. Endocrinol Diabetes Metab Case Rep 2017;2017:16-0089.
10. Feine U, Lietzenmayer R, Hanke JP, Wöhrle H, Müller-Schauenburg W. 18FDG-Ganzkörper-PET bei differenzierten Schilddrüsenkarzinomen. Flipflop im Speichermuster von 18FDG und 131J [18FDG whole-body PET in differentiated thyroid carcinoma. Flipflop in uptake patterns of 18FDG and 131I]. Nuklearmedizin 1995;34:127-134.
11. Jung JH, Kim CY, Son SH, Kim DH, Jeong SY, Lee SW, Lee J, Ahn BC. Preoperative Prediction of Cervical Lymph Node Metastasis Using Primary Tumor SUVmax on 18F-FDG PET/CT in Patients with Papillary Thyroid Carcinoma. PLoS One 2015;10:e0144152.
12. Chong A, Ha JM, Han YH, Kong E, Choi Y, Hong KH, Park JH, Kim SH, Park JM. Preoperative Lymph Node Staging by FDG PET/CT With Contrast Enhancement for Thyroid Cancer: A Multicenter Study and Comparison With Neck CT. Clin Exp Otorhinolaryngol 2017;10:121-128.
13. Tuttle M, Morris LF, Haugen B, Shah J, Sosa JA, Rohren E, Subramaniam RM, Hunt JL, Perrier ND. Thyroid-differentiated and anaplastic carcinoma. AJCC Cancer Staging Manual. 8th edition. New York (NY, USA): Springer International Publishing; 2017.
14. Bertagna F, Bosio G, Biasiotto G, Rodella C, Puta E, Gabanelli S, Lucchini S, Merli G, Savelli G, Giubbini R, Rosenbaum J, Alavi A. F-18 FDG-PET/CT evaluation of patients with differentiated thyroid cancer with negative I-131 total body scan and high thyroglobulin level. Clin Nucl Med 2009;34:756-761.
15. Schlüter B, Bohuslavizki KH, Beyer W, Plotkin M, Buchert R, Clausen M. Impact of FDG PET on patients with differentiated thyroid cancer who present with elevated thyroglobulin and negative 131I scan. J Nucl Med 2001;42:71-76.
16. Shammas A, Degirmenci B, Mountz JM, McCook BM, Branstetter B, Bencherif B, Joyce JM, Carty SE, Kuffner HA, Avril N. 18F-FDG PET/CT in patients with suspected recurrent or metastatic well-differentiated thyroid cancer. J Nucl Med 2007;48:221-226.
17. Gim H, Lee DK, Park HS, Jeong YJ. Diagnostic Value of SUV in 18F-FDG PET/CT for Papillary Thyroid Cancer. Int J Thyroidol 2020;13:37-42.
18. Grabellus F, Nagarajah J, Bockisch A, Schmid KW, Sheu SY. Glucose transporter 1 expression, tumor proliferation, and iodine/glucose

uptake in thyroid cancer with emphasis on poorly differentiated thyroid carcinoma. Clin Nucl Med 2012;37:121-127.

19. Robbins RJ, Wan Q, Grewal RK, Reibke R, Gonen M, Strauss HW, Tuttle RM, Drucker W, Larson SM. Real-time prognosis for metastatic thyroid carcinoma based on 2-[18F]fluoro-2-deoxy-D-glucose-positron emission tomography scanning. J Clin Endocrinol Metab 2006;91:498-505.
20. Ha LN, Iravani A, Nhung NT, Hanh NTM, Hutomo F, Son MH. Relationship between clinicopathologic factors and FDG avidity in radioiodine-negative recurrent or metastatic differentiated thyroid carcinoma. Cancer Imaging 2021;21:8.
21. Kang JH, Jung DW, Pak KJ, Kim IJ, Kim HJ, Cho JK, Shin SC, Wang SG, Lee BJ. Prognostic implication of fluorine-18 fluorodeoxyglucose positron emission tomography/computed tomography in patients with recurrent papillary thyroid cancer. Head Neck 2018;40:94-102.
22. Cho SG, Kwon SY, Kim J, Cho DH, Na MH, Kang SR, Yoo SW, Song HC. Risk factors of malignant fluorodeoxyglucose-avid lymph node on preablation positron emission tomography in patients with papillary thyroid cancer undergoing radioiodine ablation therapy. Medicine (Baltimore) 2019;98:e14858.
23. Piccardo A, Foppiani L, Morbelli S, Bianchi P, Barbera F, Biscaldi E, Altrinetti V, Villavecchia G, Cabria M. Could [18]F-fluorodeoxyglucose PET/CT change the therapeutic management of stage IV thyroid cancer with positive (131)I whole body scan? Q J Nucl Med Mol Imaging 2011;55:57-65.

Original Article
Mol Imaging Radionucl Ther 2021;30:144-149 DOI:10.4274/mirt.galenos.2021.59254

Is SUV Corrected for Lean Body Mass Superior to SUV of Body Weight in ^{68}Ga-PSMA PET/CT?

^{68}Ga PSMA PET/BT'de Yağsız Vücut Kütlesine Göre Düzeltilmiş SUV Vücut Ağırlığına Göre Hesaplanan SUV'den Daha mı Üstün?

Ayşegül Aksu[1], Gamze Çapa Kaya[2]

[1]*University of Health Sciences Turkey, Başakşehir Çam and Sakura City Hospital, Clinic of of Nuclear Medicine, İstanbul, Turkey*
[2]*Dokuz Eylül University Faculty of Medicine, Department of Nuclear Medicine, İzmir, Turkey*

Abstract

Objectives: This study aimed to investigate the relationship between the standard uptake value (SUV) of body weight and SUV corrected for lean body mass (SUL) parameters obtained from the prostate gland in gallium-68 (^{68}Ga)-prostate-specific membrane antigen (PSMA) positron emission tomography-computed tomography (PET/CT) with Gleason grade (GG) groups, D'Amico risk groups, and presence of metastases.

Methods: Patients with prostate adenocarcinoma who underwent ^{68}Ga-PSMA PET/CT for staging at our center between February 2017 and October 2018 were evaluated retrospectively. Maximum SUV (SUV_{max}), SUV_{peak}, SUL_{max}, SUL_{peak}, SUV_{mean}, and SUL_{mean} values of the prostate tumor were obtained. The difference in these values between GG groups (≥3, <3) and D'Amico risk (low-moderate/high) groups was evaluated with the Mann-Whitney U test. The area under the curve values of SUV and SUL parameters were compared. In addition, SUV_{mean} and SUL_{mean} values were obtained from the right liver lobe, and their correlation with body weight was evaluated.

Results: A total of 79 patients were included in the study. Significant differences were found in the prostate SUV_{max}, SUL_{max}, SUV_{peak}, SUL_{peak}, SUV_{mean}, and SUL_{mean} values between the GG (≥3 and <3) groups and between D'Amico risk (low-moderate and high) groups. However, no significant difference was found in the discriminative power of any SUV or SUL parameter when compared with each other. A significant difference in any SUV and SUL parameters was found in patients with and without metastasis. Neither liver SUV_{mean} value nor SUL_{mean} value correlated with the body weight.

Conclusion: The superiority of SUL values obtained from ^{68}Ga-PSMA PET to SUV was not determined in our study. SUV parameters can also be used for quantitative analysis in ^{68}Ga-PSMA PET.

Keywords: SUV, SUL, lean body mass, prostate specific membrane antigen

Öz

Amaç: Amacımız, galyum-68 (^{68}Ga)-prostat spesifik membran antijeni (PSMA) pozitron emisyon tomografisi-bilgisayarlı tomografide (PET/BT) prostat bezinden elde edilen standart uptake değeri (SUV) ve yağsız vücut kütlesine göre düzeltilmiş SUV (SUL) parametrelerinin Gleason grade (GG) grupları, D'Amico risk grupları, metastaz varlığı değerlendirmedeki ilişkilerinin araştırılmasıdır.

Yöntem: Merkezimizde Şubat 2017-Ekim 2018 tarihleri arasında prostat adenokarsinomu tanısı ile evreleme amaçlı ^{68}Ga-PSMA PET/BT görüntülemesi yapılan hastalar retrospektif olarak değerlendirildi. Prostat bezinde görülen tümörden SUV_{maks}, SUV_{peak}, SUL_{maks}, SUL_{peak}, SUV_{mean} ve SUL_{mean} değerleri elde edildi. GG grupları (≥3, <3), D'Amico risk grupları (düşük-orta/yüksek) arasında bu değerler arasındaki fark Mann-Whitney

Address for Correspondence: Ayşegül Aksu MD, University of Health Sciences Turkey, Başakşehir Çam and Sakura City Hospital, Clinic of of Nuclear Medicine, İstanbul, Turkey
Phone: +90 507 962 35 75 **E-mail:** aaysegulgedikli@gmail.com ORCID ID: orcid.org/0000-0002-6239-0660
Received: 15.02.2021 **Accepted:** 02.05.2021

U testi ile değerlendirildi. SUV ve SUL parametrelerinin eğri altındaki alan değerleri karşılaştırıldı. Ayrıca karaciğer sağ lobundan SUV_{mean} ve SUL_{mean} değerleri alınarak vücut ağırlığı ile korelasyonları değerlendirildi.

Bulgular: GG grupları (≥3 ve <3) arasında ve D'Amico risk grupları (düşük-orta ve yüksek) arasında prostat SUV_{maks}, SUL_{maks}, SUV_{peak}, SUL_{peak}, SUV_{mean} ve SUL_{mean} değerlerinde istatistiksel olarak anlamlı farklılıklar izlendi. Bununla birlikte, herhangi bir SUV veya SUL parametresinin bu grupları ayırt etme gücünde diğerine kıyasla önemli bir fark elde edilemedi. Metastaz olan ve olmayan hasta gruplarında hiçbir SUV ve SUL parametresinde istatistiksel olarak anlamlı bir fark saptanamadı. Ne karaciğer SUV_{mean} değeri ne de SUL_{mean} değeri vücut ağırlığı ile ilişkili değildi.

Sonuç: ^{68}Ga-PSMA PET'den elde edilen SUL değerlerinin SUV'ye üstünlüğü çalışmamızda belirlenememiştir. ^{68}Ga-PSMA PET'de SUV parametrelerinin kantitatif analiz için de kullanılabileceği düşünülmektedir.

Anahtar kelimeler: SUV, SUL, yağsız vücut kütlesi, prostat spesifik membran antijeni

Introduction

Positron emission tomography/computed tomography (PET/CT) is becoming a standard component of the diagnosis and staging in the field of oncology. Especially, ^{18}flourine-fluorodeoxyglucose (^{18}F-FDG) PET/CT is used to quantify radiopharmaceutical uptake and quantitatively determine treatment response in the evaluation of the metabolic response in various tumors (1,2,3). PET images are analyzed in clinical practice either qualitatively using visual comparison of metabolism in lesions with normal tissue or semi-quantitatively using standard uptake values (SUV). SUV is obtained as the tissue concentration (MBq/mL) divided by the injected activity (MBq/g) per body weight (BW). Factors affecting SUV have been discussed in many studies (4,5,6). Since fat contributes to BW but accumulates very little ^{18}F-FDG in a starvation state, SUV is relatively increased in patients who are obese than in thinner ones. A study found that lean body mass (LBM) SUV (SUL) correction is a more suitable quantitative method than BW or body surface area for patients who are obese (7).

Prostate-specific membrane antigen (PSMA) is a highly expressed human transmembrane protein that is low or moderate in normal or hyperplastic prostate tissues and high in primary adenocarcinomas and distinguishes malignant lesions from benign lesions with high accuracy and positively correlates with the degree of expression, tumor aggression, metastatic disease, and recurrence (8,9,10,11). In the literature, studies have shown that the SUV values obtained from a prostate tumor are higher as the Gleason score (GS) and prostate-specific antigen (PSA) value increase. Gafita et al. (12) investigated whether SUL is a more appropriate quantitative method than SUV, which is normalized by BW in gallium-68 (^{68}Ga)-PSMA 11 PET/CT. They found that correction with lean BW disrupts positive correlations between absolute SUV and BW and that SUL may be preferred over SUV for quantitative analysis in ^{68}Ga-PSMA 11 PET (12).

This study aimed to investigate the relationship between the SUV and SUL parameters obtained from the prostate tumor according to Gleason grade (GG) groups, D'Amico risk groups, and presence of metastasis in ^{68}Ga-PSMA PET/CT and to determine whether SUL is superior to SUV.

Materials and Methods

Patients

Patients with prostate adenocarcinoma who underwent ^{68}Ga-PSMA PET/CT for staging at our center between February 2017 and October 2018 were evaluated retrospectively. GG groups of patients were obtained from prostatectomy material in patients undergoing prostatectomy and fine-needle biopsy results in other patients. D'Amico criteria was considered for risk stratification [low risk group (PSA <10 ng/mL and GS <7 and T1-T2a), intermediate-risk group (PSA 10-20 ng/mL or GS 7 or T2b-T2c), and high-risk group (PSA >20 ng/mL or GS 8-10 or T3-T4)] (13). Patients were divided into two groups according to their GG (≥3 vs <3).

PET Image Analysis

Patients signed the informed consent form, and radiation safety and imaging protocol were described. An average of 3.2 millicurie (mCi) ^{68}Ga-PSMA Imaging and Therapy was injected intravenously. Low-dose CT was used for attenuation correction an hour after injection. PET images were obtained for 1.5 min in each bed position in the supine position from the vertex to the toe tip in Philips Gemini TF PET/CT (Eindhoven, Netherlands). Row action maximum likelihood algorithm was used for reconstruction.

Patients who had PSMA expression on ^{68}Ga-PSMA PET/CT images, which could be differentiated from background activity and thought to be related to prostate adenocarcinoma metastasis (PSMA-RADs 4 and 5) were considered to have metastatic disease (14).

Weights and heights of the patients were measured before imaging. LBM was calculated with the formula developed by Janmahasatian (15,16).

$LBM = (9.27\times10^3\times BW)/(6.68\times10^3+216\times BMI)$

In the prostate gland, a region of interest was drawn on the area where PSMA expression was observed above background activity. Maximum SUV (SUV_{max}), SUV_{mean}, and SUV_{peak} values were obtained from this area. SUL_{max}, SUL_{mean}, and SUL_{peak} values were calculated from SUV_{max}, SUV_{mean}, and SUV_{peak} values using the LBM value obtained from the Janmahasatian formula.

SUL = SUV × LBM/BW

In addition, a 3-cm volume of interest (VOI) was drawn to the right liver lobe to determine liver background activity. Liver SUV_{mean} and liver SUL_{mean} values were obtained from this VOI (17).

Statistical Analysis

The free version of the Statistical Package for the Social Sciences v. 26.0 was used for statistical analysis. The correlations among liver SUV_{mean}, liver SUL_{mean}, and BW were evaluated by Spearman correlation analysis. A $p<0.05$ value was considered significant.

The difference in SUV_{max}, SUL_{max}, SUV_{mean}, SUL_{mean}, SUV_{peak}, and SUL_{peak} values from the prostate tumor between low-moderate and high-risk groups was analyzed with the Mann-Whitney U test. In addition, the difference in the SUV and SUL values between GG groups, between PSA groups (≥10 and <10 ng/mL), and between D'Amico risk groups (low-moderate and high) was evaluated with the Mann-Whitney U test.

The potential of SUV and SUL parameters in distinguishing GG groups and risk groups was evaluated by the receiver operating characteristics analysis. The area under the curve (AUC) values were compared, and significant difference between them was evaluated.

Ethics Approval

Dokuz Eylül University Ethics Committee approval was obtained (decision no: 2020/18-37, date: 10.08.2020). All procedures performed in studies involving human participants were in accordance with the ethical standards of the institutional research committee and with the 1964 Helsinki declaration and its later amendments or comparable ethical standards. All patients gave their informed consent before their inclusion in the study.

Results

The study included 79 patients with a mean age of 65±7 (range, 44-78) years and mean BW of 81.5±14.5 (range, 53-125) kg. The median PSA value was 16 (range, 0.02-527.00) ng/mL. A total of 13 patients had a history of radical prostatectomy.

In this study, 7 (9%) patients had GG 1, 21 (27%) had GG 2, 12 (15%) had GG 3, 15 (19%) had GG 4, and 24 (30%) had GG 5. In ^{68}Ga-PSMA PET/CT, 41 (52%) patients did not have metastasis, while 38 patients had PSMA expression suggesting metastasis. Moreover, 33 (41.8%) patients had lymph node metastasis. Five of these patients had PSMA expression in cervical/mediastinal lymph nodes, 16 in abdominal lymph nodes, and 33 in pelvic lymph nodes. In addition, 19 (24.1%) patients had PSMA expression suggesting bone metastasis, whereas 2 (2.5%) patients had PSMA expression suggesting pulmonary metastasis. In the study group, no patient had liver metastasis. According to the D'Amico risk groups, two patients had low risk, 18 (22.8%) patients had moderate risk, and 59 (74.7%) patients had high-risk.

The mean ± standard deviation and median (range) values from the prostate tumor were calculated as follows: SUV_{max}, 11.5±9.3 and 8.0 (3.0-49.8); SUL_{max} value, 8.4±6.1 and 6.1 (2.2-34.4); SUV_{peak} value, 8.6±7.2 and 5.8 (2.4-37.6); SUL_{peak} value, 6.3±4.5 and 4.5 (1.7-25.9); SUV_{mean} value, 5.0±2.6 and 4.2 (1.9-13.8); and SUL_{mean} value, 3.7±3.3 and 3.2 (1.3-9.4).

A significant difference was found in the prostate SUV_{max}, SUL_{max}, SUV_{peak}, SUL_{peak}, SUV_{mean}, and SUL_{mean} values between patients with GG ≥3 and <3 (Table 1). However, when comparing AUC values of SUV and SUL parameters in distinguishing GG groups, no SUV/SUL parameters were superior to the other (Table 2).

No significant difference was observed in any SUV and SUL parameters between patients with GS 3+4 and 4+3.

Prostate SUV_{max}, SUL_{max}, SUV_{peak}, SUL_{peak}, SUV_{mean}, and SUL_{mean} values were significantly higher in the high-risk group than in the other D'Amico risk groups (Table 1). However, no SUV/SUL parameter was superior to others in distinguishing risk groups (Table 2).

While all SUV and SUL parameters were higher in patients with a PSA value ≥10 ng/mL than in those with <10 ng/mL (Table 1), no significant difference was found in the discrimination power of any SUV and SUL parameters (Table 2).

No significant difference was found in any SUV and SUL parameters in patient groups with and without metastasis.

The mean liver SUV_{mean} value was calculated as 4.0±1.1 (1.8-7.6), and the liver SUL_{mean} value was 3.0±1.4 (1.4-5.5). The liver SUV_{mean} and SUL_{mean} values did not correlate with BW ($p=0.387$ and 0.132, respectively).

Discussion

In this study, a significant correlation was found with the BW of neither SUV_{mean} nor SUL_{mean} obtained from the liver. Gafita et al. (12) reported that SUL can be preferred over SUV in ^{68}Ga-PSMA 11 PET/CT. In this study, while the liver SUV_{mean} value showed a significant correlation with BW, no significant correlation was found in the SUL_{mean} value. Despite the few studies on this subject, similar to our study, Li et al. (2) evaluated the ^{18}F-DCFPyL uptake but could not detect a significant correlation between liver SUV_{mean} and SUL_{mean} values and BW; as a result, they suggested using the SUV.

Several studies have also shown that PSMA SUV data are successful in differentiating GG groups and risk groups (18,19,20,21). Likewise, we were able to obtain significant differences in SUV parameters between these groups. However, our study is the first to evaluate the relationship between the success of SUL and SUV parameters obtained from ^{68}Ga-PSMA PET in differentiating GG groups and risk groups. In our study, SUL parameters obtained from ^{68}Ga-PSMA PET were not superior to SUV parameters in distinguishing GG groups and in distinguishing risk groups. Moreover, the studies that quantified uptake with body-weight-corrected SUV and LBM-corrected SUV have shown that the repeatability coefficient of SUL_{max} and SUV_{max} within the same patient in a test-retest setting is comparable (22,23,24). These results show that SUL and SUV parameters are not superior to each other in ^{68}Ga-PSMA PET in clinical practice.

Prostate SUV and SUL parameters were significantly higher in patients with GG ≥3 than in GG ≤2, and this is similar to the findings in the literature. Onal et al. (25) reported that SUV_{max} values obtained from primary tumors in 191 patients were significantly higher in patients with GS >7.

Table 1. Evaluation of SUV and SUL parameters in Gleason grade, D'Amico risk, and PSA groups

		GG		D'Amico risk groups		PSA	
		GG <3	**GG ≥3**	**Low-moderate**	**High**	**<10 ng/mL**	**≥10 ng/mL**
SUV_{max}	Mean ± standard	7.6±4.5	13.7±10.5	6.6±3.9	13.2±10.0	8.1±5.6	13.8±10.5
	Median (range)	5.4 (3.1-17.5)	10.5 (3.0-49.8)	5.2 (3.0-15.4)	10.2 (3.4-49.8)	3.6 (3.0-26.7)	11.0 (3.5-49.8)
	p value	0.003		0.001		0.001	
	AUC (95% CI)	0.706 (0.588-0.823)		0.755 (0.637-0.872)		0.705 (0.587-0.823)	
SUL_{max}	Mean ± standard	5.6±3.4	9.9±7.4	4.9±2.9	9.6±7.3	5.9±4.1	10±7.4
	Median (range)	4.0 (2.4-12.7)	7.5 (2.2-34.4)	3.8 (2.2-11.1)	7.3 (2.4-34.4)	4.4 (2.2-19.9)	8.4 (2.5-34.4)
	p value	0.002		0.001		0.001	
	AUC (95% CI)	0.709 (0.592-0.826)		0.760 (0.644-0.875)		0.707 (0.589-0.825)	
SUV_{mean}	Mean ± standard	3.8±1.6	5.6±2.9	3.4±1.1	5.5±2.8	3.8±1.6	5.7±2.9
	Median (range)	3.2 (2.1-7.6)	4.9 (1.9-13.8)	3.2 (1.9-5.5)	4.9 (2.1-13.8)	3.3 (2.0-8.0)	4.9 (1.9-13.8)
	p value	0.002		0.001		0.001	
	AUC (95% CI)	0.707 (0.591-0.823)		0.750 (0.636-0.863)		0.703 (0.588-0.819)	
SUL_{mean}	Mean ± standard	2.8±1.2	4.1±2.0	2.5±0.9	4.1±3.5	2.8±2.4	4.2±3.7
	Median (range)	2.4 (1.3-5.8)	3.5 (1.4-9.4)	2.4 (1.9-4.4)	3.5 (1.3-9.4)	2.4 (1.5-6.0)	3.0 (1.3-9.4)
	p value	0.002		0.001		0.001	
	AUC (95% CI)	0.714 (0.597-0.830)		0.756 (0.643-0.870)		0.703 (0.587-0.819)	
SUV_{peak}	Mean ± standard	5.6±3.5	10.2±8.1	3.5±2.8	9.9±7.7	5.9±4.2	10.3±8.2
	Median (range)	3.9 (2.5-13.3)	7.7 (2.4-37.6)	3.5 (2.4-11.3)	7.7 (2.6-37.6)	4.3 (2.5-19.0)	8.2 (2.4-37.6)
	p value	0.003		<0.001		0.001	
	AUC (95% CI)	0.701 (0.582-0.820)		0.767 (0.649-0.884)		0.706 (0.588-0.824)	
SUL_{peak}	Mean ± standard	4.1±2.6	7.4±5.5	3.5±2.2	7.2±5.5	4.4±3.0	7.5±5.8
	Median (range)	2.8 (1.9-2.5)	5.5 (1.7-25.9)	2.7 (1.7-9.0)	5.5 (1.9-25.9)	3.1 (1.8-14.2)	6.0 (1.7-25.9)
	p value	0.003		<0.001		0.001	
	AUC (95% CI)	0.705 (0.586-0.825)		0.769 (0.651-0.887)		0.700 (0.582-0.819)	

SUV: Standard uptake value, SUL: Lean body mass SUV, PSA: Prostate-specific antigen, GG: Gleason grade, AUC: Area under the curve, CI: Confidence interval, max: Maximum

Table 2. P values obtained in the comparison of the AUC of SUV and SUL parameters

	GG (≥3 and <3)	D'Amico risk groups (low-moderate and high)	PSA (≥10 and <10 ng/mL)
SUV_{max}-SUL_{max}	0.732	0.668	0.838
SUV_{max}-SUV_{peak}	0.721	0.324	0.935
SUV_{max}-SUL_{peak}	0.983	0.420	0.744
SUV_{max}-SUV_{mean}	0.945	0.808	0.933
SUV_{max}-SUL_{mean}	0.750	0.953	0.943
SUL_{max}-SUV_{peak}	0.578	0.666	0.945
SUL_{max}-SUL_{peak}	0.761	0.560	0.595
SUL_{max}-SUV_{mean}	0.916	0.617	0.850
SUL_{max}-SUL_{mean}	0.830	0.883	0.848
SUV_{peak}-SUL_{peak}	0.664	0.829	0.484
SUV_{peak}-SUV_{mean}	0.746	0.383	0.891
SUV_{peak}-SUL_{mean}	0.574	0.696	0.905
SUL_{peak}-SUV_{mean}	0.924	0.333	0.869
SUL_{peak}-SUL_{mean}	0.660	0.573	0.868
SUV_{mean}-SUL_{mean}	0.577	0.654	1.000

SUV: Standard uptake value, SUL: Lean body mass SUV, PSA: Prostate-specific antigen, GG: Gleason grade, AUC: Area under the curve, max: Maximum

In their study, Uprimny et al. (18) did not find a significant difference in SUV_{max} values between GG 2 and 3 tumors. Similarly, Ergül et al. (19) did not found a significant difference in SUV_{max} values between grade 2 and 3 tumors. In addition, in our study, neither SUV_{max} values nor other SUV and SUL values were detected differently in tumors with GG 2 and 3.

In a previous study, Ergül et al. (19) analyzed 78 patients and found a significant difference in SUV_{max} values of prostate tumors with and without metastasis. However, Liu et al. (20) did not observe a significant difference in SUV_{max} in patients with and without metastasis. In the present study, similar to the study of Liu et al. (20), no significant difference was found in any SUV and SUL parameters between these groups.

Study Limitations

First, the retrospective design limits the generalizability of the results. Second, histopathological correlation is not technically and ethically possible from all foci considered metastasis. Finally, prostatectomy could not be applied to all patients, and the GS of some patients could only be obtained from the biopsy sample.

Conclusion

In this study, the superiority of SUL values obtained from ^{68}Ga-PSMA PET to SUV was not determined. We think that both SUV and SUL parameters can be used for quantitative analysis in ^{68}Ga-PSMA PET.

Ethics

Ethics Committee Approval: Dokuz Eylül University Ethics Committee approval was obtained (decision no: 2020/18-37, date: 10.08.2020).

Informed Consent: Retrospective cross sectional study.

Peer-review: Externally peer-reviewed.

Authorship Contributions

Surgical and Medical Practices: A.A., Concept: A.A., G.Ç.K., Design: A.A., G.Ç.K., Data Collection or Processing: A.A., Analysis or Interpretation: A.A., Literature Search: A.A., G.Ç.K., Writing: A.A., G.Ç.K.

Conflict of Interest: No conflict of interest was declared by the authors.

Financial Disclosure: The authors declared that this study has received no financial support.

References

1. O JH, Lodge MA, Wahl RL. Practical PERCIST: A Simplified Guide to PET Response Criteria in Solid Tumors 1.0. Radiology 2016;280:576-584.
2. Li X, Rowe SP, Leal JP, Gorin MA, Allaf ME, Ross AE, Pienta KJ, Lodge MA, Pomper MG. Semiquantitative Parameters in PSMA-Targeted PET Imaging with 18F-DCFPyL: Variability in Normal-Organ Uptake. J Nucl Med 2017;58:942-946.
3. Sheikhbahaei S, Wray R, Young B, Mena E, Taghipour M, Rahmim A, Subramaniam RM. 18F-FDG-PET/CT therapy assessment of locally advanced pancreatic adenocarcinoma: impact on management and utilization of quantitative parameters for patient survival prediction. Nucl Med Commun 2016;37:231-238.
4. Keyes JW Jr. SUV: standard uptake or silly useless value? J Nucl Med 1995;36:1836-1839.
5. Lee JR, Madsen MT, Bushnel D, Menda Y. A threshold method to improve standardized uptake value reproducibility. Nucl Med Commun 2000;21:685-690.
6. Ramos CD, Erdi YE, Gonen M, Riedel E, Yeung HW, Macapinlac HA, Chisin R, Larson SM. FDG-PET standardized uptake values in normal anatomical structures using iterative reconstruction segmented attenuation correction and filtered back-projection. Eur J Nucl Med 2001;28:155-164.
7. Sugawara Y, Zasadny KR, Neuhoff AW, Wahl RL. Reevaluation of the standardized uptake value for FDG: variations with body weight and methods for correction. Radiology 1999;213:521-525.
8. Perner S, Hofer MD, Kim R, Shah RB, Li H, Möller P, Hautmann RE, Gschwend JE, Kuefer R, Rubin MA. Prostate-specific membrane antigen expression as a predictor of prostate cancer progression. Hum Pathol 2007;38:696-701.
9. Afshar-Oromieh A, Malcher A, Eder M, Eisenhut M, Linhart HG, Hadaschik BA, Holland-Letz T, Giesel FL, Kratochwil C, Haufe S, Haberkorn U, Zechmann CM. PET imaging with a [68Ga]gallium-labelled PSMA ligand for the diagnosis of prostate cancer: biodistribution in humans and first

evaluation of tumour lesions. Eur J Nucl Med Mol Imaging 2013;40:486-495.

10. Eiber M, Maurer T, Souvatzoglou M, Beer AJ, Ruffani A, Haller B, Graner FP, Kübler H, Haberkorn U, Eisenhut M, Wester HJ, Gschwend JE, Schwaiger M. Evaluation of Hybrid ^{68}Ga-PSMA Ligand PET/CT in 248 Patients with Biochemical Recurrence After Radical Prostatectomy. J Nucl Med 2015;56:668-674.
11. Rahbar K, Weckesser M, Huss S, Semjonow A, Breyholz HJ, Schrader AJ, Schäfers M, Bögemann M. Correlation of Intraprostatic Tumor Extent with ^{68}Ga-PSMA Distribution in Patients with Prostate Cancer. J Nucl Med 2016;57:563-567.
12. Gafita A, Calais J, Franz C, Rauscher I, Wang H, Roberstson A, Czernin J, Weber WA, Eiber M. Evaluation of SUV normalized by lean body mass (SUL) in ^{68}Ga-PSMA11 PET/CT: a bi-centric analysis. EJNMMI Res 2019;9:103.
13. D'Amico AV, Whittington R, Malkowicz SB, Schultz D, Blank K, Broderick GA, Tomaszewski JE, Renshaw AA, Kaplan I, Beard CJ, Wein A. Biochemical outcome after radical prostatectomy, external beam radiation therapy, or interstitial radiation therapy for clinically localized prostate cancer. JAMA 1998;280:969-974.
14. Rowe SP, Pienta KJ, Pomper MG, Gorin MA. PSMA-RADS Version 1.0: A Step Towards Standardizing the Interpretation and Reporting of PSMA-targeted PET Imaging Studies. Eur Urol 2018;73:485-487.
15. Janmahasatian S, Duffull SB, Ash S, Ward LC, Byrne NM, Green B. Quantification of lean bodyweight. Clin Pharmacokinet 2005;44:1051-1065.
16. Tahari AK, Chien D, Azadi JR, Wahl RL. Optimum lean body formulation for correction of standardized uptake value in PET imaging. J Nucl Med 2014;55:1481-1484.
17. Wahl RL, Jacene H, Kasamon Y, Lodge MA. From RECIST to PERCIST: Evolving Considerations for PET response criteria in solid tumors. J Nucl Med 2009;50 Suppl 1:122S-150S.
18. Uprimny C, Kroiss AS, Decristoforo C, Fritz J, von Guggenberg E, Kendler D, Scarpa L, di Santo G, Roig LG, Maffey-Steffan J, Horninger W, Virgolini IJ. ^{68}Ga-PSMA-11 PET/CT in primary staging of prostate cancer: PSA and Gleason score predict the intensity of tracer accumulation in the primary tumour. Eur J Nucl Med Mol Imaging 2017;44:941-949.
19. Ergül N, Yilmaz Güneş B, Yücetaş U, Toktaş MG, Çermik TF. 68Ga-PSMA-11 PET/CT in Newly Diagnosed Prostate Adenocarcinoma. Clin Nucl Med 2018;43:e422-e427.
20. Liu C, Liu T, Zhang N, Liu Y, Li N, Du P, Yang Y, Liu M, Gong K, Yang X, Zhu H, Yan K, Yang Z. ^{68}Ga-PSMA-617 PET/CT: a promising new technique for predicting risk stratification and metastatic risk of prostate cancer patients. Eur J Nucl Med Mol Imaging 2018;45:1852-1861.
21. Demirci E, Kabasakal L, Şahin OE, Akgün E, Gültekin MH, Doğanca T, Tuna MB, Öbek C, Kiliç M, Esen T, Kural AR. Can SUVmax values of Ga-68-PSMA PET/CT scan predict the clinically significant prostate cancer? Nucl Med Commun 2019;40:86-91.
22. Pollard JH, Raman C, Zakharia Y, Tracy CR, Nepple KG, Ginader T, Breheny P, Sunderland JJ. Quantitative Test-Retest Measurement of ^{68}Ga-PSMA-HBED-CC in Tumor and Normal Tissue. J Nucl Med 2020;61:1145-1152.
23. Jansen BHE, Cysouw MCF, Vis AN, van Moorselaar RJA, Voortman J, Bodar YJL, Schober PR, Hendrikse NH, Hoekstra OS, Boellaard R, Oprea-Lager DE. Repeatability of Quantitative ^{18}F-DCFPyL PET/CT Measurements in Metastatic Prostate Cancer. J Nucl Med 2020;61:1320-1325.
24. Olde Heuvel J, de Wit-van der Veen BJ, Donswijk ML, Slump CH, Stokkel MPM. Day-to-day variability of [68Ga]Ga-PSMA-11 accumulation in primary prostate cancer: effects on tracer uptake and visual interpretation. EJNMMI Res 2020;10:132.
25. Onal C, Torun N, Akyol F, Guler OC, Hurmuz P, Yildirim BA, Cağlar M, Reyhan M, Ozyigit G. Integration of 68Ga-PSMA-PET/CT in Radiotherapy Planning for Prostate Cancer Patients. Clin Nucl Med 2019;44:e510-e516.

Original Article
Mol Imaging Radionucl Ther 2021;30:150-157 DOI:10.4274/mirt.galenos.2021.78055

The Relationship Between HER-2 Expression Levels and ^{18}F-FDG PET/CT Parameters in Gastric Cancer

Mide Kanseri Hastalarında HER-2 Ekspresyon Düzeyleri ve ^{18}F-FDG PET/BT Parametreleri Arasındaki İlişki

Seyit Ahmet Ertürk[1], Zekiye Hasbek[2], Hatice Özer[3]

[1]T.R. Ministry of Health, Tokat State Hospital, Nuclear Medicine Unit, Tokat, Turkey
[2]Sivas Cumhuriyet University Faculty of Medicine, Department of Nuclear Medicine, Sivas, Turkey
[3]Sivas Cumhuriyet University Faculty of Medicine, Department of Pathology, Sivas, Turkey

Abstract

Objectives: Human epidermal growth factor receptor-2 (HER-2) is a protooncogene encoded by ERBB2 on chromosome 17. ^{18}Fluoride-fluorodeoxyglucose positron emission tomography/computed tomography (^{18}F-FDG PET/CT) examination is frequently used to detect distant metastasis in gastric cancer imaging. This study aimed to investigate the relationship between the data obtained in the ^{18}F-FDG PET/CT examination and HER-2 expression status in patients with gastric cancer.

Methods: A total of 115 patients diagnosed with gastric cancer between 2016 and 2020, with HER-2 immunohistochemical followed by ^{18}F-FDG PET/CT examination for staging purposes were included.

Results: HER-2 immunohistochemical examination revealed 71 patients (61.7%) with negative and 44 (38.3%) with positive results. The median maximum standardized uptake value (SUV_{max}), mean standardized uptake value (SUV_{mean}), metabolic tumor volume (MTV), and total lesion glycolysis (TLG) values of patients positive with HER-2 were 9.95, 5, 30.44, and 139.16, respectively, whereas patients negative with HER-2 were 9.3,5.4,36.62, and 190.424, respectively (p>0.05). The median cancer antigen 19-9 (CA 19-9) levels of patients positive with HER-2 was 33.52, whereas 11.79 in those who were negative (p=0.016). The mean age was 69.3±9.35 years in patients with distant metastases, whereas 65.2±10.9 in those without distant metastases (p=0.042). Median SUV_{max} and SUV_{mean} values in patients with distant metastases were 11.1 and 6.3, respectively, and 8.2 and 4.5 in those without distant metastases (p=0.002 and p=0.001, respectively). The median CA 19-9 and carcinoembryonic antigen (CEA) levels in patients with distant metastases were 31.34 and 9.20, respectively, whereas those without distant metastases were 11.55 and 2.26, respectively (p=0.011 and p=0.001, respectively).

Conclusion: In our study, no statistically significant difference was found in terms of HER-2 status, SUV_{max}, SUV_{mean}, MTV, TLG, distant metastasis, presence of lymph node metastasis, age, gender, tumor diameter, grade, and localization, and CEA levels in patients with gastric cancer. A statistically significant difference was found between HER-2 status and CA 19-9 levels. A statistically significant relationship was found between distant metastases in the ^{18}F-FDG PET/CT examination and SUV_{max}, SUV_{mean}, age, CEA levels, and histopathologic diagnosis; however, the relationship between distant metastasis in the ^{18}F-FDG PET/CT scan and MTV, TLG, tumor diameter, localization, and grade was not statistically significant.

Keywords: Gastric cancer, PET/CT, HER-2, ^{18}F-FDG

Öz

Amaç: İnsan epidermal büyüme faktörü reseptörü-2 (HER-2) kromozom 17 üzerinde ERBB2 tarafından kodlanan bir protoonkogendir. Mide kanseri görüntülemesinde ^{18}fluoride-florodeoksiglikoz pozitron emisyon tomografi/bilgisayarlı tomografi (^{18}F-FDG PET/BT) tetkiki uzak metastaz taraması için sıklıkla kullanılmaktadır. Bizim bu çalışmadaki amacımız patolojik olarak mide kanseri tanısı konmuş hastalarda ^{18}F-FDG PET/BT tetkikinde elde edilen veriler ile HER-2 ekspresyonu arasındaki ilişkinin araştırılmasıdır.

Address for Correspondence: Seyit Ahmet Ertürk MD, T.R. Ministry of Health, Tokat State Hospital, Nuclear Medicine Unit, Tokat, Turkey
Phone: +90 346 258 02 61 **E-mail:** seyitahmet1988@gmail.com ORCID ID: orcid.org/0000-0002-6030-9662
Received: 21.01.2021 **Accepted:** 12.05.2021

Yöntem: Çalışmamıza 2016 ve 2020 yılları arasında mide kanseri tanısı konulmuş, evreleme amacıyla ^{18}F-FDG PET/BT tetkiki yapılmış ve patolojik olarak HER-2 incelemesi yapılmış 115 mide kanseri hastası dahil edilmiştir.

Bulgular: Çalışmamızdaki hastaların HER-2 immünohistokimyasal incelemesine göre 71'i (%61,7) negatif, 44'ü (%38,3) pozitif olarak değerlendirilmiştir. HER-2 pozitif olan hastaların medyan maksimum standartlaştırılmış alım değeri (SUV_{maks}), ortalama standartlaştırılmış alım değeri ($SUV_{ortalama}$), metabolik tümör hacmi (MTV), toplam lezyon glikoliz (TLG) değeri sırasıyla 9,95, 5, 30,44, 139,16 iken, HER-2 negatif olan hastaların ise sırasıyla 9,3, 5,4, 36,62 ve 190,424 idi (p>0,05). HER-2 pozitif olan hastaların medyan CA 19-9 değeri 33,52 iken, negatif olan hastaların 11,79 idi (p=0,016). ^{18}F-FDG PET/BT tetkikinde uzak metastaz bulunan hastalarda ortalama yaş 69,3±9,35 iken, uzak metastaz olmayanlarda ortalama yaş 65,2±10,9 idi (p=0,042). ^{18}F-FDG PET/BT tetkikinde uzak metastaz bulunan hastalarda medyan SUV_{maks} ve $SUV_{ortalama}$ değerleri sırasıyla 11,1 ve 6,3 iken, uzak metastaz olmayanlarda sırasıyla 8,2 ve 4,5 idi (p=0,002, p=0,001 sırasıyla). Uzak metastaz bulunan hastalarda medyan CA 19-9 ve CEA düzeyleri sırasıyla 31,34 ve 9,20 iken, uzak metastaz olmayanlarda sırasıyla 11,55 ve 2,26 idi (p=0,011 ve p=0,001 sırasıyla).

Sonuç: Çalışmamızda mide kanseri hastalarında HER-2 durumu ile SUV_{maks}, $SUV_{ortalama}$, MTV, TLG, uzak metastaz varlığı, lenf nodu metastazı varlığı, yaş, cinsiyet, tümör çapı, tümör derecesi, tümör lokalizasyonu ve CEA düzeyleri açısından istatistiksel olarak anlamlı bir farklılık yoktu ancak HER-2 durumu ile CA 19-9 değerleri arasında istatistiksel olarak anlamlı bir fark bulundu. ^{18}F-FDG PET/BT tetkikinde uzak metastaz bulunması ile SUV_{maks}, $SUV_{ortalama}$, yaş, CEA düzeyleri ve histopatolojik tanı arasında istatistiksel olarak anlamlı bir ilişki saptanırken, MTV, TLG, tümör çapı, tümör lokalizasyonu ve tümör derecesi arasındaki ilişki istatistiksel olarak anlamlı değildi.

Anahtar kelimeler: Mide kanseri, PET/BT, HER-2, ^{18}F-FDG

Introduction

Gastric cancer is one of the most common cancers worldwide (1). Gastric cancer was the most important part of cancer-related deaths until the 1980s but was replaced by lung cancer after these years (2,3). However, most patients with gastric cancer in western society are currently diagnosed as advanced, and despite advances in understanding the biology of gastric cancer, median survival is still under 12 months. Therefore, personalized treatment development is important (4).

Human epidermal growth factor receptor-2 (HER-2) is a protooncogene encoded by ERBB2 on chromosome 17. The main role of HER-2 protein in these tissues is to support cell proliferation and prevent apoptosis. Therefore, it facilitates excessive uncontrolled cell growth and tumorigenesis processes (5). The importance of this protein is understood in patients with breast cancer, and the developed antagonists gave positive results in the treatment, thus, other types of cancer have been investigated. Patients with gastric cancer constitute a significant part of the research carried out in this regard (5,6). The National Comprehensive Cancer Network (NCCN) guidelines recommended tumor HER-2 overexpression assessment using immunohistochemistry and in situ hybridization method in patients with inoperable locally advanced, recurrent, or metastatic gastric adenocarcinoma for whom HER-2 receptor antagonist therapy are considered (6).

^{18}Fluoride-fluorodeoxyglucose positron emission tomography/computed tomography (^{18}F-FDG PET/CT) examination is frequently used for the detection of distant metastasis in gastric cancer imaging. The role of ^{18}F-FDG PET/CT in the initial diagnosis of gastric cancer is not established. However, ^{18}F-FDG PET/CT examination is recommended in all patients who are clinically indicated according to the NCCN guidelines, without metastases detected by other radiological imaging methods (7).

The determination of HER-2 status became standard in patients with gastric cancer; however, its evaluation requires an invasive procedure. Therefore, the development of noninvasive techniques to predict the HER-2 status is important. Limited publications investigated the relationship between HER-2 status and tumor markers in patients with gastric cancer. Thus, evaluation of PET/CT as a technique for this purpose is important. However, study findings are conflicting on this subject.

This study aimed to investigate the relationship between the data obtained in the ^{18}F-FDG PET/CT examination, HER-2 expression status and histopathological features, the usage of ^{18}F-FDG PET/CT, and level of tumor markers in predicting the HER-2 status in patients with gastric cancer.

Materials and Methods

A total of 115 patients diagnosed with gastric cancer between 2016 March and 2020 January, with HER-2 immunohistochemical examination followed by ^{18}F-FDG PET/CT examination for staging purposes were included in this study. Operable patients diagnosed with endoscopic biopsy were included in the study using ^{18}F-FDG PET/CT examination for staging before surgery, whereas inoperable patients diagnosed with endoscopic biopsy were included in the study with ^{18}F-FDG PET/CT examination before chemotherapy or radiotherapy. A total of 63 patients had a history of operation after diagnosis, wherein 52 were not operated on. Out of 63 patients who were operated on, 11 had distant metastasis on FDG PET/CT examination and 52 had none. This study was conducted following the principles of the Declaration of Helsinki. This study was approved by Cumhuriyet University Non-interventional

Clinical Research Ethics Committee with decision number: 2019-09/05. Verbal and written consent forms were obtained from all study participants.

Imaging Protocol with ^{18}F-FDG PET/CT: Patients were asked for at least 4-6 hours of fasting, and blood glucose measurements of all patients were done before the imaging. Radiopharmaceutical injection was given to patients with fasting blood glucose <200 mg/dL. An average of 10 mCi of ^{18}F-FDG was administered to the patients during the ^{18}F-FDG PET/CT examination.

All patients were kept in the restroom for 45-60 min after the injection. The imaging of patients was performed with a General Electric Discovery PET/CT 600 device (GE Medical Systems, LLC, 3000 N. GRANDVIEW BLVD., WAUKESHA, WI., U.S.A.). CT imaging was performed at 120 kV, 172 mAs with a spiral 16 slice scanner for attenuation correction and anatomical correlation. PET imaging was performed in 3 dimensions to cover the body part from the vertex to the middle of the thigh, including the cranium with 3 dimensions, and PET imaging was performed for approximately 2 min in each bed position. Axial, coronal, and sagittal fusion images were created using the iterative reconstruction method. Maximum standardized uptake value (SUV_{max}), mean standardized uptake value (SUV_{mean}), metabolic tumor volume (MTV), and total lesion glycolysis (TLG) values were calculated from the PET images. An adaptive threshold setting of 42% of the maximum lesional metabolic activity was used for PET images and the region of interest (ROI) was placed within the primary tumor in the stomach while avoiding the peripheral area. SUV_{max} measurement of metastatic lymph nodes and distant metastatic lesions was not evaluated.

The SUV was calculated with the following formula:

[Activity in ROI (mCi/mL) × Bodyweight (gram)] ÷ Injected Dose (mCi)

TLG reflects the metabolic activity of the entire tumor and was calculated by multiplying the MTV by the SUV_{mean} value. An adaptive threshold setting of 42% of the maximum lesional metabolic activity was used for PET images and the ROI was placed within the tumor while avoiding the peripheral area (8).

Immunohistochemical Staining: Hematoxylin-eosin stained sections prepared from formalin-fixed paraffin blocks were examined, and from the paraffin blocks of these preparations, 3 micron thick sections were taken into the positively charged slide. Immunohistochemical staining of tissues with completed deparaffinization was performed in ROCHE VENTANA BENCHMARK XT (Ventana Medical Systems, Tucson, Arizona, USA) automated staining device using a c-erbB-2 antibody (PATHWAY anti-HER-2/neu clone 4B5, Rabbit Monoclonal Primary Antibody, Ventana Medical Systems, Tucson, Arizona, USA, 2017) in a ready-to-use form. HER-2 positivity was determined using a light microscope.

Immunohistochemical Assessment: Only the membranous staining was considered significant in the immunohistochemical c-erbB-2 staining evaluation, whereas the cytoplasmic granular and nuclear staining were not evaluated. The modified form of the HercepTest scoring system was used for gastric cancers (9,10). All cases were divided into four groups as score 0, score 1+, score 2+, and score 3+. Patients with immunohistochemical staining scores of 0 and 1+ were considered negative, whereas scores 2+ and 3+ were accepted as positive (11).

Statistical Analysis

The data obtained were evaluated with Statistical Package for the Social Sciences 23.0 program (SPSS Inc., Chicago). The Kolmogorov-Smirnov test was used to check the normality of the data. An independent sample t-test for two independent groups and the F-test [analysis of variance (ANOVA)] test for more than two groups were used for data with parametric conditions. ANOVA was used to compare more than two groups, whereas the Tukey tests were used in those with homogeneity assumption and Tamhane's T2 tests in those without homogeneity assumption to determine which group is different from the others. The Mann-Whitney U test was used for two independent groups and the Kruskal-Wallis test for more than two independent groups if any or all assumptions are not provided. Chi-square test was used to evaluate the data obtained by counting. The margin of error was taken as 0.05. The tests performed for sample volume calculation revealed a standard deviation related to the A event as 6, with the margin of error as 1.2, whereas the sample volume calculation before the study determined the sample size as 96.

Results

A total of 115 patients [85 men (73.9%), 30 women (26.1%)] were included in this study, with the patient tumor characteristics presented in Table 1. The histopathological subtypes of patients by Lauren classification revealed 9 (7.8%) with diffuse type, 101 (87.8%) with intestinal type, and 5 (4.3%) with mixed type. The group with intestinal-type gastric carcinoma revealed 4 (3.5%) patients with intramucosal carcinoma. The group with diffuse-type gastric carcinoma revealed four (3.5%) patients with signet ring cell carcinoma and five (4.3%) with poorly cohesive carcinoma. Patients with adenocarcinoma revealed 29 with poorly differentiated adenocarcinoma, 30 with

Table 1. Age, gender, histopathological diagnosis, tumor location, presence of distant metastasis, and lymph node metastasis in ^{18}F-FDG PET/CT, HER-2 expression distribution of patients

	Number (n)	Percentage (%)
Gender		
Male	85	73.9%
Female	30	26.1%
Total	115	100%
Age (mean ± standard deviation)	66.70±10.52	-
Histopathologic diagnosis		
Diffuse type	9	7.8%
Signet ring cell carcinoma	4	3.5%
Poorly cohesive carcinoma	5	4.3%
Intestinal type	101	87.8%
Invasive adenocarcinoma	97	84.3%
Intramucosal carcinoma	4	3.5%
Mixed carcinoma	5	4.3%
Total	115	100%
Tumor localization		
Cardia	34	29.6%
Non-cardia	81	70.4%
Corpus	29	25.2%
Antrum	45	39.1%
Lesser curvature	4	3.5%
Fundus	1	0.9%
Greater curvature	1	0.9%
Diffuse	1	0.9%
Total	115	100%
Distant metastasis in ^{18}F-FDG PET/CT		
Absent	73	63.5%
Present	42	36.5%
Total	115	100%
Lymph node metastasis ^{18}F-FDG PET/CT		
Absent	55	47.8%
Present	60	52.2%
Total	115	100%
HER-2 expression status		
Negative	71	61.7%
Positive	44	38.3%
Total	115	100%
HER-2 expression score		
0	58	50.4%
1+	13	11.3%
2+	29	25.2%
3+	15	13%
Total	115	100%

HER-2: Human epidermal growth factor receptor-2, ^{18}F-FDG PET/CT: ^{18}Fluoride-fluorodeoxyglucose positron emission tomography/computed tomography

moderately differentiated adenocarcinoma, and 2 with well-differentiated adenocarcinoma.

HER-2 immunohistochemical examinations were performed in all patients, wherein 58 (50.4%) were negative, 13 (11.3%) were 1+, 29 (25.2%) were 2+, and 15 (13%) were 3+. According to the HER-2 immunohistochemical examination of patients, 71 (61.7%) were negative and 44 (38.3%) were positive.

No statistically significant relation was found between HER-2 and age, gender, SUV_{max}, SUV_{mean}, MTV, TLG, tumor diameter, presence of distant metastasis and lymph node metastasis in ^{18}F-FDG PET/CT, tumor histopathologic subtype, tumor grade, and tumor localization (p=1.0, 0.507, 0.959, 0.751, 0.661, 0.627, 0.802, 0.086, 0.418, 0.371, 0.713, and 0.677, respectively). Median tumor SUV_{max} of patients was 10.73±6.35 [minimum (min): 3.2, maximum (max): 49.6]; tumor SUV_{mean} value was 6.07±3.92 (min: 1.7, max: 30.7); TLG value was 295.981±464 (min: 4.428, max: 3438.400); and MTV value was 44.4±41.01 (min: 1.64, max: 228). The median SUV_{max} of patients positive with HER-2 was 9.95 (min: 3.2, max: 49.6), whereas the median SUV_{max} of patients with negative HER-2 was 9.3 (min: 3.3, max: 31.7) (p=0.959). The median SUV_{mean} value of patients with positive HER-2 was 5 (min: 1.7, max: 30.7), whereas 5.4 for patients with negative HER-2 (min: 1.7, max: 19.5) (p=0.751). The median MTV value of patients with positive HER-2 was 30.44 (min: 1.64, max: 205), whereas 36.62 for patients with negative HER-2 (min: 1.86, max: 228) (p=0.661). The median TLG value of patients positive with HER-2 was 139.16 (min: 4.428, max: 3438.400), where 190.424 for patients with negative HER-2 (min: 8.624, max: 2553.600) (p=0.627). The separate statistical group evaluation of patients with positive and negative HER-2 in terms of distant metastasis revealed 45.5% of patients with positive HER-2 had distant metastasis on PET/CT examination, whereas 31% of patients with negative HER-2 had distant metastasis (p=0.117). The mean tumor diameter of patients with positive HER-2 was 4.93±2.11 cm, whereas 5.25±2.68

cm in patients with negative HER-2 (p=0.802) (Table 2). ^{18}F-FDG PET/CT examination of patients with positive HER-2 revealed 20 (45.5%) patients with distant metastasis and 24 (54.5%) without distant metastasis. ^{18}F-FDG PET/CT examination of patients with negative HER-2 revealed 22 (31%) patients with distant metastasis and 49 (69%) without distant metastasis (p>0.05, p=0.086).

Table 2. Relationship between HER-2 and age, gender, metabolic PET parameters, tumor diameter, presence of distant metastasis and lymph node metastasis in ^{18}F-FDG PET/CT, tumor grade, tumor localization, CA 19-9 levels, and CEA levels

	HER-2 (+) n (%)	HER-2 (-) n (%)	p
Age	66.7±10.2	66.7±10.8	1.0
Gender			
Female	11 (25%)	19 (26.8%)	0.507
Male	33 (75%)	52 (73.2%)	
SUV_{max} (median)	9.95	9.3	0.959
SUV_{mean} (median)	5	5.4	0.751
MTV (median)	30.44	36.62	0.661
TLG (median)	139.16	190.424	0.627
Tumor diameter	4.93±2.11 cm	5.25±2.68 cm	0.802
Distant metastasis in ^{18}F-FDG PET/CT			
Present	20 (45.5%)	22 (31%)	0.086
Absent	24 (54.5%)	49 (69%)	
Lymph node metastasis ^{18}F-FDG PET/CT			
Present	24 (54.5%)	36 (50.7%)	0.418
Absent	29 (45.5%)	35 (49.3%)	
Tumor grade			
Grade 1	2 (9.5%)	3 (6.8%)	0.713
Grade 2	13 (61.9%)	24 (54.5%)	
Grade 3	6 (28.6%)	17 (38.6%)	
Tumor localization			
Cardia	14 (31.8%)	20 (28.2%)	0.677
Non-cardia	30 (68.2%)	51 (71.8%)	
Corpus	11 (25%)	18 (25.4%)	
Antrum	16 (36.4%)	29 (40.8%)	
Lesser curvature	1 (2.3%)	3 (4.2%)	
Fundus	1 (2.3%)	0	
Greater curvature	0	1 (1.4%)	
Diffuse	1 (2.3%)	0	
CA 19-9	33.52	11.79	**0.016***
CEA	3.23	2.31	0.158

HER-2: Human epidermal growth factor receptor-2, ^{18}F-FDG PET/CT: ^{18}Fluoride-fluorodeoxyglucose positron emission tomography/computed tomography, SUV_{max}: Maximum standardized uptake value, SUV_{mean}: Mean standardized uptake value

^{18}F-FDG PET/CT examination of patients with positive HER-2 revealed 24 (54.5%) patients with lymph node metastasis and 20 patients (45.5%) without lymph node metastasis. ^{18}F-FDG PET/CT examination of patients with positive HER-2 revealed 36 (50.7%) patients with lymph node metastasis in and 35 (49.3%) without lymph node metastasis (p=0.418).

No statistically significant relationship was found between HER-2 status and tumor grade. Two (9.5%) patients with positive HER-2 had grade 1, 13 (61.9%) had grade 2, and 6 (28.6%) had grade 3. Three (6.8%) of the patients with negative HER-2 had grade 1, 24 (54.5%) had grade 2, and 17 (38.6%) had grade 3 (p=0.713). No statistically significant relationship was found between the HER-2 status and tumor localization (p=0.677).

The median CA 19-9 value of patients with positive HER-2 was 33.52 U/mL (min: 2.52, max: 36310), whereas 11.79 U/mL in patients with negative HER-2 (min: 0.95, max: 1000), which was statistically significant (p=0.016). However, no significant relationship was found between the CEA and HER-2, and the median CEA value of patient with positive HER-2 was 3.23 ng/mL (min: 0.75, max: 415.3), whereas 2.31 ng/mL in patients with negative HER-2 (min: 0.53, max: 1000) (p=0.158) (Table 2).

^{18}F-FDG PET/CT evaluation of the relationship between the distant metastasis and tumor histopathological subtype revealed no distant metastases in nine patients with diffuse-type tumor, whereas four had lymph node metastasis. A total of 60 patients with intestinal-type tumors did not have metastases, whereas 41 had distant metastases. Four patients with mixed tumors did not have distant metastases, whereas one patient had distant metastases, which was statistically significant (p=0.039).

The relationship between presence of distant metastasis in ^{18}F-FDG PET/CT and CA 19-9 levels revealed a median CA 19-9 level of 31.34 U/mL (min: 4.30, max: 36.310) in patients with distant metastasis, whereas 11.55 U/mL (min: 0.95, max: 1.000) in patients without distant metastasis (p=0.011). The relationship between the presence of distant metastasis in ^{18}F-FDG PET/CT and CEA levels revealed a median CEA level of 9.20 ng/mL (min: 0.74, max: 1.000) in patients with distant metastases, whereas 2.26 ng/mL (min: 0.53, max: 280) in patients without distant metastases (p=0.001) (Table 3).

Discussion

Study results revealed the mean SUV_{max} value of patients with positive HER-2 of 9.95, whereas 9.3 in patients with negative HER-2, which was not statistically significant. CA 19-9 levels and the incidence of distant metastasis

were higher in patients with positive HER-2. Contrarily, a statistically significant relationship was found between the distant metastasis in ^{18}F-FDG PET/CT examination and SUV_{max}, SUV_{mean}, age, histopathologic subtype, and CEA levels.

Table 3. The relationship between the presence of distant metastasis in ^{18}F-FDG PET/CT and age, gender, metabolic PET parameters, tumor diameter, grade, and localization, CA 19-9, and CEA levels

	Patients with distant metastasis in ^{18}F-FDG PET/CT	Patients without distant metastasis in ^{18}F-FDG PET/CT	p
Age	69.3±9.35	65.2±10.9	**0.042***
Gender			
Female	12 (28.6%)	18 (24.7%)	0.402
Male	30 (71.4%)	55 (75.3%)	
SUV_{max}	11.1	8.2	**0.002***
SUV_{mean}	6.3	4.5	**0.001***
MTV	32.75	35.82	0.822
TLG	187.62	133.635	0.180
Tumor diameter	5.5	4.75	0.552
Tumor grade			
Grade 1	0	5 (100%)	0.297
Grade 2	9 (24.3%)	28 (75.7%)	
Grade 3	3 (13%)	20 (87%)	
Tumor localization			
Cardia	14 (41.2%)	20 (58.8%)	0.502
Non-cardia	28 (34.6%)	53(64.4%)	
Corpus	10 (34.4%)	19 (65.6%)	
Antrum	16 (35.6%)	29 (64.4%)	
Lesser curvature	2 (50%)	2 (50%)	
Fundus	0	1 (100%)	
Greater curvature	0	1 (100%)	
Diffuse	0	1 (100%)	
Histopathologic diagnosis			
Diffuse type	0	9 (100%)	**0.039***
Intestinal type	41 (40.6%)	60 (59.4%)	
Mixed carcinoma	1 (20%)	4 (80%)	
CA 19-9	31.34	11.55	**0.011***
CEA	9.20	2.26	**0.001***

*p<0.05, HER-2: Human epidermal growth factor receptor-2, ^{18}F-FDG PET/CT: ^{18}F-fluorodeoxyglucose positron emission tomography/computed tomography, MTV: Metabolic tumor volume, TLG: Total lesion glycolysis, SUV_{max}: Maximum standardized uptake value, SUV_{mean}: Mean standardized uptake value

A limited number of publications evaluated the HER-2 status in patients with gastric cancer, together with the parameters obtained in the ^{18}F-FDG PET/CT examination. One of these limited studies was by Park et al. (12) compared the parameters obtained in PET/CT in 124 patients with gastric cancer who had ^{18}F-FDG PET/CT before the first stage of chemotherapy and the HER-2 status of the patient. In their study, mean SUV_{max} values were 12.1 in patients with gastric cancer having positive HER-2, whereas 7.4 in patients with gastric cancer having negative HER-2, which was statistically significant. Patients with positive HER-2 with higher metabolic tumor burden among those treated with Trastuzumab had worse overall survival but without difference in progression-free survival. In the same study, SUV_{mean}, MTV, and TLG values were also higher in a patient with positive HER-2, whereas no statistically significant differences were found in our study. However, only metastatic and recurrent patients with gastric cancer were included in this study, whereas all patients with or without metastases who underwent PET/CT scans for primary staging were included in our study. The difference between the studies between HER-2 examination and PET/CT parameters is due to the difference in the patient population. In a study by Kim and Young Park (13) comparing HER-2 expression status and SUV_{max} values of 109 patients who were operated on for gastric cancer and had preoperative ^{18}F-FDG PET/CT, SUV_{max} values were significantly higher in patients with positive HER-2.

According to the study conducted by Celli et al. (14), similar to our study, no statistically significant difference was found between the SUV_{max} value obtained in PET/CT and HER-2 status of patients, and the cumulative death incidence was 60% in patients whose SUV_{max} value was above 6.6 during the study period, whereas the cumulative death incidence was 18% in patients below 6.6. Similar to our study, no significant relationship was found between the tumor size, presence of lymph node metastasis in patients, and HER-2 status. In the same study, the average age of patients with positive HER-2 was 70 years, whereas the mean age of patients with negative HER-2 was 67 years, which was not statistically significant. In our study, the mean age of patients with positive HER-2 was 66.7±10.2 years, whereas the mean age of patients with negative HER-2 was 66.7±10.8 years. Similarly, no statistically significant difference was found between the mean ages.

The study of Chen et al. (15) compared the data obtained in the ^{18}F-FDG PET/CT examination with the HER-2 status in 64 patients with gastric cancer who were not operated on. This study revealed a statistically significant correlation between the HER-2 expression and SUV_{max} when the signet ring cell carcinomas were included. The mean SUV_{max}

values of patients with positive HER-2 were 6.893±5.495, whereas 3.673±2.352 in patients with negative HER-2. A significant relationship was found between the HER-2 status and SUV_{max} values when signet ring cell carcinomas were excluded, and the mean SUV_{max} values of patients with positive HER-2 were 8.619±5.878, whereas 3.789±2.613 in patients with negative HER-2. They were able to detect HER-2 status with 64.4% accuracy when the SUV_{max} cut-off value was 6.2. Therefore, PET/CT examination is used to predict HER-2 status when signet ring cell carcinomas were excluded. However, our study revealed that the relationship between the HER-2 and PET/CT parameters remained even when signet ring cell carcinomas were excluded.

The study conducted by Bai et al. (16) revealed a mean SUV_{max} value in patients with gastric adenocarcinoma of 9.22 in HER-2 positive tumors and 5.02 in HER-2 negative tumors, which was statistically significant. In this study, only operable patients were evaluated, and inoperable patients were not evaluated. However, in our study, both operable and inoperable patients were evaluated. The difference between the studies between HER-2 examination and PET/CT parameters is due to the difference in the patient population. In the same study, SUV_{max} values were linearly correlated with CA 19-9 values. Therefore, the CA 19-9 value was a parameter used to predict the SUV_{max} value. Likewise, the SUV_{max} value is used to predict the HER-2 status. The study conducted by Zhou et al. (17) including 256 gastric cancer patients revealed no statistically significant correlation between the CA 19-9 levels and HER-2. However, they concluded that HER-2 and CA 19-9 levels are independent prognostic factors in patients with gastric cancer. In our study, the median CA 19-9 value of patients with positive HER-2 was 33.52, whereas 11.79 in patients with negative HER-2, which was statistically significant (p=0.011).

Study Limitations

One of the main limitations of our study was that HER-2 immunohistochemical analysis was performed on all patients, gene amplification analysis was performed with the *in situ* hybridization technique in addition to 17 of the patients with 2+HER-2 immunohistochemical analysis result; however, this analysis was not done to the 12 patients. All patients had a pathological diagnosis and macroscopic type of tumor and tumor diameter parameters were included in the operated patients, but these parameters were not included in the non-operated patients.

Conclusion

A significant relationship was not found between the PET/CT parameters and HER-2 status in patients with gastric cancer; however, a statistically significant relationship was found between the HER-2 expression level and CA 19-9 values. Contrarily, a statistically significant relationship was found between the distant metastasis in ^{18}F-FDG PET/CT examination and SUV_{max}, SUV_{mean}, age, histopathologic subtype, and CEA levels, thus evaluating these data primarily in the treatment plan and follow-up of patients is important. In addition, the rate of distant metastasis increases with age in patients with gastric cancer, and increased CA 19-9 and CEA levels raise suspicion of distant metastasis in patients. However, the use of immunohistochemical and *in situ* hybridization techniques together with the addition of survival data in a wider patient population of this study will contribute more to the literature.

Ethics

Ethics Committee Approval: This study was approved by Cumhuriyet University Non-interventional Clinical Research Ethics Committee with decision number 2019-09/05.

Informed Consent: Verbal and written consent forms were obtained from all study participants.

Peer-review: Externally peer-reviewed.

Authorship Contributions

Surgical and Medical Practices: S.A.E, Z.H., H.Ö., Concept: S.A.E, Z.H., H.Ö., Design: S.A.E, Z.H., H.Ö., Data Collection or Processing: S.A.E., Z.H., Analysis or Interpretation: S.A.E., Z.H., Literature Search: S.A.E., Z.H., Writing: S.A.E, Z.H.,H.Ö.

Conflict of Interest: No conflict of interest was declared by the authors.

Financial Disclosure: The authors declared that this study has received no financial support.

References

1. Bray F, Ferlay J, Soerjomataram I, Siegel RL, Torre LA, Jemal A. Global cancer statistics 2018: GLOBOCAN estimates of incidence and mortality worldwide for 36 cancers in 185 countries. CA Cancer J Clin 2018;68:394-424.
2. Pisani P, Parkin DM, Ferlay J. Estimates of the worldwide mortality from eighteen major cancers in 1985. Implications for prevention and projections of future burden. Int J Cancer 1993;55:891-903.
3. Parkin DM. Epidemiology of cancer: global patterns and trends. Toxicol Lett 1998;102-103:227-34.
4. Digklia A, Wagner AD. Advanced gastric cancer: Current treatment landscape and future perspectives. World J Gastroenterol 2016;22:2403-2414.
5. Boku N. HER2-positive gastric cancer. Gastric Cancer 2014;17:1-12.
6. Meric-Bernstam F, Johnson AM, Dumbrava EEI, Raghav K, Balaji K, Bhatt M, Murthy RK, Rodon J, Piha-Paul SA. Advances in HER2-Targeted Therapy: Novel Agents and Opportunities Beyond Breast and Gastric Cancer. Clin Cancer Res 2019;25:2033-2041.

7. Nicole McMillian N, Lenora Pluchino MA, Ajani JA, D TA, Chair V, Bentrem DJ, et al. Gastric Cancer Continue NCCN Guidelines Panel Disclosures. 2019.
8. Fox JJ, Autran-Blanc E, Morris MJ, Gavane S, Nehmeh S, Van Nuffel A, Gönen M, Schöder H, Humm JL, Scher HI, Larson SM. Practical approach for comparative analysis of multilesion molecular imaging using a semiautomated program for PET/CT. J Nucl Med 2011;52:1727-1732.
9. Bartley AN, Washington MK, Ventura CB, Ismaila N, Colasacco C, Benson AB 3rd, Carrato A, Gulley ML, Jain D, Kakar S, Mackay HJ, Streutker C, Tang L, Troxell M, Ajani JA. HER2 Testing and Clinical Decision Making in Gastroesophageal Adenocarcinoma: Guideline From the College of American Pathologists, American Society for Clinical Pathology, and American Society of Clinical Oncology. Am J Clin Pathol 2016;146:647-669.
10. Hofmann M, Stoss O, Shi D, Büttner R, van de Vijver M, Kim W, Ochiai A, Rüschoff J, Henkel T. Assessment of a HER2 scoring system for gastric cancer: results from a validation study. Histopathology 2008;52:797-805.
11. Wolff AC, Hammond ME, Hicks DG, Dowsett M, McShane LM, Allison KH, Allred DC, Bartlett JM, Bilous M, Fitzgibbons P, Hanna W, Jenkins RB, Mangu PB, Paik S, Perez EA, Press MF, Spears PA, Vance GH, Viale G, Hayes DF; American Society of Clinical Oncology; College of American Pathologists. Recommendations for human epidermal growth factor receptor 2 testing in breast cancer: American Society of Clinical Oncology/College of American Pathologists clinical practice guideline update. Arch Pathol Lab Med 2014;138:241-256.
12. Park JS, Lee N, Beom SH, Kim HS, Lee CK, Rha SY, Chung HC, Yun M, Cho A, Jung M. The prognostic value of volume-based parameters using 18F-FDG PET/CT in gastric cancer according to HER2 status. Gastric Cancer 2018;21:213-224.
13. Kim JS, Young Park S. (18)F-FDG PET/CT of advanced gastric carcinoma and association of HER2 expression with standardized uptake value. Asia Ocean J Nucl Med Biol 2014;2:12-18.
14. Celli R, Colunga M, Patel N, Djekidel M, Jain D. Metabolic Signature on 18F-FDG PET/CT, HER2 Status, and Survival in Gastric Adenocarcinomas. J Nucl Med Technol 2016;44:234-238.
15. Chen R, Zhou X, Liu J, Huang G. Relationship Between 18F-FDG PET/CT Findings and HER2 Expression in Gastric Cancer. J Nucl Med 2016;57:1040-1044.
16. Bai L, Guo CH, Zhao Y, Gao JG, Li M, Shen C, Guo YM, Duan XY. SUVmax of 18F-FDG PET/CT correlates to expression of major chemotherapy-related tumor markers and serum tumor markers in gastric adenocarcinoma patients. Oncol Rep 2017;37:3433-3440.
17. Zhou H, Dong A, Xia H, He G, Cui J. Associations between CA19-9 and CA125 levels and human epidermal growth factor receptor 2 overexpression in patients with gastric cancer. Oncol Lett 2018;16:1079-1086.

Original Article
Mol Imaging Radionucl Ther 2021;30:158-168 DOI:10.4274/mirt.galenos.2021.82584

Prognostic Prediction of BRCA Mutations by ^{18}F-FDG PET/CT SUV_{max} in Breast Cancer

Meme Kanserlerinde BRCA Mutasyonlarının ^{18}F-FDG PET/BT SUV_{max} Değeri ile Prognostik Tahmini

Semra Özdemir[1], Fatma Sılan[2], Mehmet Yılmaz Akgün[3], Nilgün Aracı[4], İsmail Çırpan[5], Fulya Koç Öztürk[1], Öztürk Özdemir[2]

[1]*Çanakkale Onsekiz Mart University Faculty of Medicine, Department of Nuclear Medicine, Çanakkale, Turkey*
[2]*Çanakkale Onsekiz Mart University Faculty of Medicine, Department of Medical Genetics, Çanakkale, Turkey*
[3]*Çanakkale Onsekiz Mart University Faculty of Medicine, Department of General Surgery, Çanakkale, Turkey*
[4]*Çanakkale State Hospital, Clinic of Nuclear Medicine, Çanakkale, Turkey*
[5]*Çanakkale State Hospital, Clinic of Pathology, Çanakkale, Turkey*

Abstract

Objectives: This study aimed to investigate the prognostic prediction of germline BRCA1 and BRCA2 mutations by comparing the maximum standardized uptake value (SUV_{max}) obtained from ^{18}fluoride-fluorodeoxyglucose positron emission tomography/computed tomography (^{18}F-FDG PET/CT), which is considered a prognostic factor in breast cancer (BC).

Methods: Retrospective interdisciplinary laboratory results of 92 patients with BC who had germline BRCA1 or BRCA2 mutation profiles and underwent ^{18}F-FDG PET/CT were compared. Genotyping was made by next-generation sequencing, and PET/CT scans were re-evaluated. The histopathological data, genetic results, and clinical demographics of all patients were recorded. Patients were divided into two groups in accordance with the presence of germline BRCA1 and/or BRCA2 mutations. Between-group statistical comparison was performed.

Results: In PET/CT performed for primary staging, patients with BRCA-positive BC had significantly higher SUV_{max} (p=0.039), larger tumor size (p=0.025), and presence of axillary nodal metastases (p=0.023) than patients with BRCA-negative BC. Although the Ki-67 index was higher in the BRCA-positive group than BRCA-negative group, this difference was not significant (p=0.157). Moreover, in the BRCA-positive and negative groups, SUV_{max}, Ki-67 index, and tumor size, grade, and stage were significantly correlated with each other.

Conclusion: The results of this study showed a strong association between BRCA mutations and SUV_{max}, which indicates the poor prognosis of BC.

Keywords: BRCA1-2 mutation, SUV_{max}, ^{18}F-FDG PET/CT, breast cancer

Öz

Amaç: Bu çalışmanın amacı, meme kanserlerinde (MK) germline BRCA1-BRCA2 mutasyonlarının tahmini prognostik değerini, ^{18}F-florodeoksiglikoz pozitron emisyon tomografi/bilgisayarlı tomografi (^{18}F-FDG PET/BT) tetkikinden elde edilen ve prognostik bir faktör olduğu kabul edilen maksimum standardize tutulum değeri (SUV_{maks}) ile karşılaştırarak araştırmaktır.

Yöntem: Germline BRCA1 veya BRCA2 mutasyon profilleri olan ve ^{18}F-FDG PET/BT taraması yapılan MK'li 92 hastanın retrospektif olarak laboratuvar sonuçları karşılaştırıldı. Genotipleme yeni nesil sıralama tekniği ile yapıldı ve PET/BT taramaları yeniden değerlendirilerek tüm hastaların histopatolojik, genetik sonuçları ve klinik demografik özellikleri not edildi. Hastalar germline BRCA1 ve/veya BRCA2 mutasyonlarının varlığına göre iki gruba ayrıldı ve gruplar arasında istatistiksel karşılaştırma yapıldı.

Address for Correspondence: Semra Özdemir Prof. MD, Çanakkale Onsekiz Mart University Faculty of Medicine, Department of Nuclear Medicine, Çanakkale, Turkey
Phone: +90 286 263 59 50 **E-mail:** semozdemir@yahoo.com ORCID ID: orcid.org/0000-0003-1302-9630
Received: 11.04.2021 **Accepted:** 26.05.2021

Bulgular: BRCA pozitif MK hastalarının, primer evreleme için yapılan ^{18}F-FDG PET/BT görüntülemesinde, SUV_{maks} değerleri (p=0,039), tümör boyutu (p=0,025) ve aksiller nodal metastaz varlığı (p=0,023) BRCA negatif MK hastalarından önemli ölçüde daha yüksek bulundu. Ki-67 değeri, BRCA pozitif grupta BRCA negatif gruba göre daha yüksek olmasına rağmen, bu fark istatistiksel olarak anlamlı değildi (p=0,157). Ayrıca BRCA pozitif ve negatif gruplarında; SUV_{maks}, Ki-67, tümör boyutu, grade ve evre değerlerinin birbirleriyle anlamlı korelasyon gösterdiği bulundu.

Sonuç: Mevcut çalışma sonuçlarına göre, BRCA mutasyonları ile SUV_{maks} değerleri arasında MK için kötü prognozu gösteren güçlü bir ilişki vardır.

Anahtar kelimeler: BRCA1-2 mutasyonu, SUV_{maks}, ^{18}F-FDG PET/BT, meme kanseri

Introduction

Breast cancer (BC) is one of the most common types of cancer in women and has a variable spectrum of phenotypic and clinical behaviors, which are caused by genetics, lifestyle, and environmental factors (1,2). One of the main genetic risk factors is the presence of BRCA1-2 mutations. BRCA1-2 germline mutations contribute to 5-10% of BC in most populations. BRCA1 and BRCA2 provide instructions for making a protein that acts as a tumor suppressor (3,4). Tumor suppressor proteins prevent cancer formation by preventing the uncontrolled growth and division of cells or by promoting apoptosis. Hence, mutations in *BRCA* genes can lead to irregular cell growth and tumor development.

These mutations are inherited in an autosomal dominant manner and show a high degree of penetrance. A meta-analysis indicated that BRCA1 and BRCA2 carriers have 57-65% and 45-49% probability of developing BC throughout their life, respectively (5). BRCA1-associated BC types often have high histological grade and are triple-negative. BRCA2-associated breast tumors are usually high-grade, estrogen receptor positive, and human epidermal growth factor receptor-2 (HER-2)-negative (3,6). However, the effect of BRCA mutation carrier on prognosis is still controversial. While some studies have claimed that patients with BC who are BRCA carriers have reduced overall survival compared with patients with sporadic BC, some studies have also stated that it does not affect surveillance or even results in better surveillance (7,8,9,10).

In BC, ^{18}fluoride-fluorodeoxyglucose positron emission tomography/computed tomography (^{18}F-FDG PET/CT) is frequently performed for staging to obtain long-term prognostic information, evaluation of recurrent disease, and estimation of therapeutic response. Through radiolabeled glucose with ^{18}F-FDG PET/CT, the presence of the primary tumor, nodal involvement, and distant metastasis can be displayed simultaneously; as a result, tumor-node-metastasis (TNM) classification can be most accurately performed (11,12,13). The maximum standardized uptake value (SUV_{max}) obtained from ^{18}F-FDG PET/CT, which is a metabolic indicator, is an accepted parameter in determining BC prognosis. Many studies have shown that high SUV_{max} is an indicator of poor prognosis (13,14,15). Therefore, this study aimed to investigate the relationship between SUV_{max} and BRCA positivity to predict the effect of BRCA mutation on prognosis.

Materials and Methods

Study Groups

A total of 92 female patients were selected retrospectively among patients with BC who had germline BRCA1 or BRCA2 analysis and who underwent PET/CT between 2017 and 2020. All patients received routine PET/CT imaging protocol. Imaging was completed with a Biograph Duo LSO ^{18}F-FDG PET/CT scanner (Siemens, Germany). Patients who were pathologically diagnosed with BC and underwent PET for primary staging were included in this study. Multidisciplinary laboratory results from histopathology, genetics, and PET/CT and some clinical demographics of all patients were noted. All patients had a family history of BC. None of the patients had undergone surgery, and *BRCA* gene analyses were made before surgery. Patients were divided into two groups in accordance with the presence of germline BRCA1 and/or BRCA2 mutations. Group 1 (BRCA-positive group) was composed of patients who had BRCA1 and/or BRCA2 mutation (n=18), while group 2 (BRCA-negative group) comprised patients who had no germline BRCA1 and BRCA2 mutations (n=74). In the BRCA-positive group (mean age, 50.11±11.98 years), 11 women were 50 years old or younger. In the BRCA-negative group (mean age, 51.36±10.86 years), 37 women were 50 years old or younger. The clinical characteristics, histopathological features, and PET/CT parameters of the cohorts are shown in Table 1. Only patients who underwent PET/CT for primary staging were included in this study. Patients whose pathology results could not be obtained and who did not undergo PET/CT for primary staging were excluded from the study.

All patients provided written informed consent. The archives of the university and state hospital were used with the permission of the institution. The study was approved by the Çanakkale Onsekiz Mart University Ethics Committee (protocol no: 2020-04, date: 26.02.2020).

Table 1. Laboratory and clinical characteristics of patients with breast cancer			
Clinical characteristics	**Patient cohort (n=92)**		
	BRCA1-2-positive group (n=18)	**BRCA1-2-negative group (n=74)**	**p value**
Mean age (years) Mean ± SD Median Min-max ≤50, n (%) >50, n (%)	 50.11±11.98 49 31-74 11 (61.1) 7 (38.9)	 51.36±10.86 51 32-78 37 (50.0) 37 (50.0)	 0.629 0.397
Smoke (+)	8 (44.4)	20 (27.0)	0.248
Alcohol (+)	1 (5.6)	8 (10.8)	0.817
Ki-67 Mean ± SD Median Min-max	 32.89±19.16 32.50 (5.00-70.00)	 26.17±16.72 20.00 (2.00-70.00)	 0.157
Histopathologic feature	**n (%)**	**n (%)**	**p value**
Tumor histotype Invasive ductal carcinoma (IDC) IDC (papillary type) IDC (mucinous type) IDC (medullary type) IDC (tubular type) Invasive lobular carcinoma	 14 (77.8) 0 (0.0) 1 (5.6) 1 (5.6) 0 (0.0) 2 (11.1)	 62 (83.8) 2 (2.7) 2 (2.7) 0 (0.0) 1 (1.4) 5 (6.8)	 0.411
Progesterone receptor status Positive Negative	 8 (44.4) 10 (55.6)	 45 (60.8) 29 (39.2)	 0.320
Estrogen receptor status Positive Negative	 9 (50.0) 9 (50.0)	 56 (75.7) 18 (24.3)	 0.063
Hormone receptor status Positive Negative	 9 (50.0) 9 (50.0)	 61 (82.4) 13 (17.6)	 **0.010****
Molecular subtypes HR+/HER-2- (luminal A) HR-/HER-2- (triple-negative) HR+/HER-2 (luminal B) HR-/HER-2+ (HER-2 enriched)	 4 (22.2) 4 (22.2) 5 (27.7) 5 (27.7)	 41 (55.4) 11 (14.8) 20 (27.2) 2 (2.7)	 **0.024**** 0.578 0.949 **0.002**
Grades 1 2 3	 4 (22.2) 13 (72.2) 1 (5.6)	 31 (41.9) 35 (47.3) 8 (10.8)	 0.165*
Stage I II A II-B III A III B III C IV	 1 (5.6) 5 (27.8) 5 (27.8) 3 (16.7) 1 (5.6) 0 (0) 3 (16.7)	 24 (32.4) 17 (23.0) 11 (14.9) 7 (9.4) 4 (5.4) 6 (8.1) 5 (6.8)	 0.080**
PET/CT parameters			**p value**
Primary tumor size (max) (mm) Mean ± SD Min-max	 30.11±10.90 15-51	 24.69±11.31 8-60	 **0.025***

Table 1. Continued

Clinical characteristics	Patient cohort (n=92)		
	BRCA1-2-positive group (n=18)	BRCA1-2-negative group (n=74)	p value
Primary lesion SUV_{max} Mean ± SD Min-max	 10.93±8.29 2.60-30.72	 6.76±3.90 2.0-17.3	**0.039****
Axillary nodal metastasis, n (%) Positive Negative	 15 (83.3) 3 (16.7)	 40 (54.1) 34 (45.9)	**0.023***
Distant metastasis, n (%) Positive Negative	 3 (16.7) 15 (83.3)	 6 (8.1) 68 (91.9)	0.371***

*Pearson chi-square, **Mann-Whitney U test, ***Fisher's Exact test, SD: Standard deviation, min: Minimum, max: Maximum, HER-2: Human epidermal growth factor receptor-2, SUV_{max}: Maximum standardized uptake value

^{18}F-FDG PET/CT and Data Analysis

Before PET/CT was performed, patients were instructed to fast for at least 6 h, and serum glucose levels should be <160 mg/dL. All images were acquired approximately 1 h later by a PET/CT scanner after intravenous injection of 3.7 MBq/kg of ^{18}F-FDG. Initial guideline scout images were obtained, and non-contrasted CT images were taken for the body regions from the vertex to 1/3 proximal thigh, followed by PET. PET/CT images were taken with mean 7-8 bed positions and 2 mm slices. PET/CT images were re-evaluated independently by two nuclear medicine physicians. The SUV_{max} of the primary tumor lesion was automatically calculated according to the region of interest. The TNM classification was made according to PET/CT data.

Tumor size, presence of axillary node metastasis, and distant metastasis parameters, which are obtained from PET/CT images used for TNM classification, were statistically compared. The obtained SUV_{max} values of the two groups were also compared.

Genotyping of Target *BRCA* Genes

Targeted next-generation sequencing (NGS) of candidate BC-associated genes was performed on blood samples from patients with BC. Total genomic DNA was extracted from whole-blood samples and submitted at recruitment for BRCA1 and BRCA2 genotyping. The mutational profiles of 43 patients with primary breast tumors were correlated with clinicopathological data and compared with individuals without BC (non-BC controls). DHS-102Z Human BRC1 and BRCA2 multiplex amplicon-based library preparation panel and Qiagen Illumina NGS run system (Qiagen, QIAseq, Germany) were used for target gene profiling of breast-cancer-susceptibility genes including BRCA1 and BRCA2. For sequencing, an Illumina HiSeq2500 NDS Platform (Illumina, Little Chesterford, UK; appendix pp. 20-21) was used. In this study, predicted variants of missense, silent, frameshift, non-sense, and other splice site exchanges were defined and confirmed by Sanger sequencing. DNAs were isolated by sample preparation nucleic acid kit (Qiagen, MiniseqMN00813), and amplifications of target breast-cancer-susceptibility genes were performed by QIAseq targeted DNA panel Illumina NGS run and evaluated by QIAseq targeted DNA panel analysis pipeline. All data were interpreted by ingenuity variant analysis. Some variants of uncertain significance (VUS) and/or specific variants were evaluated by ExAC, GnomAD, ClinVAR, Varsome, GERP, LRT, MetaLR, MetaSVM, MutationAssesor, MutationTaster, DANN, dbNSFP.FATHMM, and Provean.

Statistical Analysis

All data analysis was performed using statistical package software SPSS (Statistical Package for Social Sciences) version 20.0. Descriptive data were presented as frequency, percentage, mean, standard deviation, median, minimum, and maximum values. According to the number of patients in the groups, the compatibility of variables to normal distribution was examined using the Shapiro-Wilk test. Non-parametric tests were preferred as the analysis method by examining the sample size and compliance tests with normal distribution. Mann-Whitney U test was used to compare age and continuous variables between groups. Pearson chi-square and Fisher's exact test were used to compare categorical variables between groups. A value of $p<0.05$ was considered significant.

Relationships between PET/CT and histopathological parameters were analyzed with Spearman correlation analysis. Correlation was interpreted as follows: 0.00-0.24, weak; 0.25-0.49, medium; 0.50-0.74, strong; 0.75-1.00, very strong relationship.

Results

The study population consisted of 92 female patients with BC who underwent ^{18}F-FDG PET/CT for primary staging and who also had germline BRCA1 or BRCA2 analysis. The mean age of the patients was 51.13±11.01 (minimum-maximum: 32-78) years. The mean ages of patients in the germline BRCA1 or BRCA2-positive (n=18) and BRCA-negative (n=74) groups were 50.11±11.98 and 51.36±10.86 years, respectively (Table 1). Although the number of patients aged <50 years was higher in the BRCA-positive group (61.1%) than in the BRCA-negative group (50%), the difference was not significant. All patients who were evaluated in this study had a family history of BC. No significant difference was found between both groups in terms of smoking and alcohol use. Other details about the demographic and clinical characteristics of the cohorts are summarized in Table 1.

Table 1 also shows the histopathological types, hormone receptor status, and molecular subtypes for the BC cohort in this study. The mean Ki-67 index was lower in the BRCA-positive group than in the BRCA-negative group, but the difference was not significant (p=0.157). While no significant difference was found between the two groups in terms of histopathological type, grade, and stage of the tumor, differences were found in the molecular subtypes. The rate of hormone receptor (estrogen and/or progesterone) positivity was significantly higher in the BRCA-negative group (82.4%) than in the BRCA-positive group (50%), (p=0.010). The most common subtype was Luminal A (HR+/HER-2-) in 55.4% of the BRCA-negative group, and the difference between the two groups of patients was significant (p=0.024). The least common subtype was HER-2 enriched (HR-/HER-2+) in 2.7% of the BRCA-negative group, and this difference was also significant (p=0.002) (Table 1).

Considering the PET/CT parameters between the groups, the size and SUV_{max} of the primary breast tumor lesion were significantly higher in the BRCA-positive group (p=0.025, p=0.039) according to the TNM criteria. After the diagnosis of cancer, results of PET/CT performed for staging purposes revealed that axillary node involvement was significantly higher in the BRCA-positive group than in the BRCA-negative group (Table 1). However, the presence of distant metastases at the time of primary staging was not significantly different in both groups.

Correlation analyses among SUV_{max}, Ki-67 index, tumor size, tumor grade, tumor stage, and age were performed in all groups. All parameters, except for age, showed a significant correlation with each other at a medium-strong level. These correlation rates were nearly comparable in both groups, so the difference was not significant (Table 2, 3).

In this study, we found a strong correlation between SUV_{max} and Ki-67 values (Table 1, Figure 1). In addition, SUV_{max} correlated moderately with tumor size and highly correlated with tumor grade and stage (Table 1).

Table 2. Significant relationship between SUV_{max} values of histopathological variables such as Ki-67 value, primary tumor size, tumor stage, and age at diagnosis of patients with mutated breast tumors (group 1)

Spearman's correlation analysis group 1 (n=18)	SUV_{max}	Ki-67	Tumor			Age
			Size	Grade	Stage	
SUV_{max} rho p value						
Ki-67 rho p value	**0.678** **<0.001***					
Tumor size rho p value	**0.462** **<0.001***	**0.308** **0.003***				
Tumor grade rho p value	**0.533** **<0.001***	**0.551** **<0.001***	**0.357** **<0.001***			
Tumor stage rho p value	**0.594** **<0.001***	**0.364** **<0.001***	**0.692** **<0.001***	**0.514** **<0.001***		
Age rho p value	-0.069 0.513	0.150 0.154	0.127 0.226	0.034 0.747	0.086 0.415	

*Correlation is significant at the 0.05 level (two-tailed). Rho: Correlation coefficient, p: Spearman correlation analysis, SUV_{max}: Maximum standardized uptake value

Various structural point mutations were detected in *BRCA1* and *BRCA2* genes in the current cohort. In addition, 4 (4.3%) patients showed BRCA1 mutation, 11 (11.9%) showed BRCA2 mutation, and 3 (3.2%) showed mutations in both BRCA1 and BRCA2. No point mutation was detected in the remaining patients (80.5%) with BC (Table 4). Moreover, 2 frameshift and 3 missense point mutations were detected in BRCA1, and 4 frameshift and 12 missense point mutations were detected in BRCA2 (Table 4). All missense and frameshift mutations were located in various exonic frames for both genes. The detected point mutations showed different levels of clinical significance

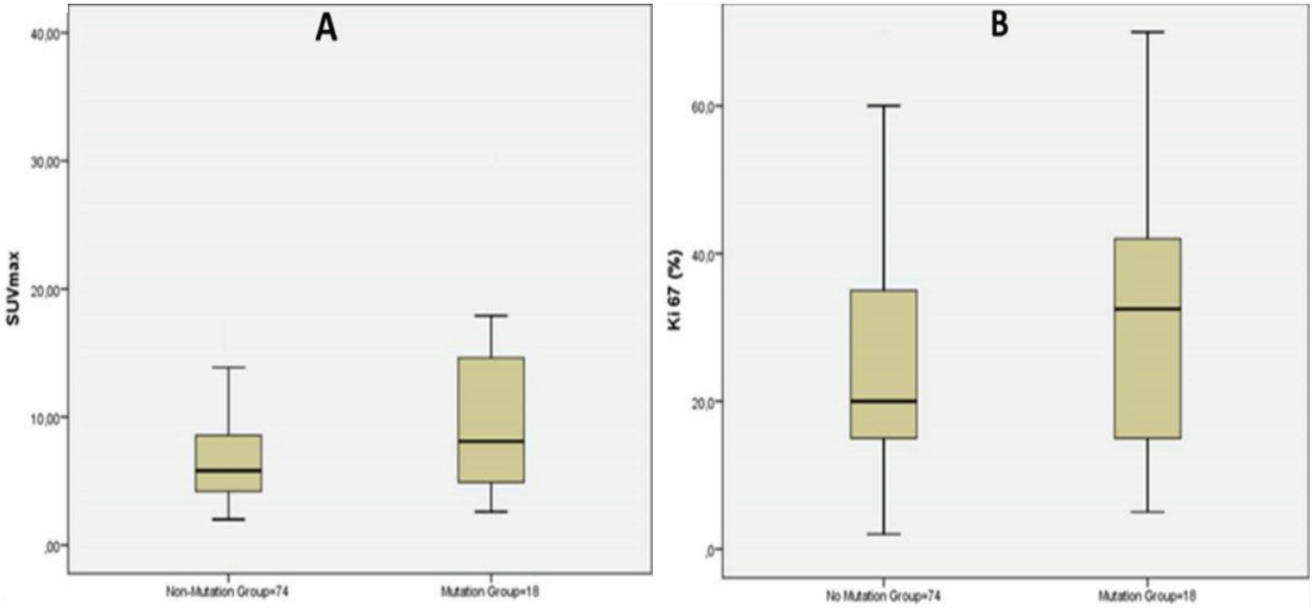

Figure 1. Median SUV_{max} (A) and Ki-67 (B) values between mutated and non-mutated groups
SUV_{max}: Maximum standardized uptake value

Table 3. Significant relationship between the SUV_{max} values of histopathological variables such as Ki-67 value, primary tumor size, tumor stage, and age at diagnosis in patients without mutated breast tumors (group 2)

Spearman's correlation analysis group 2 (n=74)	SUV_{max}	Ki-67	Tumor			Age
			Size	Grade	Stage	
SUV_{max} rho p value						
Ki-67 rho p value	**0.731** **<0.001***					
Tumor size rho p value	**0.379** **<0.001***	**0.397** **0.003***				
Tumor grade rho p value	**0.512** **<0.001***	**0.564** **<0.001***	**0.294** **<0.011***			
Tumor stage rho p value	**0.579** **<0.001***	**0.408** **<0.001***	**0.676** **<0.001***	**0.495** **<0.001***		
Age rho p value	-0.092 0.438	-0.147 0.213	0.051 0.664	-0.027 0.820	0.008 0.947	

*Correlation is significant at the 0.05 level (two-tailed). Rho: Correlation coefficient, p: Spearman correlation analysis, SUV_{max}: Maximum standardized uptake value

when compared with the latest literature findings. One missense point mutation in exon 27 of BRCA2 was likely benign, and five missense point mutation in various exons in BRCA2 were of VUS. Two pathogenic and 16 pathogenic point mutations were detected in the present breast tumor cohort (Table 4).

An example of case of BRCA1-positive BC is shown in Figure 2, 3. Figure 2 shows the NGS mutated profiles for BRCA1 for this case. Figure 3 shows the ^{18}F-FDG PET/CT of axial slices of the same case. In this BRCA1-positive case, the high SUV_{max} and the presence of a conglomerate of metastatic axillary LAP are observed as indicators of poor prognosis.

Discussion

This study was conducted to investigate the prognostic value of BRCA1-2 germline mutations in patients with BC by comparing ^{18}F-FDG PET/CT findings. Various clinical and meta-analytic studies indicate that patients with cancer having a high primary SUV_{max} may have a worse prognosis (16,17,18). Moreover, SUV_{max} has been reported to be a prognostic factor of BC (16,19,20). For example, Kitajima et al. (21) performed a prospective study to compare PET/CT and magnetic resonance imaging findings and reported that the preoperative SUV_{max} of primary BC lesion is a prognostic factor, but not apparent diffusion coefficient. In addition, Ravina et al. (12) claimed that the pretreatment tumor SUV_{max} could be used as an independent imaging biomarker of poor prognosis. In a review study, Caresia Aroztegui et al. (22) revealed that baseline tumor glycolytic activity is associated with biology and prognosis.

Many parameters affecting prognosis such as patient age, tumor size, expression of HER-2, and estrogen and progesterone hormone receptors have also been defined in BC (23,24,25,26). However, data about the effect of BRCA mutation on BC prognosis are limited and varied. Many studies have indicated that the presence of BRCA mutations reduces or does not affect overall survival of patients with BC when compared with those having sporadic BC and even leads to good surveillance (8,10,27,28,29,30). A meta-analysis assessing the association of BRCA mutations with survival in patients with BC claimed that BRCA1 and BRCA2 mutations were associated with poor overall survival in patients with BC, but had no significant impact on BC-specific survival or event-free survival (31). Similarly, Taneja et al. (32) reported that BRCA1/2 carriers with BC often show high nuclear grades and, thus, are associated with poor prognosis.

However, De Talhouet et al. (3) reported that the effect of mutation on prognosis depends on BC subtypes; in the non-triple-negative BC group, the BRCA1/2 mutations did not have any impact on survival, whereas in the triple-negative BC group, BRCA1/2 germline mutations are associated with prolonged survival.

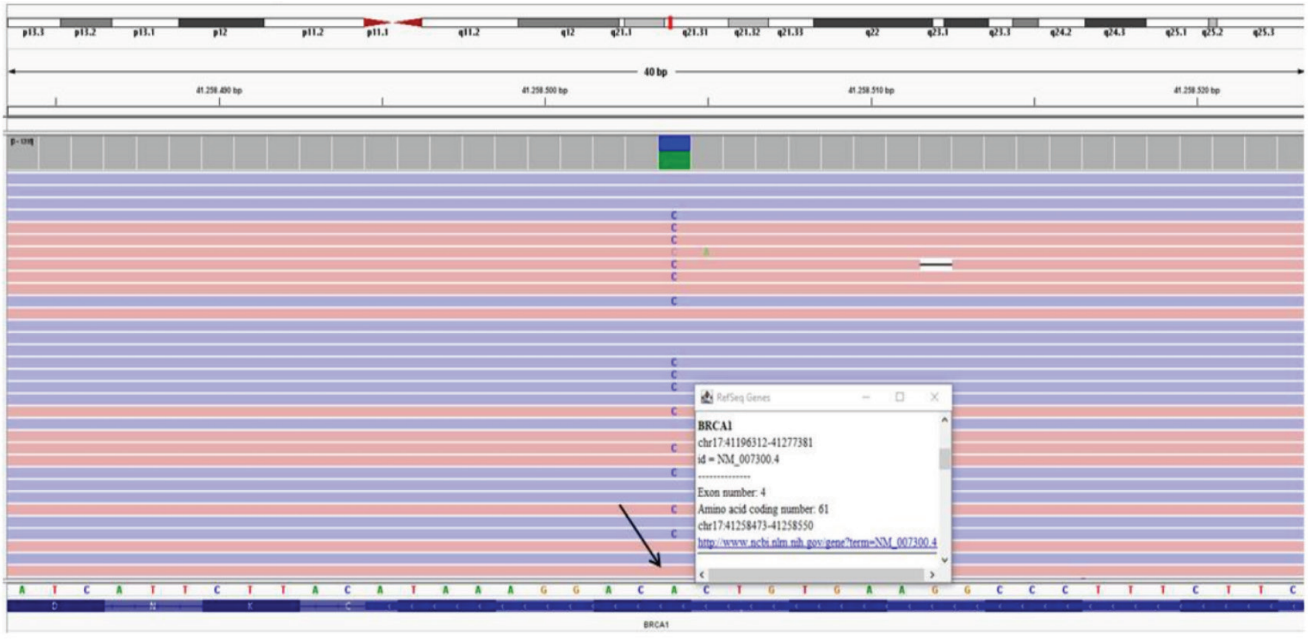

Figure 2. NGS mutated profiles of *BRCA1* gene for a 54-year-old patient with breast cancer. Arrow indicates the germline A>C transversion in codon 61 for exon 4

NGS: Next-generation sequencing

Table 4. Mutated genes, exon, codon, base substitution, mutation type, and clinical significance of germline BRCA1-2 mutation profiles detected in patients with breast cancer

Case no	*BRCA* gene		Mutation		Clinical significance			
	1	2	Location	Type	LB	VUS	PP	P
1	+		Exon 10 c.3835G>A (p.Ala1279Thr)	Missense				+
		+	Exon 27 c.9934A>G (p.lle3312Val)	Missense			+	
2		+	Exon 10 c.943T>A (p.Cys315Ser)	Missense		+		
3		+	Exon 27 c.9976A>T (p.Lys3326Ter)	Missense		+		
4	+		Exon 4 c.181T>G (p.Cys61Gly)	Missense				+
		+	Exon 10 c.1792A>G (p.Thr598Ala)	Missense		+		
5	+		Exon 10 c.2800C>T (p.Q934*)	Frameshift				+
6		+	Exon 11 c.44914_4915insA (p.val1639fs)	Missense				+
7		+	Exon 26 c.9586A>G (p.Lys3196Glu)	Missense				+
8		+	Exon 11 c.6613G>A (p.Val2205Met)	Missense		+		
9		+	Exon 27 c.9934A>G (p.I3312V)	Missense		+		
10		+	Exon 22 c.8940delA (p.Glu298ILysfs*7)	Frameshift				+
11	+		Exon 4 c.182T>G (p.Cys61Gly)	Missense				+
12	+		Exon 11 c.3333delA (p.E1112fs*5)	Frameshift				+
13		+	Exon 19 c.8452G>A (p.Val281Ile)	Missense			+	
14		+	Exon 22 c.8940delA (p.Glu2981Lysfs*8)	Frameshift				+
15		+	Exon 7 c.599C>T (p.Thr200lle)	Missense				+
16	+		Exon 10 c.3333delA (p.Glu1112AsnfsTer5)	Frameshift				+
		+	Exon 27 c.9976A>T (p.Lys3326Ter)	Missense	+			
17	+		Exon 20 c.5329dupC (p.Gln1777fsTer*74)	Frameshift				+
18		+	Exon 11 c.5427C>A (p.Cys1809ter)	Missense				+

LB: Likely benign, VUS: Variants of uncertain significance, PP: Probably pathogenic, P: Pathogenic

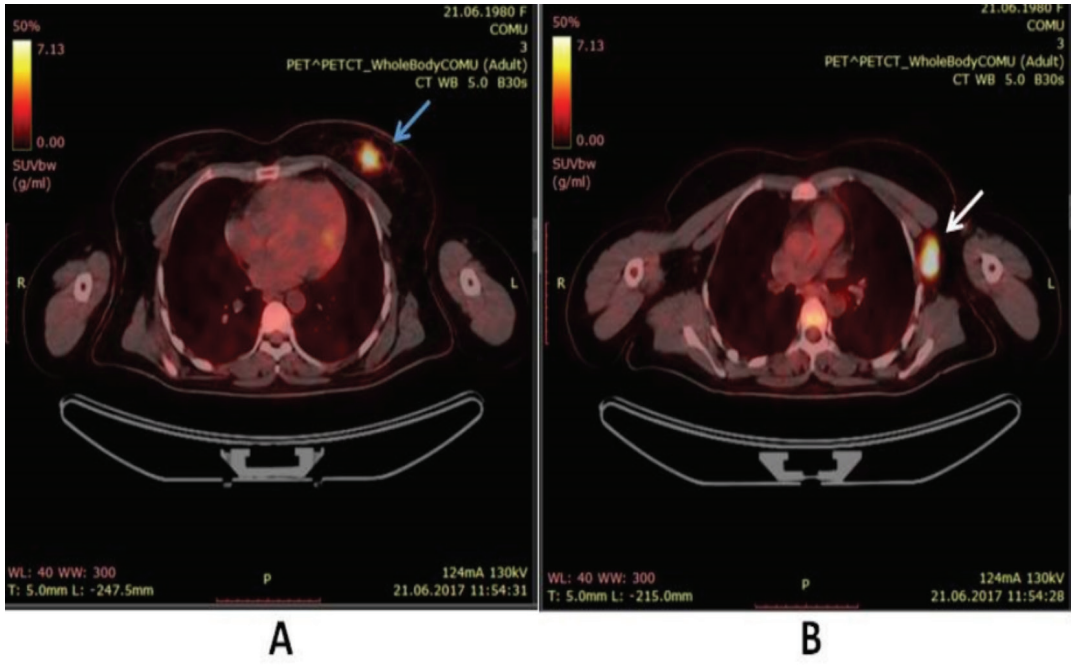

Figure 3. ^{18}F-FDG PET/CT images of axial slices. The blue arrow indicates increased ^{18}F-FDG (SUV_{max} of 8.6) uptake of 25-mm primary breast lesion in the left breast of the patient with germline *BRCA1* gene point mutation shown in Figure 2. The white arrow also indicates increased ^{18}F-FDG (SUV_{max} of 9.7) uptake in conglomerate LAP in left axillary level III in the same case

^{18}F-FDG PET/CT: ^{18}Fluoride-fluorodeoxyglucose positron emission tomography/computed tomography, SUV_{max}: Maximum standardized uptake value

In this study, BRCA mutations were detected in 19.5% of 92 patients with BC. The mutation rate is higher than that in the normal population because *BRCA* gene analyses were performed in patients with a family history of BC. BRCA1/2 germline mutations are more common in patients with a family history of BC. The incidence of BRCA1-2 mutation in unselected patients with BC is 5-10% in most populations. In the literature, the age at BC diagnosis is lower in patients with germline BRCA mutation than in those with sporadic cancer (33,34). However, our cohort consisted of BRCA-positive and wild-type BC cases with positive BC family histories, and no significant difference was found between the groups in terms of age at diagnosis and the number of patients aged <50 years.

The Ki-67 index, which is a cell proliferation marker in predicting BC prognosis, has also been investigated, and conflicting results have been reported. In addition, correlation levels between Ki-67 index and SUV_{max} varied from low to high (35,36,37). The results of the present study showed a strong correlation between SUV_{max} and Ki-67 values. SUV_{max} also correlated moderately with tumor size and highly correlated with tumor grade and stage. The finding of comparable correlation rates between the groups and the lack of difference was consistent with other results.

Remarkably, in the present study, the rate of hormone receptor (estrogen and/or progesterone) positivity was significantly higher in the BRCA-negative group (p=0.010). In the literature, BRCA1 carriers were more likely to be estrogen or progesterone receptor-negative, whereas those with BRCA2-mutated BC were more likely to be estrogen-negative or progesterone-positive (33). However, owing to the small number of our patients, we could not analyze the difference between BRCA1 and BRCA2 in terms of the presence of hormone receptors. Likewise, the most common subtype was Luminal A (HR+/HER-2-) in 55.4% and the least common subtype was HER-2 enriched (HR-/HER-2+) in 2.7% of the BRCA-negative group. Hormone receptor-positive BC has a better prognosis. Therefore, based on this information alone, it would not be wrong to claim that BRCA-negative BC will show a better prognosis. Moreover, the SUV_{max}, which is already used routinely to predict prognosis, was higher in the BRCA-positive group, which supports the prediction of poor prognosis. In addition, the rate of having a larger tumor size and axillary lymph node involvement was higher in the BRCA-positive group than in the BRCA-negative group, and this finding support our claim for a worse prognosis.

In a Chinese cohort, BRCA mutation carriers were more likely to have lymph node involvement upon BC diagnosis.

Even after adjusting the clinical prognostic factors, the results were significantly worse, suggesting that BRCA mutation is an independent factor of poor prognosis (38). Mori et al. (39) also have published similar results that patients with BRCA tumors having a family history of BC were associated with a poor prognosis. Our results were similar to the results of these two studies.

Study Limitations

The major limitation of this study was the small population size. Thus, the results of this study needs to be confirmed by larger-scale studies to clarify the prognostic value of BRCA mutations. In addition, these results should be supported by studies evaluating the relationship of BRCA mutation status with clinical outcomes such as disease-free survival and overall survival.

Conclusion

The prognostic role of germline BRCA1 or BRCA2 point mutations in patients with BC is unclear. In this retrospective study, we analyzed and compared the interdisciplinary laboratory findings derived from 92 patients with BC of which 18 were BRCA mutation carriers. Various structural point mutations were also found, e.g., 6 missense and 15 frameshift mutations were detected in 19.5% of BRCA mutation carriers, and a strong association was found between SUV_{max} values. The results of this study show a strong correlation between BRCA mutations and SUV_{max}, which indicate the poor prognosis of BC. Risk stratification based on this finding can play a very important role in the management of patients with BRCA-positive BC. Based on the current results, it is possible to estimate the strong association of BC-susceptible *BRCA* gene variants with SUV_{max} criteria that indicates the poor prognosis of BC. However, the interpretation of the results of this study are limited by the retrospective study design, high risk of selection bias, lack of data about disease treatment related to BRCA mutation carriers and non-carriers, and the relatively small sample size. The results of this study suggest that germline BRCA1 and BRCA2 mutation status has a significant prognostic value and those remarks are strongly supported by SUV_{max}. Clearly, further prospective and/or retrospective studies with larger sample size are needed to clarify the interdisciplinary laboratory corrections in patients with BC.

Acknowledgments

The authors thank the family members who agreed to participate in this study.

Ethics

Ethics Committee Approval: The study was approved by the Çanakkale Onsekiz Mart University Ethics Committee (protocol no: 2020-04, date: 26.02.2020).

Informed Consent: All patients provided written informed consent.

Peer-review: Externally peer-reviewed.

Authorship Contributions

Surgical and Medical Practices: S.O., Y.A., Concept: S.O., F.S., O.O., Design: S.O., F.S., O.O., Data Collection or Processing: S.O., N.A., F.K.O., I.C., Analysis or Interpretation: S.O., F.K.O., Literature Search: S.O., O.O., F.S., Writing: S.O., O.O.

Conflict of Interest: No conflict of interest was declared by the authors.

Financial Disclosure: The authors declared that this study has received no financial support.

References

1. Baglia ML, Cook LS, Mei-Tzu C, Wiggins C, Hill D, Porter P, Li CI. Alcohol, smoking, and risk of Her2-overexpressing and triple-negative breast cancer relative to estrogen receptor-positive breast cancer. Int J Cancer 2018;143:1849-1857.
2. Brewer HR, Jones ME, Schoemaker MJ, Ashworth A, Swerdlow AJ. Family history and risk of breast cancer: an analysis accounting for family structure. Breast Cancer Res Treat 2017;165:193-200.
3. De Talhouet S, Peron J, Vuilleumier A, Friedlaender A, Viassolo V, Ayme A, Bodmer A, Treilleux I, Lang N, Tille JC, Chappuis PO, Buisson A, Giraud S, Lasset C, Bonadona V, Trédan O, Labidi-Galy SI. Clinical outcome of breast cancer in carriers of BRCA1 and BRCA2 mutations according to molecular subtypes. Sci Rep 2020;10:7073.
4. Kemp Z, Turnbull A, Yost S, Seal S, Mahamdallie S, Poyastro-Pearson E, Warren-Perry M, Eccleston A, Tan MM, Teo SH, Turner N, Strydom A, George A, Rahman N. Evaluation of Cancer-Based Criteria for Use in Mainstream BRCA1 and BRCA2 Genetic Testing in Patients With Breast Cancer. JAMA Netw Open 2019;2:e194428.
5. Kim EK, Park SY, Kim SW. Clinicopathological characteristics of BRCA-associated breast cancer in Asian patients. J Pathol Transl Med 2020;54:265-275.
6. Nicolini A, Ferrari P, Duffy MJ. Prognostic and predictive biomarkers in breast cancer: Past, present and future. Semin Cancer Biol 2018;52:56-73.
7. Huszno J, Kołosza Z, Grzybowska E. BRCA1 mutation in breast cancer patients: Analysis of prognostic factors and survival. Oncol Lett 2019;17:1986-1995.
8. Copson ER, Maishman TC, Tapper WJ, Cutress RI, Greville-Heygate S, Altman DG, Eccles B, Gerty S, Durcan LT, Jones L, Evans DG, Thompson AM, Pharoah P, Easton DF, Dunning AM, Hanby A, Lakhani S, Eeles R, Gilbert FJ, Hamed H, Hodgson S, Simmonds P, Stanton L, Eccles DM. Germline BRCA mutation and outcome in young-onset breast cancer (POSH): a prospective cohort study. Lancet Oncol 2018;19:169-180.
9. van den Broek AJ, Schmidt MK, van 't Veer LJ, Tollenaar RA, van Leeuwen FE. Worse breast cancer prognosis of BRCA1/BRCA2 mutation carriers: what's the evidence? A systematic review with meta-analysis. PLoS One 2015;10:e0120189.
10. Baretta Z, Mocellin S, Goldin E, Olopade OI, Huo D. Effect of BRCA germline mutations on breast cancer prognosis: A systematic review and meta-analysis. Medicine (Baltimore) 2016;95:e4975.

11. Ulaner GA, Castillo R, Goldman DA, Wills J, Riedl CC, Pinker-Domenig K, Jochelson MS, Gönen M. (18)F-FDG-PET/CT for systemic staging of newly diagnosed triple-negative breast cancer. Eur J Nucl Med Mol Imaging 2016;43:1937-1944.
12. Ravina M, Saboury B, Chauhan MS, Jacob MJ, Pandit AG, Sanchety N, Werner TJ, Alavi A. Utility of 18 F-FDG PET/CT in pre-surgical risk stratification of patients with breast cancer. Hell J Nucl Med 2019;22:165-171.
13. Kang S, Kim EH, Hwang JE, Shin JH, Jeong YS, Yim SY, Joo EW, Eun YG, Lee DJ, Sohn BH, Lee SH, Lim B, Lee JS. Prognostic significance of high metabolic activity in breast cancer: PET signature in breast cancer. Biochem Biophys Res Commun 2019;511:185-191.
14. Has Şimşek D, Şanli Y, Külle CB, Karanlik H, Kiliç B, Kuyumcu S, Önder S, Özmen V. Correlation of 18F-FDG PET/CT with pathological features and survival in primary breast cancer. Nucl Med Commun 2017;38:694-700.
15. Diao W, Tian F, Jia Z. The prognostic value of SUVmax measuring on primary lesion and ALN by 18F-FDG PET or PET/CT in patients with breast cancer. Eur J Radiol 2018;105:1-7.
16. Yoo J, Yoon HJ, Kim BS. Prognostic value of primary tumor SUVmax on F-18 FDG PET/CT compared with semi-quantitative tumor uptake on Tc-99m sestamibi breast-specific gamma imaging in invasive ductal breast cancer. Ann Nucl Med 2017;31:19-28.
17. Pahk K, Joung C, Kim S. Visceral fat metabolic activity evaluated by preoperative 18F-FDG PET/CT significantly affects axillary lymph node metastasis in postmenopausal luminal breast cancer. Sci Rep 2020;10:1348.
18. Refaat R, Abd Alkhalik Basha M, Sobhi Hassan M, Hussein RS, Al-Molla RM, Awad NM, Elkholy E. Is FDG maximum standardized uptake value of primary breast cancer a prognostic factor for locoregional axillary lymph node metastasis? Acta Radiol 2019;60:1241-1250.
19. Taghipour M, Wray R, Sheikhbahaei S, Wright JL, Subramaniam RM. FDG Avidity and Tumor Burden: Survival Outcomes for Patients With Recurrent Breast Cancer. AJR Am J Roentgenol 2016;206:846-855.
20. Ahn SG, Park JT, Lee HM, Lee HW, Jeon TJ, Han K, Lee SA, Dong SM, Ryu YH, Son EJ, Jeong J. Standardized uptake value of ^{1} F-fluorodeoxyglucose positron emission tomography for prediction of tumor recurrence in breast cancer beyond tumor burden. Breast Cancer Res 2014;16:502.
21. Kitajima K, Miyoshi Y, Yamano T, Odawara S, Higuchi T, Yamakado K. Prognostic value of FDG-PET and DWI in breast cancer. Ann Nucl Med 2018;32:44-53.
22. Caresia Aroztegui AP, García Vicente AM, Alvarez Ruiz S, Delgado Bolton RC, Orcajo Rincon J, Garcia Garzon JR, de Arcocha Torres M, Garcia-Velloso MJ; Oncology Task Force of the Spanish Society of Nuclear Medicine and Molecular Imaging. 18F-FDG PET/CT in breast cancer: Evidence-based recommendations in initial staging. Tumour Biol 2017;39:1010428317728285.
23. Allison KH, Hammond MEH, Dowsett M, McKernin SE, Carey LA, Fitzgibbons PL, Hayes DF, Lakhani SR, Chavez-MacGregor M, Perlmutter J, Perou CM, Regan MM, Rimm DL, Symmans WF, Torlakovic EE, Varella L, Viale G, Weisberg TF, McShane LM, Wolff AC. Estrogen and Progesterone Receptor Testing in Breast Cancer: ASCO/CAP Guideline Update. J Clin Oncol 2020;38:1346-1366.
24. Park C, Park K, Kim J, Sin Y, Park I, Cho H, Yang K, Bae BN, Kim KW, Ahn S, Gwak G. Prognostic values of negative estrogen or progesterone receptor expression in patients with luminal B HER2-negative breast cancer. World J Surg Oncol 2016;14:244.
25. Li S, Wu J, Huang O, He J, Zhu L, Chen W, Li Y, Chen X, Shen K. HER2 positivity is not associated with adverse prognosis in high-risk estrogen receptor-positive early breast cancer patients treated with chemotherapy and trastuzumab. Breast 2020;54:235-241.
26. Provencher L, Diorio C, Hogue JC, Doyle C, Jacob S. Does breast cancer tumor size really matter that much? Breast 2012;21:682-685.
27. Maksimenko J, Irmejs A, Nakazawa-Miklasevica M, Melbarde-Gorkusa I, Trofimovics G, Gardovskis J, Miklasevics E. Prognostic role of BRCA1 mutation in patients with triple-negative breast cancer. Oncol Lett 2014;7:278-284.
28. Ruiz de Sabando A, Urrutia Lafuente E, García-Amigot F, Alonso Sánchez A, Morales Garofalo L, Moreno S, Ardanaz E, Ramos-Arroyo MA. Genetic and clinical characterization of BRCA-associated hereditary breast and ovarian cancer in Navarra (Spain). BMC Cancer 2019;19:1145.
29. Song Y, Barry WT, Seah DS, Tung NM, Garber JE, Lin NU. Patterns of recurrence and metastasis in BRCA1/BRCA2-associated breast cancers. Cancer 2020;126:271-280.
30. Zhu Y, Wu J, Zhang C, Sun S, Zhang J, Liu W, Huang J, Zhang Z. BRCA mutations and survival in breast cancer: an updated systematic review and meta-analysis. Oncotarget 2016;7:70113-70127.
31. Jacot W, Lopez-Crapez E, Mollevi C, Boissière-Michot F, Simony-Lafontaine J, Ho-Pun-Cheung A, Chartron E, Theillet C, Lemoine A, Saffroy R, Lamy PJ, Guiu S. BRCA1 Promoter Hypermethylation is Associated with Good Prognosis and Chemosensitivity in Triple-Negative Breast Cancer. Cancers (Basel) 2020;12:828.
32. Taneja P, Maglic D, Kai F, Zhu S, Kendig RD, Fry EA, Inoue K. Classical and Novel Prognostic Markers for Breast Cancer and their Clinical Significance. Clin Med Insights Oncol 2010;4:15-34.
33. Foulkes WD, Metcalfe K, Sun P, Hanna WM, Lynch HT, Ghadirian P, Tung N, Olopade OI, Weber BL, McLennan J, Olivotto IA, Bégin LR, Narod SA. Estrogen receptor status in BRCA1- and BRCA2-related breast cancer: the influence of age, grade, and histological type. Clin Cancer Res 2004;10:2029-2034.
34. Rosenberg SM, Ruddy KJ, Tamimi RM, Gelber S, Schapira L, Come S, Borges VF, Larsen B, Garber JE, Partridge AH. BRCA1 and BRCA2 Mutation Testing in Young Women With Breast Cancer. JAMA Oncol 2016;2:730-736.
35. Surov A, Meyer HJ, Wienke A. Associations Between PET Parameters and Expression of Ki-67 in Breast Cancer. Transl Oncol 2019;12:375-380.
36. Soliman NA, Yussif SM. Ki-67 as a prognostic marker according to breast cancer molecular subtype. Cancer Biol Med 2016;13:496-504.
37. Deng SM, Zhang W, Zhang B, Chen YY, Li JH, Wu YW. Correlation between the Uptake of 18F-Fluorodeoxyglucose (18F-FDG) and the Expression of Proliferation-Associated Antigen Ki-67 in Cancer Patients: A Meta-Analysis. PLoS One 2015;10:e0129028.
38. Chen L, Fu F, Huang M, Lv J, Zhang W, Wang C. The spectrum of BRCA1 and BRCA2 mutations and clinicopathological characteristics in Chinese women with early-onset breast cancer. Breast Cancer Res Treat 2020;180:759-766.
39. Mori H, Kubo M, Kai M, Velasquez VV, Kurata K, Yamada M, Okido M, Kuroki S, Oda Y, Nakamura M. BRCAness Combined With a Family History of Cancer Is Associated With a Poor Prognosis for Breast Cancer Patients With a High Risk of BRCA Mutations. Clin Breast Cancer 2018;18:e1217-e1227.

Original Article
Mol Imaging Radionucl Ther 2021;30:169-176 DOI:10.4274/mirt.galenos.2021.26056

The Comparison of Quantitative Evaluation Results of the MPS SPECT/CT and Coronary Angiography: Determining the Most Valuable Quantitative Evaluation Score

MPS SPECT/BT Kantitatif Değerlendirme Sonuçlarının Koroner Anjiyografi Sonuçları ile Karşılaştırılması: En Değerli Kantitatif Değerlendirme Skorunun Belirlenmesi

Nazlı Pınar Karahan Şen[1], Recep Bekis[1], Bihter Şentürk[2], Bahri Akdeniz[2]

[1]*Dokuz Eylül University Faculty of Medicine, Department of Nuclear Medicine, İzmir, Turkey*
[2]*Dokuz Eylül University Faculty of Medicine, Department of Cardiology, İzmir, Turkey*

Abstract

Objectives: This study aimed to determine the most important perfusion score in patient selection for coronary angiography (CA) by quantitatively evaluating myocardial perfusion scintigraphy (MPS).

Methods: Patients who underwent MPS single-photon emission computerized tomography/computed tomograph imaging in our clinic between December 2017 and January 2019, without coronary artery disease (CAD) history, followed by CA were included in the study. CA was considered positive when there is a stenosis of 70% or more in at least one coronary vessel. The summed stress score, rest score, and differential score; total perfusion deficit (TPD); and the defect's extent obtained from non-attenuation-corrected (NC) and attenuation-corrected (AC) images of 80 patients were evaluated using the Mann-Whitney U test. A p value of <0.05 was considered significant. Receiver operating characteristic (ROC) analysis was performed.

Results: The scores obtained from NC and AC images showed a significant difference between the two groups for all scores except for the extent and TPD scores at rest from AC images. The applied ROC curves' highest diagnostic value was determined as the TPD score at stress (TPDS) obtained from NC images (area under the curve: 0.880, 95% confidence interval, 0.807-0.952, p<0.001). The cut-off value obtained for the TPDS from the ROC curve was found to be 5.5.

Conclusion: The scores obtained from NC images have more power to detect CAD than those obtained from AC images. Patients with no prior CAD history with TPDS score higher than 5 in MPS should be referred for CA with priority.

Keywords: Myocardial perfusion imaging, SPECT/CT, coronary angiography

Öz

Amaç: Bu çalışmada miyokard perfüzyon sintigrafisinin (MPS) kantitatif değerlendirilmesiyle koroner anjiyografi (KAG) yapılacak hastalarının seçiminde en önemli perfüzyon skorunun belirlenmesi amaçlandı.

Yöntem: Aralık 2017-Ocak 2019 tarihleri arasında kliniğimizde MPS tek foton emisyon tomografisi/bilgisayarlı tomografi (SPECT/BT) görüntüleme uygulanan ve daha önce koroner arter hastalığı (KAH) tanısı bulunmayan ve MPS sonrası KAG yapılan hastalar çalışmaya dahil edildi. KAG sonucunda en az bir koroner damarda %70 veya daha fazla darlık izlenen hastalar koroner arter darlığı (KAD) açısından pozitif kabul edildi. Seksen hastanın atenüasyon düzeltilmemiş (NC) ve SPECT/BT ile atenüasyon düzeltilmiş (AC) görüntülerden elde edilen toplam stres skoru, toplam rest skoru, toplam perfüzyon bozukluğu ve extent puanları Mann-Whitney U testi ile değerlendirildi. P<0,05 değeri anlamlı kabul edildi. Alıcı işlem karakteristikleri (ROC) analizi yapıldı.

Address for Correspondence: Nazlı Pınar Karahan Şen MD, Dokuz Eylül University Faculty of Medicine, Department of Nuclear Medicine, İzmir, Turkey
Phone: +90 232 412 42 90 **E-mail:** drpinarkarahan@hotmail.com ORCID ID: orcid.org/0000-0002-1562-9085
Received: 15.02.2021 **Accepted:** 03.07.2021

Bulgular: NC ve AC görüntülerinden elde edilen skorlar, ExtentRac ve TPDRac dışındaki tüm skorlar için iki grup arasında anlamlı fark görüldü. ROC eğrilerindeki en yüksek tanı değeri NC görüntülerinden elde edilen TPDS değeri olarak belirlendi (eğrinin altında kalan alan: 0,880, %95 güven aralığı, 0,807-0,952, p<0,001). TPDS için ROC eğrisinden elde edilen kesim değeri 5,5 olarak bulundu.

Sonuç: NC görüntülerden elde edilen skorların AC görüntülerden elde edilen skorlara göre daha fazla KAD saptama gücü vardır. Daha önceden bilinen KAH olmayan ve MPS'de TPDS skoru 5'in üzerinde olan hastalar KAG'ye öncelikli olarak yönlendirilmelidir.

Anahtar kelimeler: Miyokard perfüzyon görüntüleme, SPECT/BT, koroner anjiyografi

Introduction

Coronary artery disease (CAD) is a result of atherosclerosis of coronary arteries, which restricts the heart's blood flow (1,2). Myocardial ischemia can occur, and patients may experience ischemic symptoms like typical angina, depending on the degree of the coronary artery stenosis. Myocardial perfusion scintigraphy (MPS) is one of the frequently used non-invasive diagnostic tests of CAD. An unbalanced cardiac oxygen support mechanism in CAD results in ischemia, which causes a reversible perfusion defect occurring in scintigraphy images (3). Coronary angiography (CA) is the gold standard method for CAD diagnosis. Since it is an invasive and expensive method and carries the mortality risks, selecting patients suitable for CA is important (4,5).

Scanning MPS with computerized tomography (CT) combined with gated single-photon emission computerized tomography (SPECT/CT) is an emerging technique (6,7). CT being part of the SPECT/CT allows attenuation correction from the emission by extracardiac tissues and reduces false positive rates (8,9,10). Both attenuation-corrected (AC) and non-attenuation-corrected (NC) images are obtained from SPECT/CT. MPS is currently interpreted as ischemia positive or negative according to the presence of a reversible perfusion defect. Alternatively, several scores obtained from scintigraphy images depict ischemia severity or extent, such as summed stress score (SSS), rest score (SRS), and differential score (SDS); total perfusion deficit (TPD); and extent of the defect (11,12,13). While scores are calculated using automatic programs, each image requires comparison with its own normal data; therefore, scores from AC and NC images may differ. The question is that which score is valuable or do the scores have advantages over each other? We investigated patients who underwent MPS and subsequently CA. We evaluated the mentioned perfusion scores obtained from AC and NC images to identify these scores' relation with CA results and to determine the cut-off value for the most relevant score.

Materials and Methods

Study Design

This study was designed as a retrospective study.

Study Population

Patients who underwent MPS between November 2017 and February 2020 at our institution were retrospectively evaluated. Those without prior CAD history and underwent CA recently (in >6 months) after MPS were included in this study, which was approved ethically at our institution (Dokuz Eylül University Non-interventional Research Ethics Committee protocol number: 5448-GOA, decision number: 01.06.2020, 2020/11-06).

Study Protocol

Patients underwent a 1-day rest/stress or 2-day stress/rest MPS protocol. MPSs were performed using a SPECT/CT scanner (GE Healthcare). Patients discontinued beta-blockers and calcium channel blockers 48 h before the study, and nitrate derivative drugs were stopped for 24 h. Following a 6-h fasting period, MPS was performed. In the 1-day protocol rest, images were obtained 1 h after the injection of 8 millicuries (mCi) technetium-99m methoxy-isobutyl-isonitrile (Tc-99m-MIBI). Three hours after the rest procedure, exercise stress tests were performed on a treadmill following the BRUCE protocol. Those who could not tolerate exercise stress test, pharmacological stress test was applied with adenosine. The dobutamine stress test was preferred if the patient had dyspnea and could not tolerate the treadmill. Patients who reached 85% of the target heartbeat [(220 - age in years) × 85%] were included in the study. Stress images were obtained 30 min after 22 mCi of Tc-99m-MIBI was injected. On the first day of the 2-day protocol, patients were imaged after stress protocol with 22-mCi activity; then on another day, rest procedures were done with 22 mCi of Tc-99m-MIBI. Because both protocols have equal diagnostic value, their MPS images were included in the study (8). Patients with prior CAD history and inadequate stress test were excluded. Consequently, 80 patients were included in the study.

Rest and stress images were processed and quantitatively assessed using the Xeleris and Quantitative Perfusion SPECT (QPS) program based on a 20-segment scoring model. QPS gives scores automatically using a five-point scoring system according to the radiopharmaceutical uptake degree (0, normal; 1, mildly decreased; 2, moderately decreased; 3, severely decreased; and 4,

absence of segmental uptake) in both images. SSS, SRS, SDS, TPD, and extent values from rest (TPDR, ExtentR) and stress (TPDS, ExtentS) images are the scores automatically derived from the images. SSS and SRS provide information about hipoperfusion areas and the degree of perfusion deficient of stress and rest images, respectively. SDS is the difference between SSS and SRS. TPD represents the extent and severity of the perfusion defect. The scores obtained from NC (SSS, SRS, SDS, TPDR, TPDS, ExtentR, ExtentS) and AC images (SSSac, SRSac, SDSac, TPDRac, TPDSac, ExtentRac, ExtentSac) were recorded. In addition to the quantitative analysis of MPS, patients' CA reports were retrospectively evaluated. A significant CAD was determined as ≥70% stenosis of at least one coronary artery (left anterior descending artery, left circumflex artery, and right coronary artery) or ≥50% narrowing in the left main coronary artery (14).

Statistical Analysis

Statistical Package for the Social Sciences software version 24.0 for Windows was used to analyze the data. CA results; SSS, SRS, SDS, TPDS, and TPDR; and ExtentS and ExtentR scores from AC and NC images were evaluated using the Mann-Whitney U test. A p value of <0.05 was considered as significant. Receiver operating characteristic (ROC) analyses were performed for the scores. An area under the curve (AUC) of >0.5 was accepted as worthwhile. A cut-off value was obtained from the score with the highest AUC.

Results

Fifty-one patients were female and 29 were male, with mean age of 60.4±12.4 years (32-89 years). Among the 80 patients, 32 were CAD-positive, with mean scores detected as SSS, 13.53 (3-43); SRS, 6.00 (0-36); SDS, 6.90 (0-29); ExtentR, 10.18 (0-49); TPDR, 8.90 (1-44); ExtentS, 17.96 (3-48); TPDS, 14.87 (4-41); SSSac, 13.62 (2-40); SRSac, 5.15 (0-29); SDSac, 8.15 (2-19); ExtentRac, 7.28 (0-37); TPDRac, 6.34 (0-33); ExtentSac, 18.12 (0-49); and TPDSac, 14.15 (0-38). The mean range of all scores derived from both images was significantly higher in the CAD-positive group than the CAD-negative group ($p<0.05$) except TPDRac and ExtentRac. The results are demonstrated in Table 1. ROC analyses demonstrated that, for AC and NC images, both TPDS have the highest AUC value among the scores (0.817 and 0.880, TPDSac and TPDS, respectively). Also, AUC values of the scores from NC images were detected at higher values than those from AC images. Among all scores, TPDS derived from NC images was determined as having the highest AUC value (AUC: 0.880) (Table 2). According to the Youden index with 84.4% sensitivity and 75% specificity, the ROC curve analysis of TPDS derived from NC images provided a 5.5 cut-off value in predicting CAD (Figures 1, 2, 3).

Discussion

Our study results demonstrated the usefulness of the MPS quantitative scores in detecting significant CAD. The scores

Table 1. Univariate analysis results of the scores using the Mann-Whitney U test

	All patients' mean (n=80)	CA (-) mean (n=48)	CA (+) mean (n=32)	p value	AUC
SSS	8.17 (0-43)	4.60 (0-19)	13.53 (3-43)	0.000	0.855
SRS	3.40 (0-36)	1.66 (0-11)	6.00 (0-36)	0.000	0.735
SDS	4.47 (0-29)	2.85 (0-10)	6.90 (0-29)	0.000	0.764
ExtentR	6.77 (0-49)	4.50 (0-27)	10.18 (0-49)	0.027	0.646
TPDR	6.07 (0-44)	4.18 (0-21)	8.90 (1-44)	0.004	0.691
ExtentS	10.16 (0-48)	4.95 (0-26)	17.96 (3-48)	0.000	0.873
TPDS	8.75 (0-41)	4.66 (0-21)	14.87 (4-41)	0.000	0.880
SSSac	8.81 (0-40)	5.60 (0-27)	13.62 (2-40)	0.000	0.788
SRSac	2.91 (0-29)	1.41 (0-11)	5.15 (0-29)	0.001	0.715
SDS ac	5.72 (0-19)	4.10 (0-16)	8.15 (2-19)	0.000	0.741
ExtentRac	5.78 (0-37)	4.79 (0-34)	7.28 (0-37)	0.346	0.562
TPDRac	5.20 (0-33)	4.43 (0-26)	6.34 (0-33)	0.258	0.575
ExtentSac	10.76 (0-49)	5.85 (0-36)	18.12 (0-49)	0.000	0.816
TPDSac	8.67 (0-38)	5.02 (0-24)	14.15 (0-38)	0.000	0.817

AC: Attenuation-corrected, AUC: Area under curve, CA (-): Coronary angiography negative, CA (+): Coronary angiography positive, CI: Confidence interval, ExtentR: Extent rest, ExtentS: Extent stress, n: Number of patients, SDS: Summed differential score, SRS: Summed rest score, SSS: Summed stress score, TPDR: Total perfusion deficit rest, TPDS: Total perfusion deficit stress

Table 2. ROC analysis results of the scores					
Score	**AUC**	**p**	**Sensitivity**	**Specificity**	**Cut-off**
SSS	0.855 (0.775-0.935, 95% CI)	0.000	90.6%	70.8%	4.5
SRS	0.735 (0.623-0.846, 95% CI)	0.000	84.4%	58.3%	0.5
SDS	0.764 (0.656-0.871, 95% CI)	0.000	59.4%	83.3%	4.5
ExtentR	0.646 (0.519-0.772, 95% CI)	0.028	50%	77.1%	6.5
TPDR	0.691 (0.574-0.809, 95% CI)	0.004	50%	81.3%	6.5
ExtentS	0.873 (0.798-0.948, 95% CI)	0.000	90.6%	70.8%	5.5
TPDS	0.880 (0.807-0.952, 95% CI)	0.000	84.4%	75%	5.5
SSSac	0.788 (0.691-0.886, 95% CI)	0.000	71.9%	72.9%	7.5
SRSac	0.715 (0.598-0.832, 95% CI)	0.001	75%	60.4%	0.5
SDS ac	0.741 (0.635-0.847, 95% CI)	0.000	100%	41.7%	1.5
ExtentRac	0.562 (0.429-0.694, 95% CI)	0.351	40.6%	77.1%	6.5
TPDRac	0.575 (0.445-0.704, 95% CI)	0.261	21.9%	95.8%	11.5
ExtentSac	0.816 (0.723-0.910, 95% CI)	0.000	81.3%	72.9%	5.5
TPDSac	0.817 (0.723-0.912, 95% CI)	0.000	75%	79.2%	7.5

AC: Attenuation-corrected, AUC: Area under curve, CI: Confidence interval, ExtentR: Extent rest, ExtentS: Extent stress, SDS: Summed differential score, SRS: Summed rest score, SSS: Summed stress score, TPDR: Total perfusion deficit rest, TPDS: Total perfusion deficit stress

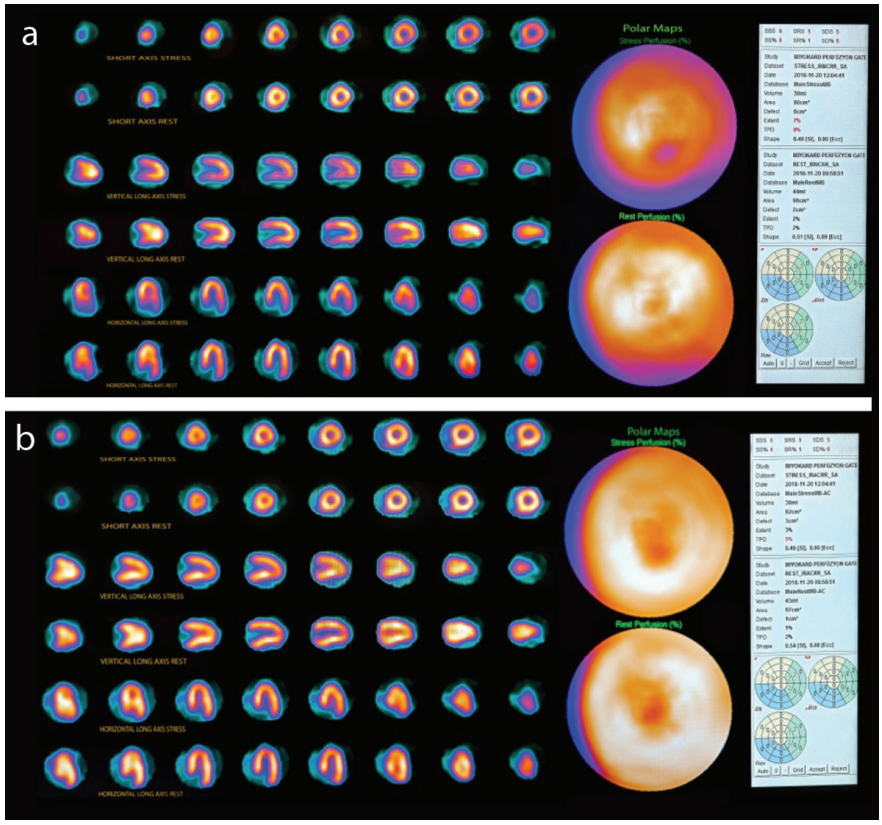

Figure 1. NC (a) and AC (b) MPS images of a 65-year-old male patient. The patient's TPDS and TPDSac scores are 6% and 5%. The patient is CAD positive according to NC images but negative in AC images. Angiography results demonstrated >70% narrowing in the LAD and RCA

LAD: Left anterior descending artery, RCA: Right coronary artery, NC: Non-attenuation-corrected, AC: Attenuation-corrected, MPS: Myocardial perfusion scintigraphy, CAD: Coronary artery disease

obtained from both images were evaluated with the CA results. It was detected that the scores from NC images have higher AUC values than those from the AC images. Furthermore, while TPDS scores demonstrated the highest significance in both images, TPDS from NC images has the highest discriminative values to detect significant CAD among the scores.

MPS is a diagnostic imaging method in which quantitative data can be obtained using programs allowing image comparison with normal data in memory using an automatic scoring system. SSS, SRS, and SDS and TPD scores are derived automatically from the segmentation of perfusion maps. Various studies have been conducted to obtain an MPS diagnostic value by comparing the main scores obtained from the polar map with methods, such as CA, fractional flow reserve, or CT angiography (15,16,17,18).

One of the major deficiencies in planar images is imaging artifacts, occurring due to patient motion, photon attenuation (breast attenuation in women and diaphragmatic attenuation in men), or extracardiac activity in the region of interest. They could mimic true abnormalities, and artifacts could be challenging while interpreting the reports (19). The widespread SPECT/CT use to prevent attenuation artifacts increased the use of AC images in MPS interpretation (20,21). The evaluation of AC images is similar to NC images, but the interpreting physician should be familiar with the AC images (22). Quantitative evaluation of the images plays an important role in the interpretation. It is recommended to report the defect's extent and severity. The scores obtained from both images could be different from each other. Therefore, knowing the difference between the scores is important to predict CAD using quantitative analyses. There are studies with different results in this regard (23,24,25,26). In a study, which evaluated the scores from both images (17), ROC analysis results were similar to our study. For SSS, SDS, and TPDS from NC images, AUC values were minimally higher than the scores obtained from AC images. Similarly, TPDS from NC images (AUC: 0.87) has the highest AUC to detect significant CAD. Xu et al. (21) reported similar AUC (0.87) values in their study for TPD from both images. On the other hand, a study compared automatic and visual evaluation of MPS.

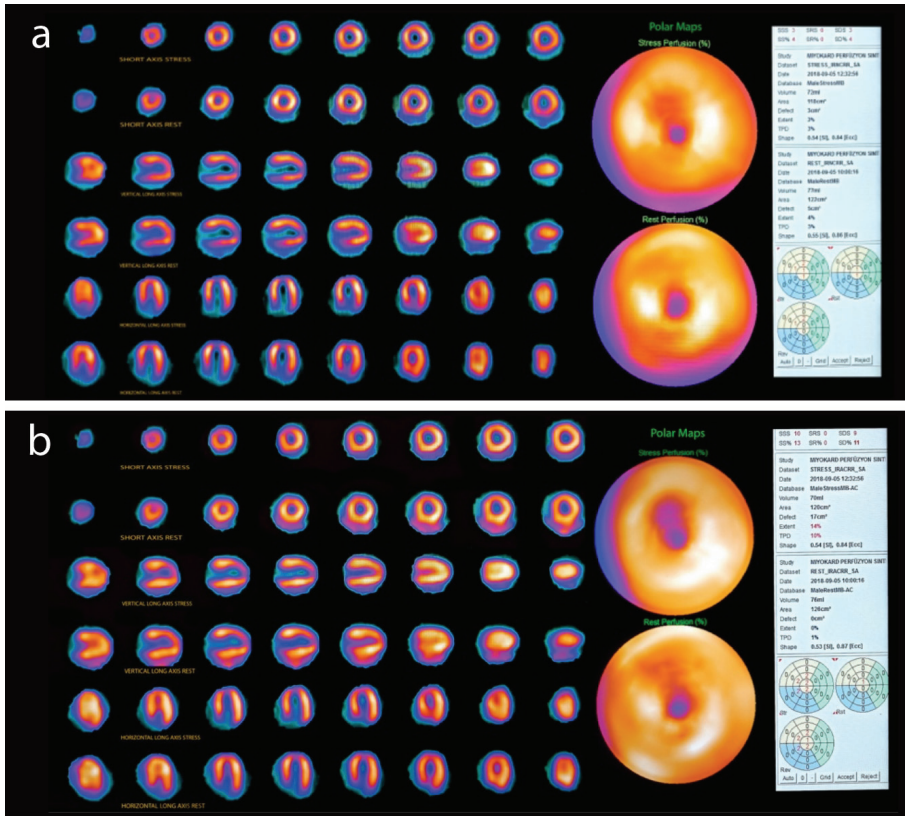

Figure 2. NC (a) and AC (b) MPS images of a 54-year-old male patient. TPDS and TPDSac scores were 3% and 10%. The patient is CAD negative according to NC images but positive in AC images. Angiography results were found to be normal

NC: Non-attenuation-corrected, AC: Attenuation-corrected, MPS: Myocardial perfusion scintigraphy, TPDS: Total perfusion deficit stress, CAD: Coronary artery disease

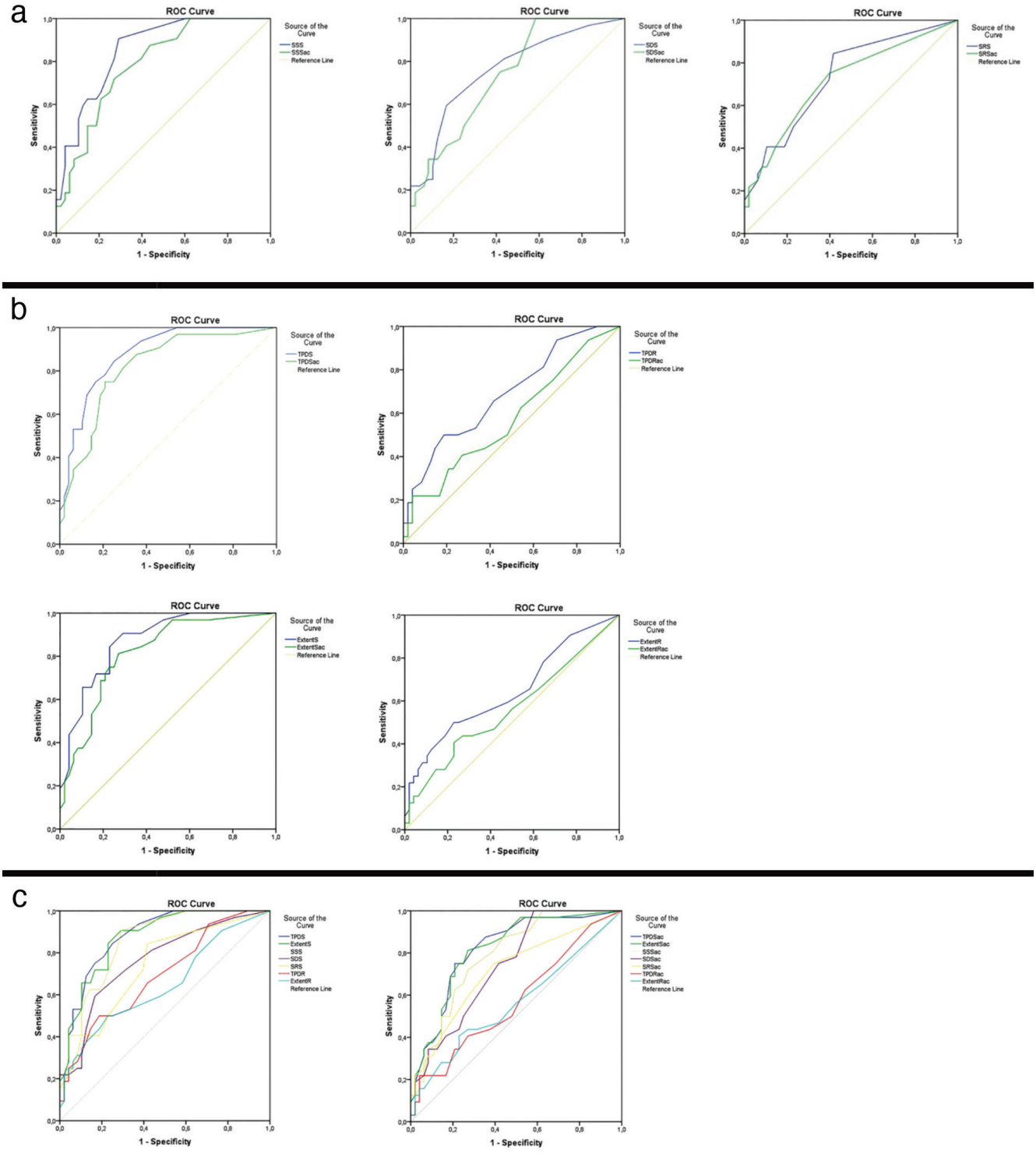

Figure 3. ROC curves of the scores: SSS, SDS, and SRS (a); TPDS, TPDR, ExtentS, and ExtentR (b); and all scores in one curve (c). Both scores obtained from AC and NC images were demonstrated

ROC: Receiver operating characteristic, SDS: Summed differential score, SRS: Summed rest score, SSS: Summed stress score, TPDS: Total perfusion deficit stress, TPDR: Total perfusion deficit rest, NC: Non-attenuation-corrected, AC: Attenuation-corrected

Arsanjani et al. (26) demonstrated a higher AUC value for TPD score from AC images in detecting significant CAD from our results (AUC: 0.92 with 84% sensitivity and 88% specificity) and detected AUC of 0.91 for TPD score from NC images with 83% sensitivity and a higher specificity than our results (81% vs. 75%). Unlike our study, they suggest scores from AC images were found to have more diagnostic power than those from NC images. Also, none of these studies mentioned of determining a cut-off value for TPD.

A study evaluated coronary vessels separately, with cut-off values determined as 8.5, 4.5, and 3.5 for TPD stress, rest, and difference, respectively (15). Another study determined cut-off values as ≥5.5 (SSS), ≥2.5 (SDS), and ≥9.5 (TPDS) to predict significant CAD (16). The AUC sensitivity and specificity values calculated for the TPD scores of our study were found to be higher than those in these studies. This difference is thought to be due to the results, which can be changed according to the processes or artifacts like motion.

There are studies related to SSS and SDS (21,27,28). Some studies suggest that SDS above 1 is an evaluable finding favoring ischemia, and some suggest a cut-off value ≥2 for SDS to determine CAD (21,27). Also, it has been reported that SSS above 4 increases the risk of cardiac events (28). However, the reproducibility of differential scores is accepted to be lower. SSS >4 was demonstrated to significant CAD with 86% sensitivity and 82% specificity, similar to our results (90.6% sensitivity, 70.8% specificity, SSS cut-off value of 4.5) (29).

The use of TPD value provides a quantitative evaluation and contributes to the visual evaluation, increasing reproducibility and reducing interobserver variability (30). TPD with ≥5% threshold was accepted for patients to undergo coronary intervention in the COURAGE study (31). However, there are studies suggesting a slightly higher TPD threshold (>7%) in MPS to detect significant ischemia. Our study demonstrates that the majority of true positive patients in MPS (84.4%) had a TPD score from NC images ≥5.5. These findings suggested that, if TPDS score in patients referred for MPS is >5, CA results are high, probably positive in terms of severe CAD in at least one coronary artery.

Using CT, a patient's low-dose extra radiation exposure could be seen as a minimal disadvantage of AC images (32). Nevertheless, studies have reported that AC image addition to the NC data improves significant CAD diagnosis. In visual evaluation, both images together provide better results than NC images only (AUC: 0.90 vs. 0.87) in determining CAD (26). Particularly, AC images are known to be successful in the correction of artifacts from attenuation (33). Superior advantages can be obtained in the visual evaluation by providing attenuation evaluation with SPECT/CT imaging. However, this is not the case in quantitative evaluation. Conversely, in our study, the scores from images without any AC have more power to detect CAD, which may be due to the compared databases or manual processes needed from attenuation images. These processes could reduce reproducibility.

Study Limitations

The retrospective design and limited number of patients are the study's main limitation.

Conclusion

Considering TPDS before CA may help select patients who need CA primarily. Patients with no prior CAD history with TPDS score >5 in MPS should be primarily advised for CA. Although the MPS evaluation from AC images has become widespread recently, according to this study's quantitative evaluation results, the scores obtained from non-corrected images have more power to detect CAD than the scores obtained from AC images.

Ethics

Ethics Committee Approval: Dokuz Eylül University Non-interventional Research Ethics Committee protocol number: 5448-GOA, decision number: 01.06.2020, 2020/11-06).

Informed Consent: Retrospective cross sectional study.

Peer-review: Externally and internally peer-reviewed.

Authorship Contributions

Surgical and Medical Practices: N.P.K.Ş., R.B., B.Ş., B.A., Concept: N.P.K.Ş., R.B., Design: N.P.K.Ş., R.B., Data Collection or Processing: N.P.K.Ş., Analysis or Interpretation: N.P.K.Ş., R.B., Literature Search: N.P.K.Ş., R.B, Writing: N.P.K.Ş., R.B.

Conflict of Interest: No conflict of interest was declared by the authors.

Financial Disclosure: The authors declared that this study has received no financial support.

References

1. Sanchis-Gomar F, Perez-Quilis C, Leischik R, Lucia A. Epidemiology of coronary heart disease and acute coronary syndrome. Ann Transl Med 2016;4:256.
2. Libby P, Theroux P. Pathophysiology of coronary artery disease. Circulation 2005;111:3481-3488.
3. Fathala A. Myocardial perfusion scintigraphy: techniques, interpretation, indications and reporting. Ann Saudi Med 2011;31:625-634.
4. Athanasiou LS, Fotiadis DI, Michalis LK. Atherosclerotic plaque characterization methods based on coronary imaging. 1st Ed. London: Elsevier; 2017. p. 23-28.

5. Noto TJ Jr, Johnson LW, Krone R, Weaver WF, Clark DA, Kramer JR Jr, Vetrovec GW. Cardiac catheterization 1990: a report of the Registry of the Society for Cardiac Angiography and Interventions (SCA&I). Cathet Cardiovasc Diagn 1991;24:75-83.
6. Notghi A, Low CS. Myocardial perfusion scintigraphy: past, present and future. Br J Radiol 2011;84:S229-236.
7. Seo Y, Mari C, Hasegawa BH. Technological development and advances in single-photon emission computed tomography/computed tomography. Semin Nucl Med 2008;38:177-198.
8. Czaja M, Wygoda Z, Duszańska A, Szczerba D, Głowacki J, Gąsior M, Wasilewski JP. Interpreting myocardial perfusion scintigraphy using single-photon emission computed tomography. Part 1. Kardiochir Torakochirurgia Pol 2017;14:192-199.
9. Lecchi M, Malaspina S, Scabbio C, Gaudieri V, Del Sole A. Myocardial perfusion scintigraphy dosimetry: optimal use of SPECT and SPECT/CT technologies in stress-first imaging protocol. Clin Transl Imaging 2016;4:491-498.
10. Hayes SW, De Lorenzo A, Hachamovitch R, Dhar SC, Hsu P, Cohen I, Friedman JD, Kang X, Berman DS. Prognostic implications of combined prone and supine acquisitions in patients with equivocal or abnormal supine myocardial perfusion SPECT. J Nucl Med 2003;44:1633-1640.
11. Kakhki VRD, Sadeghi R, Torabian-Kakhki M, Rad MP, Sadri K. Semi-quantitative segmental perfusion scoring in myocardial perfusion SPECT: Visual vs. automated analysis. Iranian Journal of Nuclear Medicine 2014;22:64-69.
12. Yoda S, Nakanishi K, Tano A, Hori Y, Suzuki Y, Matsumoto N, Hirayama A. Validation of automated quantification of nuclear cardiology in Japanese patients using total perfusion deficits: Comparison with visual assessment. J Cardiol 2014;63:350-357.
13. Berman DS, Kang X, Gransar H, Gerlach J, Friedman JD, Hayes SW, Thomson LE, Hachamovitch R, Shaw LJ, Slomka PJ, Yang LD, Germano G. Quantitative assessment of myocardial perfusion abnormality on SPECT myocardial perfusion imaging is more reproducible than expert visual analysis. J Nucl Cardiol 2009;16:45-53.
14. Neglia D, Rovai D, Caselli C, Pietila M, Teresinska A, Aguadé-Bruix S, Pizzi MN, Todiere G, Gimelli A, Schroeder S, Drosch T, Poddighe R, Casolo G, Anagnostopoulos C, Pugliese F, Rouzet F, Le Guludec D, Cappelli F, Valente S, Gensini GF, Zawaideh C, Capitanio S, Sambuceti G, Marsico F, Perrone Filardi P, Fernández-Golfín C, Rincón LM, Graner FP, de Graaf MA, Fiechter M, Stehli J, Gaemperli O, Reyes E, Nkomo S, Mäki M, Lorenzoni V, Turchetti G, Carpeggiani C, Marinelli M, Puzzuoli S, Mangione M, Marcheschi P, Mariani F, Giannessi D, Nekolla S, Lombardi M, Sicari R, Scholte AJ, Zamorano JL, Kaufmann PA, Underwood SR, Knuuti J; EVINCI Study Investigators. Detection of significant coronary artery disease by noninvasive anatomical and functional imaging. Circ Cardiovasc Imaging 2015;8:e002179.
15. Doğan C, Bayram Z, Çınaral F, Uslu A, Acar R, Önal Ç, Çap M, Güvendi B, Unkun T, Karaduman A, Hakgör A, Akbal ÖY, Kaymaz C, Özdemir N. Effect of localization of coronary artery lesions on total perfusion deficit in myocardial perfusion scintigraphy. Kosuyolu Heart Journal 2018;21:181-186.
16. Doğan C, Çınaral F, Karagöz A, Bayram Z, Önal SÇ, Candan Ö, Acar RD, Çap M, Erdoğan E, Hakgör A, Akbal ÖY, Uslu A, Kaymaz C, Özdemir N. Comparison of automated quantification and semiquantitative visual analysis findings of IQ SPECT MPI with conventional coronary angiography in patients with stable angına. Turk Kardiyol Dern Ars 2019;47:357-364.
17. Driessen RS, Raijmakers PG, Danad I, Stuijfzand WJ, Schumacher SP, Leipsic JA, Min JK, Knuuti J, Lammertsma AA, van Rossum AC, van Royen N, Underwood SR, Knaapen P. Automated SPECT analysis compared with expert visual scoring for the detection of FFR-defined coronary artery disease. Eur J Nucl Med Mol Imaging 2018;45:1091-1100.
18. Min JK, Koduru S, Dunning AM, Cole JH, Hines JL, Greenwell D, Biga C, Fanning G, LaBounty TM, Gomez M, Horowitz JM, Hadimitzsky M, Hausleiter J, Callister TQ, Rosanski AR, Shaw LJ, Berman DS, Lin FY. Coronary CT angiography versus myocardial perfusion imaging for near-term quality of life, cost and radiation exposure: a prospective multicenter randomized pilot trial. J Cardiovasc Comput Tomogr 2012;6:274-283.
19. Allie R, Hutton BF, Prvulovich E, Bomanji J, Michopoulou S, Ben-Haim S. Pitfalls and artifacts using the D-SPECT dedicated cardiac camera. J Nucl Cardiol 2016;23:301-310.
20. Chen J, Caputlu-Wilson SF, Shi H, Galt JR, Faber TL, Garcia EV. Automated quality control of emission-transmission misalignment for attenuation correction in myocardial perfusion imaging with SPECT-CT systems. J Nucl Cardiol 2006;13:43-49.
21. Xu Y, Fish M, Gerlach J, Lemley M, Berman DS, Germano G, Slomka PJ. Combined quantitative analysis of attenuation corrected and non-corrected myocardial perfusion SPECT: Method development and clinical validation. J Nucl Cardiol 2010;17:591-599.
22. Holly TA, Abbott BG, Al-Mallah M, Calnon DA, Cohen MC, DiFilippo FP, Ficaro EP, Freeman MR, Hendel RC, Jain D, Leonard SM, Nichols KJ, Polk DM, Soman P; American Society of Nuclear Cardiology. Single photon-emission computed tomography. J Nucl Cardiol 2010;17:941-973.
23. Huang JY, Huang CK, Yen RF, Wu HY, Tu YK, Cheng MF, Lu CC, Tzen KY, Chien KL, Wu YW. Diagnostic Performance of Attenuation-Corrected Myocardial Perfusion Imaging for Coronary Artery Disease: A Systematic Review and Meta-Analysis. J Nucl Med 2016;57:1893-1898.
24. Sharma P, Patel CD, Karunanithi S, Maharjan S, Malhotra A. Comparative accuracy of CT attenuation-corrected and non-attenuation-corrected SPECT myocardial perfusion imaging. Clin Nucl Med 2012;37:332-338.
25. Genovesi D, Giorgetti A, Gimelli A, Kusch A, D'Aragona Tagliavia I, Casagranda M, Cannizzaro G, Giubbini R, Bertagna F, Fagioli G, Rossi M, Romeo A, Bertolaccini P, Bonini R, Marzullo P. Impact of attenuation correction and gated acquisition in SPECT myocardial perfusion imaging: results of the multicentre SPAG (SPECT Attenuation Correction vs Gated) study. Eur J Nucl Med Mol Imaging 2011;38:1890-1898.
26. Arsanjani R, Xu Y, Hayes SW, Fish M, Lemley M Jr, Gerlach J, Dorbala S, Berman DS, Germano G, Slomka P. Comparison of fully automated computer analysis and visual scoring for detection of coronary artery disease from myocardial perfusion SPECT in a large population. J Nucl Med 2013;54:221-228.
27. Danias PG, Papaioannou GI, Ahlberg AW, O'Sullivan DM, Mann A, Boden WE, Heller GV. Usefulness of electrocardiographic-gated stress technetium-99m sestamibi single-photon emission computed tomography to differentiate ischemic from nonischemic cardiomyopathy. Am J Cardiol 2004;94:14-19.
28. Lindner O, Rusche H, Schäfers M, Schober O. Myocardial perfusion SPECT: current concepts. Burchert Dtsch Arztebl 2007;104:A952-958.
29. Slomka PJ, Nishina H, Berman DS, Akincioglu C, Abidov A, Friedman JD, Hayes SW, Germano G. Automated quantification of myocardial perfusion SPECT using simplified normal limits. J Nucl Cardiol 2005;12:66-77.
30. Slomka P, Xu Y, Berman D, Germano G. Quantitative analysis of perfusion studies: strengths and pitfalls. J Nucl Cardiol 2012;19:338-346.
31. Shaw LJ, Berman DS, Maron DJ, Mancini GB, Hayes SW, Hartigan PM, Weintraub WS, O'Rourke RA, Dada M, Spertus JA, Chaitman BR, Friedman J, Slomka P, Heller GV, Germano G, Gosselin G, Berger P, Kostuk WJ, Schwartz RG, Knudtson M, Veledar E, Bates ER, McCallister B, Teo KK, Boden WE; COURAGE Investigators. Optimal medical therapy with or without percutaneous coronary intervention to reduce ischemic burden: results from the Clinical Outcomes Utilizing Revascularization and Aggressive Drug Evaluation (COURAGE) trial nuclear substudy. Circulation 2008;117:1283-1291.
32. Wells RG, Trottier M, Premaratne M, Vanderwerf K, Ruddy TD. Single CT for attenuation correction of rest/stress cardiac SPECT perfusion imaging. J Nucl Cardiol 2018;25:616-624.
33. Tawakol AE, Tantawy HM, Elashmawy RE, Abdelhafez YG, Elsayed YM. Added Value of CT Attenuation Correction and Prone Positioning in Improving Breast and Subdiaphragmatic Attenuation in Myocardial Perfusion Imaging. J Nucl Med Technol 2021;49:23-29.

Original Article
Mol Imaging Radionucl Ther 2021;30:177-186 DOI:10.4274/mirt.galenos.2021.25633

Relationships Between DCE-MRI, DWI, and ^{18}F-FDG PET/CT Parameters with Tumor Grade and Stage in Patients with Head and Neck Squamous Cell Carcinoma

Baş Boyun Yassı Hücreli Kanser Hastalarında Tümör Derecesi ve Evre ile DK-MRG, DAG ve ^{18}F-FDG PET/BT Parametrelerinin İlişkisi

Hande Melike Bülbül[1], Ogün Bülbül[2], Sülen Sarıoğlu[3], Özhan Özdoğan[4], Ersoy Doğan[5], Nuri Karabay[6]

[1]*Recep Tayyip Erdoğan Training and Research Hospital, Clinic of Radiology, Rize, Turkey*
[2] *Recep Tayyip Erdoğan Training and Research Hospital, Clinic of Nuclear Medicine, Rize, Türkiye*
[3]*Dokuz Eylül University Faculty of Medicine, Department of Medical Pathology, İzmir, Turkey*
[4]*Dokuz Eylül University Faculty of Medicine, Department of Nuclear Medicine, İzmir, Turkey*
[5]*Dokuz Eylül University Faculty of Medicine, Department of Otorhinolaryngology, İzmir, Turkey*
[6]*Dokuz Eylül University Faculty of Medicine, Department of Radiology, İzmir, Turkey*

Abstract

Objectives: Properties of head and neck squamous cell carcinoma (HNSCC) such as cellularity, vascularity, and glucose metabolism interact with each other. This study aimed to investigate the associations between diffusion-weighted imaging (DWI), dynamic contrast-enhanced magnetic resonance imaging (DCE-MRI), and positron emission tomography/computed tomography (PET/CT) in patients with HNSCC.

Methods: Fourteen patients who were diagnosed with HNSCC were investigated using DCE-MRI, DCE, and ^{18}fluoride-fluorodeoxyglucose PET/CT and evaluated retrospectively. Ktrans, Kep, Ve, and initial area under the curve (iAUC) parameters from DCE-MRI, ADC_{max}, ADC_{mean}, and ADC_{min} parameters from DWI, and maximum standardized uptake value (SUV_{max}), SUV_{mean}, metabolic tumor volume (MTV), and total lesion glycolysis (TLG) parameters from PET were obtained. Spearman's correlation coefficient was used to analyze associations between these parameters. In addition, these parameters were grouped according to tumor grade and T and N stages, and the difference between the groups was evaluated using the Mann-Whitney U test.

Results: Correlations at varying degrees were observed in the parameters investigated. ADC_{mean} moderately correlated with Ve ($p=0.035$; $r=0.566$). Ktrans inversely correlated with SUV_{max} ($p=0.017$; $r=-0.626$). iAUC inversely correlated with SUV_{max}, SUV_{mean}, TLG, and MTV ($p<0.05$, $r\leq-0.700$). MTV (40% threshold) was significantly higher in T4 tumors than in T1-3 tumors ($p=0.020$). No significant difference was found in the grouping made according to tumor grade and N stage in terms of these parameters.

Conclusion: Tumor cellularity, vascular permeability, and glucose metabolism had significant correlations at different degrees. Furthermore, MTV may be useful in predicting T4 tumors.

Keywords: Cancer of the head and neck, squamous cell carcinoma, diffusion, permeability, positron emission tomography

Öz

Amaç: Baş boyun yassı hücreli karsinomunun (BBYHK) hücresellik, vaskülarite ve glukoz metabolizması gibi özellikleri birbirleri ile etkileşim içerisindedir. Bu çalışmanın amacı BBYHK hastalarında difüzyon ağırlıklı görüntüleme (DAG), dinamik kontrastlı manyetik rezonans görüntüleme (DK-MRG) ve pozitron emisyon tomografisi/bilgisayarlı tomografi (PET/BT) arasındaki ilişkinin araştırılmasıdır.

Address for Correspondence: Hande Melike Bülbül MD, Recep Tayyip Erdoğan Training and Research Hospital, Clinic of Radiology, Rize, Turkey
Phone: +90 506 938 93 94 **E-mail:** handemelikehalac@gmail.com ORCID ID: orcid.org/0000-0001-9492-093X
Received: 15.05.2021 **Accepted:** 19.07.2021

Yöntem: BBYHK tanısı almış ve DAG, DK-MRG ve ^{18}flor-florodeoksiglukoz (^{18}F-FDG) ile görüntüleme yapılmış 14 hasta retrospektif olarak değerlendirildi. DK-MRG'den Ktrans, Kep, Ve iAUC; DAG'den ADC_{maks}, ADC_{mean} and ADC_{min} ve ^{18}F-FDG PET/BT'den SUV_{maks}, SUV_{mean}, metabolik tümör hacmi (MTV) and toplam lezyon glikolizi (TLG) parametreleri elde edildi. Bu parametreler arasındaki ilişki Spearman korelasyon katsayısı kullanılarak değerlendirildi. Ayrıca bu parametreler tümör derecesi, T ve N evresine göre gruplandırılarak gruplar arasındaki ilişki Mann-Whitney U testi kullanılarak analiz edildi.

Bulgular: İncelenen parametreler arasında değişen düzeylerde korelasyonlar gözlendi. ADC_{mean} ve Ve arasında orta düzeyde pozitif korelasyon saptandı (p=0,035; r=0,566). Ktrans ile SUV_{maks}'ın negatif korelasyon gösterdiği (p=0,017; r=-0,626), iAUC ile SUV_{maks}, SUV_{mean}, TLG ve MTV arasında negatif yönde güçlü korelasyon olduğu gözlendi (p<0,05, r≤-0,700). MTV (%40 x SUV_{maks} eşik değer) T4 tümörlerde T1-3 tümörlere kıyasla istatistiksel olarak anlamlı düzeyde yüksekti (p=0,020). Tümör derecesi ve N evresine göre yapılan gruplamada parametreler arasında anlamlı fark saptanmadı.

Sonuç: Tümörün hücreselliği, vasküler permeabilite ve glukoz metabolizması farklı derecelerde anlamlı korelasyonlar gösterdi. Ayrıca, MTV değeri T4 tümörleri tahmin etmede faydalı olabilir.

Anahtar kelimeler: Baş boyun kanseri, yassı hücreli kanser, difüzyon, pozitron emisyon tomografisi, permeabilite

Introduction

Head and neck cancers constitute 4-5% of all malignancies. Among these, head and neck squamous cell carcinoma (HNSCC) constitutes the thumping majority with 90% (1).

Although magnetic resonance imaging (MRI) and computed tomography (CT) are indispensable for diagnosis and follow-up, functional imaging techniques such as dynamic contrast-enhanced (DCE) MRI, diffusion-weighted imaging (DWI), and positron emission tomography (PET)/CT are adjunctive modalities that give information about the underlying biology (2,3).

^{18}Fluoride-fluorodeoxyglucose (^{18}F-FDG) PET/CT is a modality with high sensitivity in the diagnosis of primary tumors and has been used for staging tumors, evaluating treatment responses, and identifying HNSCC recurrence (4,5). Besides ^{18}F-FDG PET/CT parameters like standardized uptake values (SUVs), total lesion glycolysis (TLG), and metabolic tumor volume (MTV) are important biomarkers of tumor behavior (5,6). For example, MTV and TLG are prognostic predictors of non-small cell lung cancers (NSCLC) and head and neck cancers (7,8). They are also valuable for predicting tumor responses to neoadjuvant chemotherapy in breast cancer, NSCLC, and osteosarcomas (9,10,11).

DCE-MRI and DWI are helpful methods for the characterization of the pathophysiological features of tumors (12,13). DWI provides quantitative information about tumor cellularity, and this is expressed by the apparent diffusion coefficient (ADC). DCE-MRI allows the determination of values such as tumor-vascular permeability and extracellular-extravascular volume fraction with quantitative parameters obtained by pharmacokinetic modeling by imaging the signal change with the administration of contrast agent (14).

Accordingly, DWI, DCE-MRI, and ^{18}F-FDG PET/CT can provide supplementary information about biological properties such as cellularity, metabolic activity, and angiogenesis in HNSCC (1,14).

Many multiparametric investigations were conducted including these modalities to clarify the complicated biology of HNSCC (2,3). But results were discordant. Although some authors have reported correlations between ADC and PET parameters (15,16), some did not show a correlation among them (17,18). The same discrepancy is found for the correlation between DCE-MRI and PET parameters and tumor grade in different studies (2,3,6).

Properties of tumor tissues such as cellularity, vascularity, and glucose metabolism interact with each other. It is essential to define this relationship because it can be valuable for clinical practice in predicting the tumor treatment response and locoregional recurrence and evaluating the treatment response in different tumor groups (19,20).

This study aimed to analyze associations between ^{18}F-FDG PET/CT, DWI, and DCE-MRI in patients with HNSCC.

Material and Methods

Dokuz Eylül University Institutional Ethics Board approved this study (file number: 5538-GOA). Because of its retrospective design, the necessity for written informed consent was waived.

Patients

The hospital database was used to identify patients with HNSCC between January 2018 and September 2019. The inclusion criteria were as follows: 1) Patients with HNSCC and histopathological diagnosis and 2) patients who underwent routine imaging work-up including DCE-MRI, DWI sequences, and ^{18}F-FDG PET/CT. The exclusion criteria were the following: 1) inadequate MRI images due to severe artifacts (n=1), 2) tumor treatment before MRI and ^{18}F-FDG PET/CT, 3) patients whose ^{18}F-FDG PET/CT images are ineligible for evaluation due to attenuation, and 4) MRI or ^{18}F-FDG PET/CT images that were obtained

at another hospital (n=4). After these criteria, 14 patients were included in this study.

Eight patients had a biopsy, and six had both a biopsy and an excision. MRI examinations were conducted before tissue samples were collected (average 4 days, range: 1-7 days). The mean time interval between biopsy and ^{18}F-FDG PET/CT examinations was 10 days (range: 7-15 days). A pathologist with 28 years of experience in head and neck cancer examined the specimens obtained at these procedures. The cases were divided into two groups based on the T stage, where patients in T1, T2, and T3 stages were included in group 1 (n=8) and those in T4 stages in group 2 (n=6). We divided the patients into two groups as those with (n=8) and without (n=6) lymph node metastases. For statistical purposes, all oropharyngeal carcinomas associated with HPV and well and moderately differentiated squamous cell carcinomas were grouped as low grade (n=10), whereas non-keratinizing undifferentiated laryngeal carcinomas and poorly differentiated squamous cell carcinomas were grouped as high grade (n=4).

MRI Examinations

MRI was performed for all patients using a 1.5 T MR scanner (Achieva, Philips Medical Systems, Netherlands) with an 8-channel head and neck array coil. The standard MRI protocols included axial T2-weighted (T2W) turbo spin-echo (TSE), axial and sagittal T1-weighted (T1W) spin-echo, coronal short-tau ınversion-recovery TSE, and axial, sagittal, and coronal fat-suppressed contrast-enhanced T1W TSE (spectral presaturation with ınversion recovery).

DWI was performed using an axial echo planar imaging DWI sequence (b0 and b800 s/mm^2). DWI parameters were as follows: TR/TE, 10165/111; matrix, 204×230; slice thickness, 5 mm; cross-section spacing, 0 mm. ADC maps were automatically generated by the implemented software.

DCE imaging was performed using the T1W DCE sequences (T1W single-shot turbo field echo). T1 map was calculated with two flip angles of 5° and 15° (TR: 10 ms and TE: 2.4 ms, axial plane, section thickness: 3 mm) before the DCE-MRI sequence. T1W DCE sequence was acquired with the following parameters: TR, 5 ms; TE, 2.4 ms; FOV, 220×220 mm; matrix, 140×114; flip angle, 258; slice thickness, 5 mm; 26 slices, NEX, 1.5; 50 dynamic cycles; total acquisition time, 5 min 36 s. Gadoterate meglumine was injected at a dose of 0.2 mmol/kg and at the rate of 2 mL/s, intravenously with an automatic injector, and then, 20 mL saline was injected.

Analysis of the DCE-MRI and DWI Images

One radiologist under the supervision of a senior radiologist with 6 and 11 years of experience in head and neck oncology, respectively, analyzed the DWI and DCE-MRI images. All images were transferred to a software module (IntelliSpace Portal-v8.2.20820, Philips Medical Systems), and all measurements were conducted using the workstation.

The ADC value was measured on ADC maps by drawing the region of interest (ROI) on the tumor at the level of its largest diameter that was explained previously (1). T1W and T2W MR images were used while drawing the ROI to avoid the necrotic and hemorrhagic components of the tumor. ADC_{max}, ADC_{mean}, and ADC_{min} parameters were measured using this method (Figure 1).

ROIs were manually drawn in the tumor on DCE images in the same way that explained for the ADC analysis. Tofts model was used to calculate pharmacokinetic parameters in every case according to the population-averaged arterial input function (21). The parameters were as follows:

Ktrans, volume transfer constant;

Ve, volume of the extravascular extracellular leakage space (EES);

Kep, redistribution rate constant (Kep = Ktrans × Ve^{-1});

iAUC, initial area under the curve.

^{18}F-FDG PET/CT Examinations

Whole-body ^{18}F-FDG PET/CT was performed using a combined PET/CT scanner (Philips Gemini TOF, 16 Slices). After 6-h fasting, 0.11 mCi/kg ^{18}F-FDG was injected intravenously if blood sugar was <200 mg/dL. All patients rested for an hour in a quiet and no lightroom, and then, PET/CT scanning was performed from the vertex to the upper thigh (1.5 min/bed).

SUV_{max}, SUV_{mean}, MTV, and TLG were calculated using freely available software LIFEx (version 6.3, lifexsoft.org) (22). The highest SUV in the given volume of interest (VOI) is called SUV_{max}. The average SUV of the VOI is called SUV_{mean}. MTV is a measurement of metabolically active tumor volume according to ^{18}F-FDG avidity. TLG is calculated by multiplying MTV by SUV_{mean}.

Analysis of the ^{18}F-FDG PET/CT Images

One nuclear medicine physician analyzed ^{18}F-FDG PET/CT images under the supervision of a senior nuclear medicine physician with 5 and 12 years of experience in ^{18}F-FDG PET/CT imaging for head and neck cancer, respectively. A VOI was placed around the primary tumor area in correlation with MRI, including all hypermetabolic tumor areas, excluding physiological uptake areas such as palatine

tonsils and mylohyoid muscle. For MTV, the following two methods were used: fixed absolute threshold by SUV 2.5 and fixed relative threshold by 40% of SUV_{max}. TLG was also determined using these two methods (23,24) (Figure 1).

Statistical Analysis

Descriptive statistics were presented as mean, standard deviation, median, and range. Shapiro-Wilks test was conducted to determine the distribution of normality of all data. Spearman's correlation coefficient was used to analyze the associations between investigated parameters. The Mann-Whitney U test was performed to analyze the association between DCE-MRI, DWI, and ^{18}F-FDG PET/CT with the group of grade and T stage. Receiver operating characteristics (ROC) analysis was conducted to determine the ability of MTV data to distinguish advanced-stage tumors.

All statistical analyses were performed using the SPSS version 24 software (SPSS Inc, Chicago, IL, USA). The $p<0.05$ was considered statistically significant in all analyses.

Results

Patients

All patients were male with a median age of 58 years, range 38-78 years. Lesion localization was oral cavity in 5 (35.7%) patients, larynx in 5 (35.7%), oropharynx in 2 (14.3%), and nasopharynx in 2 (14.3%). The T stages of tumor were T1 in 3 (21.4%), T2 in 3 (21.4%), T3 in 2 (14.3%), and T4 in 6 (42.9%) of patients. Of tumors, 10 (71.4%) were low grade, and 4 (28.6%) were high.

Imaging

A complete summary of the results, including mean values, standard deviation, median, and ranges, is shown in Table 1.

It was determined that in overall measurements, ADC_{mean} moderately correlated with Ve ($p=0.035$; $r=0.566$; Table 2). Ktrans inversely correlated with SUV_{max} ($p=0.017$; $r=-0.626$; Table 3). There was a strong inverse correlation of iAUC with SUV_{max}, SUV_{mean}, TLG, and MTV (both 40% and SUV 2.5 threshold; $p=0.00$; $r=-0.732$; $p=0.005$; $r=-0.700$, $p=0.002$; $r=-0.745$, $p=0.000$; $r=-0.824$, $p=0.000$; $r=-0.815$, $p=0.000$; $r=-0.815$, respectively). In addition, there was a tendency to inverse correlation between SUV_{max} and ADC_{mean}, but it was not statistically significant ($p=0.053$, $r=-0.526$).

There was no significant correlation between other parameters of DCE, DWI, and ^{18}F-FDG PET/CT (Table 3).

In the grouping made according to the T stage, MTV (40% threshold) and ADC_{max} were significantly higher in T4 lesions than in T1-3 patients ($p=0.020$ and 0.007, respectively; Table 4). Based on these findings, ROC analysis was conducted for the MTV (40% threshold) and T stage (Figure 2).

No significant differences were identified in the analyzed parameters between low- and high-grade tumors (Table 5).

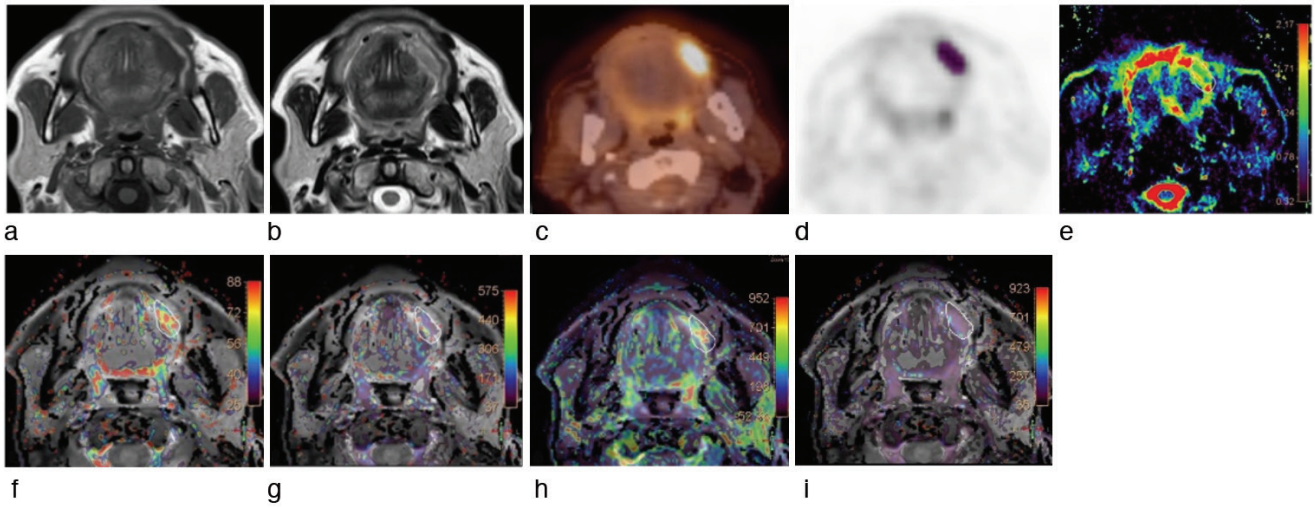

Figure 1. Imaging findings in a 61-year-old man with squamous cell carcinoma of the tongue ($T_2N_1M_0$). (a, b, c) T1- and T2-weighted images and ^{18}fluorine-fluorodeoxyglucose imaging (fused image) show left-sided tongue lesion [maximum standard uptake value (SUV_{max}): 10.2; SUV_{mean}: 5.3]. (d) Showing attenuation-corrected positron emission tomography image in LIFEx. (e) ADC map. The ADC values ($\times10^{-3}$ mm^2s^{-1}) of the lesion are as follows: ADC_{min}: 0.2, ADC_{mean}: 1.07, and ADC_{max}: 1.9. (f, g, h, i) Dynamic contrast-enhanced (DCE) imaging findings. Estimated DCE parameters are as follows: (f) Ktrans: 58.7 ($\times10^{-3}$ min^{-1}), (g) Kep: 303.1 ($\times10^{-3}$ min^{-1}), (h) Ve: 193.7 ($\times10^{-3}$), (i) iAUC: 159.1
ADC: Apparent diffusion coefficient, iAUC: Initial area under the curve

Table 1. DCE-MRI, DWI, and PET parameters in all patients

	Mean ± SD	Median	Range
SUV_{max}	12.1±1.2	11.9	3.8-20.7
SUV_{mean}	5.9±0.4	6.3	3.0-8.8
MTV (40% threshold) (mL)	11.7±2.9	9.9	1.1-35.8
TLG (40% threshold) (SUV × mL)	76.2±20.3	62.9	3.3-247.0
MTV (SUV 2.5 threshold) (mL)	20.9±5.7	15.4	2.1-72.1
TLG (SUV 2.5 threshold) (SUV × mL)	138.0±40.0	77.2	6.3-482.1
Ktrans (min^{-1})	0.05±0.04	0.05	0.03-0.09
Kep (min^{-1})	0.40±0.09	0.35	0.02-1.43
Ve	0.29±0.01	0.16	0.050-1.85
iAUC	116.6±10.2	111.1	64.6-184.1
ADC_{max} (10^{-3} mm^2/s)	2.35±0.16	2.2	1.5-3.5
ADC_{min} (10^{-3} mm^2/s)	0.3±0.1	0.2	0.1-1.0
ADC_{mean} (10^{-3} mm^2/s)	1.17±0.1	1.1	1.0-1.4

SD: Standard deviation, SUV: Standard uptake value, MTV: Metabolic tumor volume, TLG: Total lesion glycolysis, iAUC: Initial area under the curve, ADC: Apparent diffusion coefficient, DCE-MRI: Dynamic contrast-enhanced magnetic resonance imaging, DWI: Diffusion-weighted imaging, PET: Positron emission tomography, max: Maximum, min: Minimum

Table 2. Correlations* of DCE-MRI and DWI parameters in all patients

	ADC_{max}	ADC_{min}	ADC_{mean}
Ktrans	r=0.180 p=0.537	r=0.101 p=0.737	r=0.062 p=0.834
Kep	r=0.202 p=0.488	r=0.103 p=0.726	r=-0.496 p=0.072
Ve	r=-0.035 p=0.905	r=-0.110 p=0.709	**r=0.566** **p=0.035**
iAUC	r=-0.154 p=0.599	r=-0.389 p=0.169	r=0.445 p=0.111

*Spearman's correlation. iAUC: Initial area under the curve, ADC: Apparent diffusion coefficient, DCE-MRI: Dynamic contrast-enhanced magnetic resonance imaging, DWI: Diffusion-weighted imaging, max: Maximum, min: Minimum

In the grouping made according to the N stage, no significant difference was found between the parameters evaluated (Table 6).

Discussion

This study demonstrated several significant associations between PET, DCE-MRI, and DWI parameters with indicating relationships between glucose metabolism, tumor cellular density, and microvessel permeability of HNSCC.

In HNSCC, glucose metabolism is positively associated with the sum of tumor cells and growth rate. Accordingly, an inverse correlation between SUV and ADC parameters is expectable. The results of previous studies on this

Table 3. Correlations* of MRI and PET parameters in all patients

	SUV_{max}	SUV_{mean}	MTV (40% threshold)	TLG (40% threshold)	MTV (SUV 2.5 threshold)	TLG (SUV 2.5 threshold)
Ktrans	**r=-0.626** **p=0.017**	r=-0.304 p=0. 291	r=-0.196 p=0.503	r=-0.323 p=0.260	r=-0.380 p=0.180	r=-0.407 p=0.149
Kep	r=0.156 p=0.594	r=0.350 p=0.220	r=0.240 p=0.409	r=0.279 p=0.334	r=0.253 p=0.383	r=0.257 p=0.375
Ve	r=-0.380 p=0.180	r=-0.423 p=0.132	r=-0.398 p=0.159	r=-0.455 p=0.102	r=-0.459 p=0.098	r=-0.455 p=0.102
iAUC	**r=-0.732** **p=0.003**	**r=-0.700** **p=0.005**	**r=-0.745** **p=0.002**	**r=-0.824** **p=0.000**	**r=-0.815** **p=0.000**	**r=-0.815** **p=0.000**
ADC_{max}	r=-0.101 p=0.731	r=0.003 p=0.791	r=0.246 p=0.396	r=0.143 p=0.626	r=0.176 p=0.547	r=0.150 p=0.610
ADC_{min}	r=0.160 p=0.584	r=0.296 p=0.305	r=-0.018 p=0.950	r=0.110 p=0.709	r=0.062 p=0.834	r=0.071 p=0.810
ADC_{mean}	**r=-0.526** **p=0.053**	r=-0.455 p=0.102	r=-0.390 p=0.168	r=-0.456 p=0.101	r=-0.454 p=0.103	r=-0.489 p=0.076

*Spearman's correlation. SUV: Standard uptake value, MTV: Metabolic tumor volume, TLG: Total lesion glycolysis, iAUC: Initial area under the curve, ADC: Apparent diffusion coefficient, MRI: Magnetic resonance imaging, PET: Positron emission tomography, max: Maximum, min: Minimum

relationship in the literature are contradictory. For example, Zhang et al. (25) analyzed PET/MRI images of 27 patients with hypopharynx SCC, and Fruehwald-Pallamar et al. (18) analyzed ^{18}F-FDG PET/CT and MR images of 31 patients with HNSCC, and they did not observe a correlation between SUV_{max} and ADC. But Zhang et al. (25) observed an inverse correlation between MTV and ADC_{mean}. The other two studies showed that ADC_{min} tended to inversely correlate with SUV_{max} (p=0.08) (3,26). Also, Nakajo et al. (16) observed a negative correlation between SUV_{max} and ADC (20). In our study, we observed a tendency to an inverse correlation between SUV_{max} and ADC_{mean}, but it was not statistically significant (p=0.053).

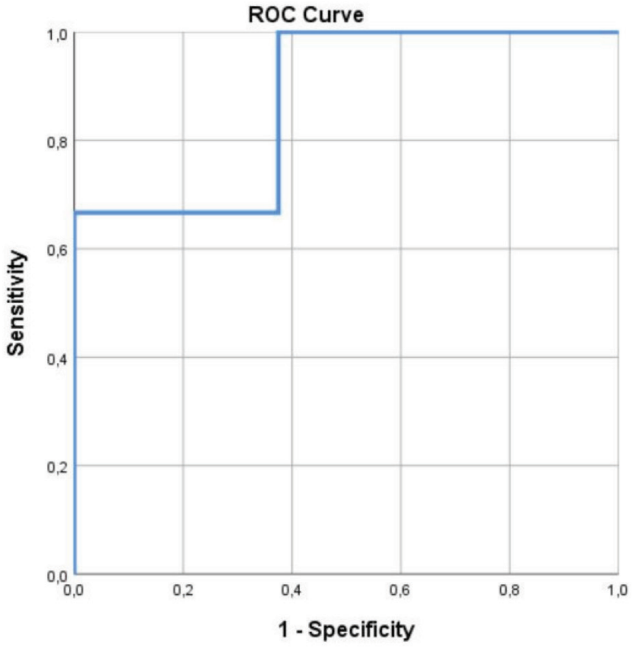

Figure 2. Receiver operating characteristics curves for advanced-stage tumor preliminary diagnosis of metabolic tumor volume (40% threshold) values. When we take the cut-off value as 5.4, the sensitivity is 100%, specificity is 62.5%, positive predictive value is 67%, negative predictive value is 100%, accuracy is 78.5%, area under curve is 0.875
ROC: Receiver operating characteristics

Many studies in the literature have investigated the relationship between T and N stages of tumors and PET parameters. Although Leifels et al. (3) did not observe significant differences in SUV_{max} between various T and N stages, Nakajo et al. (16) reported significantly higher SUV_{max} values in T3 and T4 tumors. In a previous study, T4 tumors had significantly higher SUV_{max} values than T1-3 tumors in patients with oral squamous cell carcinoma (27). In our study, we observed higher MTV (40% threshold) values in T4 tumors than T1-3 tumors. When we take the cut-off value as 5.4, the sensitivity, specificity, and AUC are 100%, 62.5%, and 0.875%, respectively. Because of the small number of patients, this cut-off value needs to be supported by studies with a higher number of patients to be more valuable. Also, TLG was higher in advanced-stage tumors but not statistically significant. T stage is determined according to the size and invasion characteristics of the tumor. As the tumor size increases, the number of tumor cells and, thus, the MTV increases. In HNSCC, T4 stage means that the tumor exceeds the limits of its primary focus and invades neighboring tissues. According to our results, MTV correlates with the tumoral invasion of adjacent tissues.

Many studies in the literature evaluated the relationship between T and N stages of the tumor and ADC values and found no significant differences (3,16,18). Zhang et al. (19) evaluated 541 cases with nasopharyngeal carcinoma, and the pretreatment ADC value in T3 and T4 tumors was significantly higher than in T1 and T2. In our study, ADC_{max}

Table 4. Comparison of PET, DCE-MRI, and DWI parameters between different T stages

Parameters	T1, T2, and T3 tumor Mean ± SD	T4 tumor Mean ± SD	p value*
SUV_{max}	11.2±4.8	13.3±4.5	0.519
SUV_{mean}	5.6±1.8	6.4±1.0	0.271
MTV (40% threshold)	6.0±4.7	19.4±12.4	**0.020**
TLG (40% threshold)	38.8±36.6	126.1±89.0	0.053
MTV (SUV 2.5 threshold)	10.3±8.9	35.0±25.7	0.053
TLG (SUV 2.5 threshold)	67.9±68.3	231.4±183.1	0.0.53
Ktrans	0.05±0.02	0.05±0.01	0.699
Kep	0.42±0.43	0.38±0.17	0.439
Ve	0.38±0.60	0.17±0.07	0.606
iAUC	126.8±45.6	102.9±21.8	0.245
ADC_{max}	2.03±0.38	2.79±0.54	**0.007**
ADC_{min}	0.386±0.3	0.213±0.2	0.179
ADC_{mean}	1.17±0.1	1.16±0.2	0.746

*Mann-Whitney U test. SUV: Standard uptake value, MTV: Metabolic tumor volume, TLG: Total lesion glycolysis, iAUC: Initial area under the curve, ADC: Apparent diffusion coefficient, PET: Positron emission tomography, DWI: Diffusion-weighted imaging, max: Maximum, min: Minimum

was significantly higher in T4 tumors than in T1-3 tumors. There was no significant difference in ADCmean and ADCmin values according to the T stage. Also, there was no significant difference in DCE, DWI, and PET parameters according to lymph node groups.

Correlations between DCE parameters and glucose metabolism and cellularity of the tumor were investigated in several studies (2,3,26). Leifel et al. (3) reported that Ktrans is significantly correlated with ADC_{max} and ADC_{mean} (3). Gawlitza et al. (26) observed a significant correlation between SUV_{mean} with Ktrans and Kep. Han et al. (2) did not observe a correlation between PET and DCE parameters. But in all three studies, a correlation was found between ADC_{mean} and Ve (p=0.0002, 0.06, and 0.000, respectively). In our research, in accordance with this result, a significant correlation was found between ADC mean and Ve (p=0.035). Ve is the indicator of EES. Accordingly, a high value of Ve implies that the number of cells in the tumor is low, which means less restricted water diffusion and, therefore, an increase in ADC value.

There are ambiguous associations described in the literature about the relationship between glucose metabolism and permeability. While one study demonstrated a correlation between SUV_{max} and Ktrans and between SUV_{mean} and Kep (26), others did not observe a correlation between perfusion and glucose metabolism parameters (2,3). In a study that involved 21 patients with advanced HCC, an inverse correlation was observed between Ktrans and SUV_{max} (28). Our results also showed an inverse correlation between Ktrans and SUV_{max}, indicating that HNSCC with higher glucose metabolism tends to have lower perfusion. This result

Table 5. Comparison of PET, DCE-MRI, and DWI parameters between low- and high-grade tumors

Parameters	Low grade Mean ± SD	High grade Mean ± SD	p value*
SUV_{max}	12.3±4.5	11.6±5.5	0.572
SUV_{mean}	5.8±1.2	6.2±2.3	0.777
MTV (40% threshold)	13.4±12.5	7.5±3.1	0.480
TLG (40% threshold)	86.5±87.1	50.4±32.2	0.671
MTV (SUV 2.5 threshold)	24.6±24.3	11.5±7.5	0.480
TLG (SUV 2.5 threshold)	161.7±169.7	78.7±66.0	0.671
Ktrans	0.05±0.01	0.06±0.02	0.120
Kep	0.39±0.39	0.44±0.12	0.322
Ve	0.34±0.54	0.16±0.09	0.572
iAUC	119.4±42.4	109.7±28.9	0.777
ADC_{max}	2.37±0.57	2.32±0.71	0.887
ADC_{min}	0.271±0.3	0.415±0.2	0.211
ADC_{mean}	1.15±0.1	1.21±0.2	0.723

*Mann-Whitney U test. SUV: Standard uptake value, MTV: Metabolic tumor volume, TLG: Total lesion glycolysis, iAUC: Initial area under the curve, ADC: Apparent diffusion coefficient, PET: Positron emission tomography, DCE-MRI: Dynamic contrast-enhanced magnetic resonance imaging, DWI: Diffusion-weighted imaging, max: Maximum, min: Minimum

Table 6. Comparison of PET, DCE-MRI, and DWI parameters between different tumor N stages

Parameters	Lymph node (-) Mean ± SD	Lymph node (+) Mean ± SD	p value*
SUV_{max}	10.5±3.6	13.3±5.2	0.245
SUV_{mean}	5.5±1.4	6.3±1.6	0.271
MTV (40% threshold)	10.9±12.9	12.3±10.1	0.439
TLG (40% threshold)	68.6±91.0	81.9±68.7	0.439
MTV (SUV 2.5 threshold)	16.8±18.6	24.0±24.1	0.606
TLG (SUV 2.5 threshold)	105.4±131.8	162.4±166.5	0.519
Ktrans	0.05±0.01	0.05±0.02	0.606
Kep	0.49±0.47	0.34±0.19	0.897
Ve	0.17±0.1	0.38±0.6	0.379
iAUC	123.0±38.7	111.8±39.7	0.439
ADC_{max}	2.23±0.33	2.44±0.73	0.747
ADC_{min}	0.308±0.35	0.312±0.27	0.545
ADC_{mean}	1.15±0.12	1.18±0.16	0.605

*Mann-Whitney U test. SUV: Standard uptake value, MTV: Metabolic tumor volume, TLG: Total lesion glycolysis, iAUC: Initial area under the curve, ADC: Apparent diffusion coefficient, PET: Positron emission tomography, DCE-MRI: Dynamic contrast-enhanced magnetic resonance imaging, DWI: Diffusion-weighted imaging, max: Maximum, min: Minimum

is contrary to the understanding that the increase in the grade would increase perfusion. In the early stage, tumor growth and vascularization are proportional. In contrast, the increase in tumor growth is faster than the increase in vascularity in the later stages, which can cause insufficient perfusion and necrosis (28,29). However, Surov et al. (30), observed a correlation between SUV_{max} and microvessel density in HNSCC. So, our results need to be supported by other studies.

This study also showed that iAUC was inversely correlated with SUV_{max}, SUV_{mean}, MTV, and TLG. Zhang et al. (31) found an inverse correlation between SUV_{mean} and iAUC in their study, in which they evaluated PET/CT and DCE-MRI images of 41 non-small cell lung cancer patients. Bisdas et al. (32) analyzed this relation in 27 patients with head and neck cancer and identified that iAUC correlated with SUV_{max} and SUV_{mean}. iAUC refers to the amount of contrast agent that reaches and retains the tumor tissue at particular time (32). iAUC is a semi-quantitative parameter of DCE- MRI. So, evaluating the correlation of iAUC with other quantitative parameters has some difficulties. It can be affected by changes in physiological conditions and differences in sequence duration (26). Cheng (33) stated that conventional iAUC could not be an alternative for quantitative parameters such as Ktrans and Kep. Still, if it becomes precise and reproducible with new methods, it can be their alternative. Considering all these, the interpretation of the inverse correlation between the iAUC and PET parameters obtained in this study will not be clear; thus, further studies are needed on this subject.

In this study, no significant association was found between tumor grade and any imaging parameters as in another study (3). Haerle et al. (6) evaluated PET/CT images of 262 patients with HNSCC and did not show a correlation between SUV_{max} and tumor grade. Choi et al. (34) and Nakajo et al. (16) also found no association between SUV_{max} and ADC with grade. Zheng et al. (27) analyzed 104 patients with oral SCC and observed an association between SUV_{max} and poor differentiation. Different grading systems in HNSCC include parameters such as lymphoplasmacytic infiltration, keratinization degree of the tumor, nuclear and cellular polymorphism, and invasion pattern (35). However, parameters such as tumor cellularity, glucose metabolism, microvessel density, and EES that were evaluated with imaging methods in this study were not considered (3). Both the small number of patients in the high-grade group (n=4) and these reasons may explain the absence of a relationship between grade and imaging parameters in our study.

Study Limitations

The most important limitations of this study are its retrospective design and the small number of patients. Additionally, the DWI and DCE parameters were obtained from freehand ROIs, whereas the PET parameters were obtained from a certain threshold automatically, and this may lead to inaccuracies to some degree. Only pretreatment imaging and histopathology data of the patients were evaluated. Therefore, their potential role in predicting treatment response or relapse has not been evaluated. In this study, all HNSCC tumors were included, and differences may arise due to different tumor localizations that were ignored.

Conclusion

We analyzed the relationships among imaging parameters derived from DCE-MRI, DWI, and ^{18}F-FDG PET/CT to reveal the complex biological structure of HNSCC with multiparametric functional imaging methods. We observed significant associations among these parameters at different degrees. MTV (40% threshold) was useful for predicting T4 tumors. Further studies are necessary to prove these results and investigate the possible complementary contribution of these techniques on explaining HNSCC characteristics.

Ethics

Ethics Committee Approval: Dokuz Eylül University Institutional Ethics Board approved this study (file number: 5538-GOA).

Informed Consent: The necessity for written informed consent was waived.

Peer-review: Externally peer-reviewed.

Surgical and Medical Practices: H.M.B., O.B., S.S., Ö.Ö., E.D., N.K., Concept: H.M.B., O.B., S.S., Ö.Ö., E.D., N.K., Design: H.M.B., O.B., S.S., Ö.Ö., E.D., N.K., Data Collection or Processing: H.M.B., O.B., S.S., Ö.Ö., E.D., N.K., Analysis or Interpretation: H.M.B., O.B., S.S., Ö.Ö., E.D., N.K., Literature Search: H.M.B., O.B., S.S., Ö.Ö., E.D., N.K., Writing: H.M.B., O.B., S.S., Ö.Ö., E.D., N.K.

Conflict of Interest: No conflict of interest was declared by the authors.

Financial Disclosure: The authors declared that this study has received no financial support.

References

1. Covello M, Cavaliere C, Aiello M, Cianelli MS, Mesolella M, Iorio B, Rossi A, Nicolai E. Simultaneous PET/MR head-neck cancer imaging: Preliminary clinical experience and multiparametric evaluation. Eur J Radiol 2015;84:1269-1276.
2. Han M, Kim SY, Lee SJ, Choi JW. The Correlations Between MRI Perfusion, Diffusion Parameters, and 18F-FDG PET Metabolic Parameters in Primary

Head-and-Neck Cancer: A Cross-Sectional Analysis in Single Institute. Medicine (Baltimore) 2015;94:e2141.

3. Leifels L, Purz S, Stumpp P, Schob S, Meyer HJ, Kahn T, Sabri O, Surov A. Associations between 18F-FDG-PET, DWI, and DCE Parameters in Patients with Head and Neck Squamous Cell Carcinoma Depend on Tumor Grading. Contrast Media Mol Imaging 2017;2017:5369625.
4. Ong SC, Schöder H, Lee NY, Patel SG, Carlson D, Fury M, Pfister DG, Shah JP, Larson SM, Kraus DH. Clinical utility of 18F-FDG PET/CT in assessing the neck after concurrent chemoradiotherapy for Locoregional advanced head and neck cancer. J Nucl Med 2008;49:532-540.
5. Surov A, Meyer HJ, Höhn AK, Sabri O, Purz S. Combined Metabolo-Volumetric Parameters of 18F-FDG-PET and MRI Can Predict Tumor Cellularity, Ki67 Level and Expression of HIF 1alpha in Head and Neck Squamous Cell Carcinoma: A Pilot Study. Transl Oncol 2019;12:8-14.
6. Haerle SK, Huber GF, Hany TF, Ahmad N, Schmid DT. Is there a correlation between 18F-FDG-PET standardized uptake value, T-classification, histological grading and the anatomic subsites in newly diagnosed squamous cell carcinoma of the head and neck? Eur Arch Otorhinolaryngol 2010;267:1635-1640.
7. Pak K, Cheon GJ, Nam HY, Kim SJ, Kang KW, Chung JK, Kim EE, Lee DS. Prognostic value of metabolic tumor volume and total lesion glycolysis in head and neck cancer: a systematic review and meta-analysis. J Nucl Med 2014;55:884-890.
8. Im HJ, Pak K, Cheon GJ, Kang KW, Kim SJ, Kim IJ, Chung JK, Kim EE, Lee DS. Prognostic value of volumetric parameters of (18)F-FDG PET in non-small-cell lung cancer: a meta-analysis. Eur J Nucl Med Mol Imaging 2015;42:241-251.
9. Im HJ, Kim YK, Kim YI, Lee JJ, Lee WW, Kim SE. Usefulness of Combined Metabolic-Volumetric Indices of (18)F-FDG PET/CT for the Early Prediction of Neoadjuvant Chemotherapy Outcomes in Breast Cancer. Nucl Med Mol Imaging 2013;47:36-43.
10. Burger IA, Casanova R, Steiger S, Husmann L, Stolzmann P, Huellner MW, Curioni A, Hillinger S, Schmidtlein CR, Soltermann A. 18F-FDG PET/CT of Non-Small Cell Lung Carcinoma Under Neoadjuvant Chemotherapy: Background-Based Adaptive-Volume Metrics Outperform TLG and MTV in Predicting Histopathologic Response. J Nucl Med 2016;57:849-854.
11. Im HJ, Kim TS, Park SY, Min HS, Kim JH, Kang HG, Park SE, Kwon MM, Yoon JH, Park HJ, Kim SK, Park BK. Prediction of tumour necrosis fractions using metabolic and volumetric 18F-FDG PET/CT indices, after one course and at the completion of neoadjuvant chemotherapy, in children and young adults with osteosarcoma. Eur J Nucl Med Mol Imaging 2012;39:39-49.
12. Bernstein JM, Homer JJ, West CM. Dynamic contrast-enhanced magnetic resonance imaging biomarkers in head and neck cancer: potential to guide treatment? A systematic review. Oral Oncol 2014;50:963-970.
13. Surov A, Meyer HJ, Wienke A. Correlation between apparent diffusion coefficient (ADC) and cellularity is different in several tumors: a meta-analysis. Oncotarget 2017;8:59492-59499.
14. Shukla-Dave A, Lee NY, Jansen JF, Thaler HT, Stambuk HE, Fury MG, Patel SG, Moreira AL, Sherman E, Karimi S, Wang Y, Kraus D, Shah JP, Pfister DG, Koutcher JA. Dynamic contrast-enhanced magnetic resonance imaging as a predictor of outcome in head-and-neck squamous cell carcinoma patients with nodal metastases. Int J Radiat Oncol Biol Phys 2012;82:1837-1844.
15. Meyer HJ, Purz S, Sabri O, Surov A. Relationships between histogram analysis of ADC values and complex 18F-FDG-PET parameters in head and neck squamous cell carcinoma. PLoS One 2018;13:e0202897.
16. Nakajo M, Nakajo M, Kajiya Y, Tani A, Kamiyama T, Yonekura R, Fukukura Y, Matsuzaki T, Nishimoto K, Nomoto M, Koriyama C. FDG PET/CT and diffusion-weighted imaging of head and neck squamous cell carcinoma: comparison of prognostic significance between primary tumor standardized uptake value and apparent diffusion coefficient. Clin Nucl Med 2012;37:475-480.
17. Varoquaux A, Rager O, Lovblad KO, Masterson K, Dulguerov P, Ratib O, Becker CD, Becker M. Functional imaging of head and neck squamous cell carcinoma with diffusion-weighted MRI and FDG PET/CT: quantitative analysis of ADC and SUV. Eur J Nucl Med Mol Imaging 2013;40:842-852.
18. Fruehwald-Pallamar J, Czerny C, Mayerhoefer ME, Halpern BS, Eder-Czembirek C, Brunner M, Schuetz M, Weber M, Fruehwald L, Herneth AM. Functional imaging in head and neck squamous cell carcinoma: correlation of PET/CT and diffusion-weighted imaging at 3 Tesla. Eur J Nucl Med Mol Imaging 2011;38:1009-1019.
19. Zhang Y, Liu X, Zhang Y, Li WF, Chen L, Mao YP, Shen JX, Zhang F, Peng H, Liu Q, Sun Y, Ma J. Prognostic value of the primary lesion apparent diffusion coefficient (ADC) in nasopharyngeal carcinoma: a retrospective study of 541 cases. Sci Rep 2015;5:12242.
20. Martens RM, Noij DP, Koopman T, Zwezerijnen B, Heymans M, de Jong MC, Hoekstra OS, Vergeer MR, de Bree R, Leemans CR, de Graaf P, Boellaard R, Castelijns JA. Predictive value of quantitative diffusion-weighted imaging and 18-F-FDG-PET in head and neck squamous cell carcinoma treated by (chemo)radiotherapy. Eur J Radiol 2019;113:39-50.
21. Gaddikeri S, Gaddikeri RS, Tailor T, Anzai Y. Dynamic Contrast-Enhanced MR Imaging in Head and Neck Cancer: Techniques and Clinical Applications. AJNR Am J Neuroradiol 2016;37:588-595.
22. Nioche C, Orlhac F, Boughdad S, Reuzé S, Goya-Outi J, Robert C, Pellot-Barakat C, Soussan M, Frouin F, Buvat I. LIFEx: A Freeware for Radiomic Feature Calculation in Multimodality Imaging to Accelerate Advances in the Characterization of Tumor Heterogeneity. Cancer Res 2018;78:4786-4789.
23. Im HJ, Bradshaw T, Solaiyappan M, Cho SY. Current Methods to Define Metabolic Tumor Volume in Positron Emission Tomography: Which One is Better? Nucl Med Mol Imaging 2018;52:5-15.
24. Fonti R, Larobina M, Del Vecchio S, De Luca S, Fabbricini R, Catalano L, Pane F, Salvatore M, Pace L. Metabolic tumor volume assessed by 18F-FDG PET/CT for the prediction of outcome in patients with multiple myeloma. J Nucl Med 2012;53:1829-1835.
25. Zhang L, Song T, Meng Z, Huang C, Chen X, Lu J, Xian J. Correlation between apparent diffusion coefficients and metabolic parameters in hypopharyngeal squamous cell carcinoma: a prospective study with integrated PET/MRI. Eur J Radiol 2020;129:109070.
26. Gawlitza M, Purz S, Kubiessa K, Boehm A, Barthel H, Kluge R, Kahn T, Sabri O, Stumpp P. In Vivo Correlation of Glucose Metabolism, Cell Density and Microcirculatory Parameters in Patients with Head and Neck Cancer: Initial Results Using Simultaneous PET/MRI. PLoS One 2015;10:e0134749.
27. Zheng D, Niu L, Liu W, Zheng C, Yan R, Gong L, Dong Z, Li K, Fei J. Correlation analysis between the SUVmax of FDG-PET/CT and clinicopathological characteristics in oral squamous cell carcinoma. Dentomaxillofac Radiol 2019;48:20180416.
28. Ahn SJ, Park MS, Kim KA, Park JY, Kim I, Kang WJ, Lee SK, Kim MJ. ^{18}F-FDG PET metabolic parameters and MRI perfusion and diffusion parameters in hepatocellular carcinoma: a preliminary study. PLoS One 2013;8:e71571.
29. Strosberg JR, Coppola D, Klimstra DS, Phan AT, Kulke MH, Wiseman GA, Kvols LK; North American Neuroendocrine Tumor Society (NANETS). The NANETS consensus guidelines for the diagnosis and management of poorly differentiated (high-grade) extrapulmonary neuroendocrine carcinomas. Pancreas 2010;39:799-800.
30. Surov A, Meyer HJ, Höhn AK, Wienke A, Sabri O, Purz S. 18F-FDG-PET Can Predict Microvessel Density in Head and Neck Squamous Cell Carcinoma. Cancers (Basel) 2019;11:543.
31. Zhang J, Chen L, Chen Y, Wang W, Cheng L, Zhou X, Wang J. Tumor vascularity and glucose metabolism correlated in adenocarcinoma, but not in squamous cell carcinoma of the lung. PLoS One 2014;9:e91649.
32. Bisdas S, Seitz O, Middendorp M, Chambron-Pinho N, Bisdas T, Vogl TJ, Hammerstingl R, Ernemann U, Mack MG. An exploratory pilot study into

the association between microcirculatory parameters derived by MRI-based pharmacokinetic analysis and glucose utilization estimated by PET-CT imaging in head and neck cancer. Eur Radiol 2010;20:2358-2366.

33. Cheng HL. Investigation and optimization of parameter accuracy in dynamic contrast-enhanced MRI. J Magn Reson Imaging 2008;28:736-743.
34. Choi SH, Paeng JC, Sohn CH, Pagsisihan JR, Kim YJ, Kim KG, Jang JY, Yun TJ, Kim JH, Han MH, Chang KH. Correlation of 18F-FDG uptake with apparent diffusion coefficient ratio measured on standard and high b value diffusion MRI in head and neck cancer. J Nucl Med 2011;52:1056-1062.
35. Sawazaki-Calone I, Rangel A, Bueno AG, Morais CF, Nagai HM, Kunz RP, Souza RL, Rutkauskis L, Salo T, Almangush A, Coletta RD. The prognostic value of histopathological grading systems in oral squamous cell carcinomas. Oral Dis 2015;21:755-761.

Interesting Image
Mol Imaging Radionucl Ther 2021;30:187-189 DOI:10.4274/mirt.galenos.2020.20981

The Role of a Bone SPECT/CT Scan in the Follow-up of a Solitary Bone Lesion in a Patient with Langerhans' Cell Histiocytosis

Langerhans Hücreli Histiyositoz Tanılı Hastada Soliter Kemik Lezyonunun Takibinde Kemik Sintigrafi ve SPECT/BT'nin Rolü

Selin Kesim, Halil Turgut Turoğlu, Sabahat İnanır, Salih Özgüven, Tanju Yusuf Erdil

Marmara University Pendik Training and Research Hospital, Clinic of Nuclear Medicine, İstanbul, Turkey

Abstract

Langerhans' cell histiocytosis (LCH) is a rare disease observed in childhood characterized by the proliferation of Langerhans' cells resulting in focal or systemic manifestations (including the bones). Here, we present a pediatric case with a localized biopsy-proven LCH, who underwent progression from solitary to multifocal form detected on bone scintigraphy and single photon emission computerized tomography/computed tomography (SPECT/CT) performed within four months. Emphasizing on localized bone pain (predictive of osseous LCH) and local tenderness and swelling usually guides the nuclear physician to perform additional SPECT/CT with presumably an improvement of the diagnostic accuracy as demonstrated in our case.

Keywords: Langerhans' cell histiocytosis, technetium-99m-methylene diphosphonate bone scintigraphy, bone SPECT/CT

Öz

Langerhans hücreli histiyositoz (LHH), genellikle çocukluk çağında görülen, Langerhans hücrelerinin çoğalmasıyla birlikte kemikler de dahil olmak üzere lokal veya sistemik tutulum ile seyreden nadir bir hastalıktır. Burada, soliter olup dört ay sonra yapılan kemik sintigrafisi ve tek foton emisyon tomografisi/bilgisayarlı tomografide (SPECT/BT) multifokal forma ilerlediği saptanan, biyopsi ile kanıtlanmış LHH tanılı pediatrik bir olgu sunulmaktadır. Bu olguda görülmektedir ki; lokalize kemik ağrısı şikayeti olan ve/veya fizik muayenede lokal hassasiyet ve şişme gibi bulguları olan hastalarda, ilgili alanın ek SPECT/BT görüntülerinin alınması ile tanısal doğrulukta iyileşme sağlamaktadır.

Anahtar Kelimeler: Langerhans hücreli histiyositoz, teknesyum-99m-metilen difosfonat kemik sintigrafisi, kemik SPECT/BT

Address for Correspondence: Selin Kesim MD, Marmara University Pendik Training and Research Hospital, Clinic of Nuclear Medicine, İstanbul, Turkey
Phone: +90 216 396 86 48 **E-mail:** selinkesim@yandex.com ORCID ID: orcid.org/0000-0002-6164-9781
Received: 28.04.2020 **Accepted:** 29.06.2020

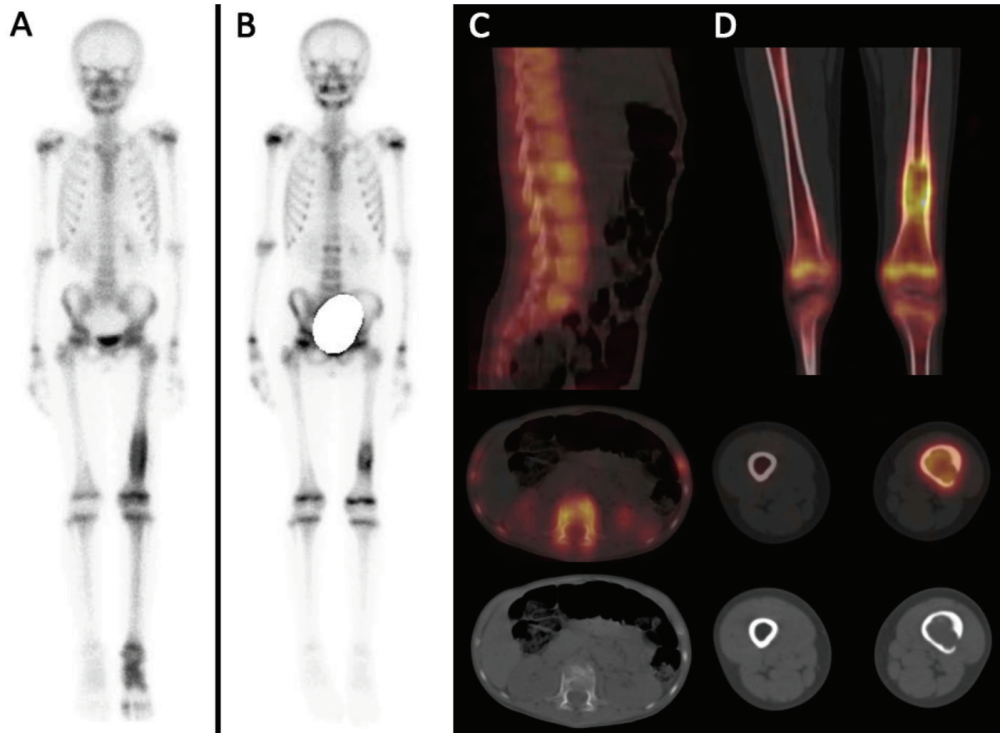

Figure 1. (A) An 11-year-old girl presented with left-leg pain and limping without history of trauma; was referred for technetium-99m-methylene diphosphonate whole-body bone scintigraphy (BS). Baseline BS revealed a marked radiotracer uptake only in the distal part of the left femoral diaphysis. In addition, an increased Tc-99m MDP uptake was observed in the left tibiotalar and tarsal region.
(B) The tru-cut biopsy demonstrated mononuclear cells with S-100 and CD1a immunoreactivity. This was consistent with Langerhans' cell histiocytosis (LCH), and the patient underwent two cycles of chemotherapy. Four months later, the patient started complaining of low back pain and was referred to do a control BS, which showed a slightly increased radiotracer uptake in the L2 vertebra.
(C) Single photon emission computerized tomography/computed tomography (SPECT/CT) images showed a new L2 lytic lesion.
(D) The initial left femoral lesion also persisted with well-defined lytic lesion, having an expanded appearance with endosteal scalloping and accompanying cortical destruction.

LCH refers to a group of diseases associated with the accumulation of Langerhans' cells, resulting in focal or systemic manifestations (involving the bone, lung, skin, central nervous system, liver, spleen, thymus, lymph nodes, and bone marrow). LCH previously known as eosinophilic granuloma (the localized form of LCH), histiocytosis X, Langerhans' cell granulomatosis, mostly occurs in childhood. Syndromes such as Hand-Schuller-Christian disease (classic triad of skull lesions, exophthalmos, and diabetes insipidus) and the Letterer-Siwe disease (disseminated lesions involving multiple visceral organs) are also included in this spectrum (1). About 50% of patients with LCH have osseous lesions only involving the cranium, legs, vertebral column, and pelvis. Early lesions tend to have an aggressive appearance, with poorly defined margins, while mature lesions depict sclerotic borders and expanded appearance. In the vertebral column, early osseous LCH lesions appear lytic, followed by a uniform collapse which result in the "coin on edge" or vertebra plana in cases of extreme vertebral collapse. The posterior elements of the vertebrae are rarely involved, thereby differentiating LCH from osseous metastases. When a single bone is involved, the disease is usually self-limited; but multiple bone involvement progresses to a systemic disease and has a less favorable prognosis (2). BS has been considered as the most sensitive test for the detection of clinically active osseous lesions of LCH. However, in patients with localized acute bone pain and/or inflammatory signs (local tenderness and swelling), an additional SPECT/CT of the involved area should be performed to enable early detection of the disease. Moreover, some studies in the literature reveal that ^{18}fluorine-fluorodeoxyglucose (^{18}F-FDG) positron emission tomography/computed tomography (PET/CT) has a higher sensitivity in detecting metabolically active lesions not detected on conventional imaging; with the advantages of providing an anatomical evaluation and identifying occult multi-organ involvements (3,4). The initial presentation of our case was an isolated bony lesion of LCH; which is associated with a good prognosis with spontaneous regression. However, follow-up BS revealed a second osseous lesion. Therefore, categorizing the case in the initial and follow-up imaging using bone scan and/or ^{18}F-FDG PET/CT for the prognosis and treatment of LCH is of utmost importance (5,6,7,8). Hybrid imaging combining SPECT with a low-dose CT has proven to improve diagnostic accuracy and to guide clinicians on decision making as demonstrated in our case.

Ethics

Informed Consent: All appropriate patient consent forms were obtained. In the form, the patient gave consent for their pictures and other clinical information to be reported in the journal.

Peer-review: Externally and internally peer-reviewed.

Authorship Contributions

Surgical and Medical Practices: S.K., H.T.T, S.İ., S.Ö., T.Y.E., Concept: S.K., H.T.T., Design: S.K., H.T.T. Data Collection or Processing: S.K., H.T.T., Analysis or Interpretation: S.K., H.T.T., Literature Search: S.K., H.T.T., Writing: S.K., H.T.T.

Conflict of Interest: No conflict of interest was declared by the authors.

Financial Disclosure: The authors declared that this study received no financial support.

References

1. Azouz EM, Saigal G, Rodriguez MM, Podda A. Langerhans' cell histiocytosis: pathology, imaging and treatment of skeletal involvement. Pediatr Radiol 2005;35:103-115.
2. Stull MA, Kransdorf MJ, Devaney KO. Langerhans cell histiocytosis of bone. Radiographics 1992;12:801-823.
3. Lee HJ, Ahn BC, Lee SW, Lee J. The usefulness of F-18 fluorodeoxyglucose positron emission tomography/computed tomography in patients with Langerhans cell histiocytosis. Ann Nucl Med 2012;26:730-737.
4. Koç ZP, Şimşek S, Akarsu S, Balcı TA, Onur MR, Kepenek F. Insufficiency of bone scintigraphy in vertebral lesions of langerhans cell histiocytosis compared to f-18 fluorodeoxyglucose positron emission tomography/computed tomography and diagnostic computed tomography. Mol Imaging Radionucl Ther 2015;24:21-24.
5. Agarwal KK, Seth R, Behra A, Jana M, Kumar R. 18F-Fluorodeoxyglucose PET/CT in Langerhans cell histiocytosis: spectrum of manifestations. Jpn J Radiol 2016;34:267-276.
6. Sasaki H, Nagano S, Shimada H, Nakamura S, Setoguchi T, Komiya S. Clinical course of the bony lesion of single-system single-site Langerhans cell histiocytosis - Is appropriate follow-up sufficient treatment? J Orthop Sci 2018;23:168-173.
7. Howarth DM, Mullan BP, Wiseman GA, Wenger DE, Forstrom LA, Dunn WL. Bone scintigraphy evaluated in diagnosing and staging Langerhans' cell histiocytosis and related disorders. J Nucl Med 1996;37:1456-1460.
8. Dogan AS, Conway JJ, Miller JH, Grier D, Bhattathiry MM, Mitchell CS. Detection of bone lesions in Langerhans cell histiocytosis: complementary roles of scintigraphy and conventional radiography. J Pediatr Hematol Oncol 1996;18:51-58.

Interesting Image
Mol Imaging Radionucl Ther 2021;30:190-192 DOI:10.4274/mirt.galenos.2020.87699

^{18}F-Sodium Fluoride (NaF) Uptake in Calcified Bladder Carcinoma: Double Density Sign

Kalsifiye Mesane Karsinomunda ^{18}F-Sodyum Florür (NaF) Tutulumu: Çift Yoğunluk İşareti

Sharjeel Usmani[1], Najeeb Ahmed[2]

[1]Kuwait Cancer Control Center, Department of Nuclear Medicine, Shuwaikh, Kuwait
[2]Jack Brignall PET/CT Centre, Castle Hill Hospital, Cottingham, United Kingdom

Abstract

^{18}F-Sodium fluoride (NaF) is primarily a skeletal imaging agent which can be localized in extraosseous calcified foci. Here, we describe a case of a 48-year-old man with bladder carcinoma referred for staging using ^{18}F-NaF positron emission tomography/computed tomography (PET/CT). ^{18}F-NaF PET/CT detected a calcified soft tissue mass in the urinary bladder. Extraosseous ^{18}F-NaF uptake is often encountered and these non-osseous findings could possibly provide important diagnostic information. Thus, recognition of extraosseous ^{18}F-NaF activity has implications for accurate staging and management.

Keywords: ^{18}F-NaF PET/CT, bladder carcinoma, extraosseous uptake, metastasis

Öz

Öncelikle bir iskelet sistemi görüntüleme ajanı olan ^{18}F-Sodyum Florür (NaF) ekstraosseöz kalsifiye odaklarda da tutulum gösterebilir. Burada, ^{18}F -NaF pozitron emisyon tomografisi/bilgisayarlı tomografi (PET/BT) kullanılarak evreleme için sevk edilen mesane karsinomu tanılı 48 yaşında bir erkek olgu sunulmuştur. ^{18}F- NaF PET/BT ile, idrar kesesinde kalsifiye yumuşak doku kitlesi tespit edilmiştir. Ekstraosseöz ^{18}F-NaF tutulumuna sıklıkla rastlanır ve bu kemik dışı bulgular önemli tanısal bilgiler sağlayabilir. Bu nedenle, ekstraosseöz ^{18}F-NaF aktivitesinin tanınmasının doğru evreleme ve tedavi açısından önemli etkileri vardır.

Anahtar Kelimeler: ^{18}F-NaF PET/BT, mesane karsinomu, ekstraosseöz tutulum, metastaz

Address for Correspondence: Sharjeel Usmani MD, Kuwait Cancer Control Center, Department of Nuclear Medicine, Shuwaikh, Kuwait
Phone: +90 96597613437 **E-mail:** dr_shajji@yahoo.com ORCID ID: orcid.org/0000-0001-9274-7571
Received: 05.05.2020 **Accepted:** 16.07.2020

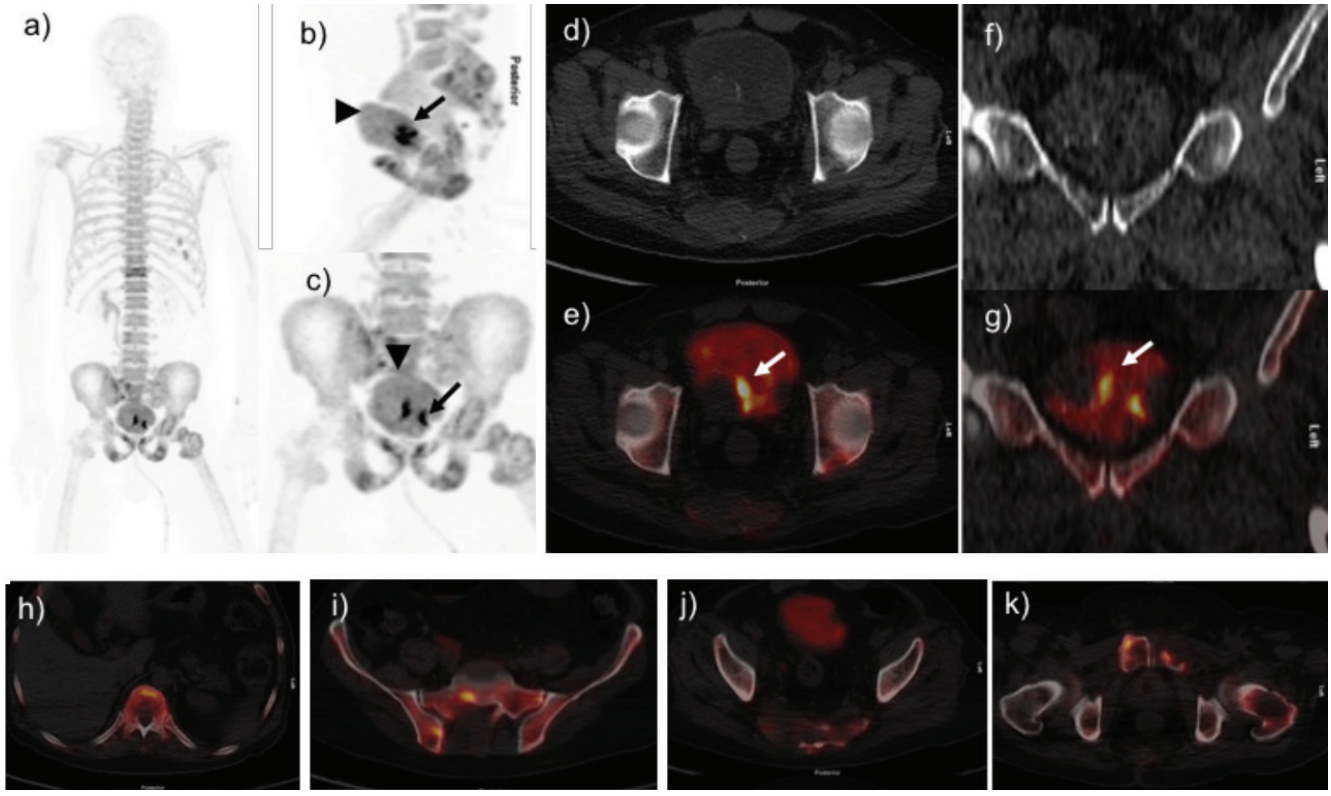

Figure 1. The profile of a 48-year-old man with bladder carcinoma. ^{18}F-Sodium fluoride (NaF) positron emission tomography/computed tomography (PET/CT) is performed after injecting 3.9 mCi of ^{18}F-NaF with urinary catheter in place and images are acquired 60 minutes post-injection. a) ^{18}F-NaF maximum intensity projection (MIP), b) zoom lateral and, c) anterior ^{18}F-NaF MIP images show two foci of intense activity in the urinary bladder (arrow) and rest of the urinary bladder is filled with mild homogenous tracer uptake (arrow head), findings appear as a double density of increase uptake in the urinary bladder. d, e, f) Non-contrast CT image in the bone window demonstrates soft tissue mass with marginal calcification and increased tracer uptake on fused images. The surveyed skeleton shows multiple aggressive lytic lesions with osteoblastic activity at D11 vertebra, sacrum, pelvic bones, and left proximal femur consistent with osteoblastic bone metastases. Double density foci (hotter spot within hot area) are due to soft tissue contrast uptake at the primary calcified urinary bladder mass and relative mild tracer uptake in the non-radioactive urine in the bladder.

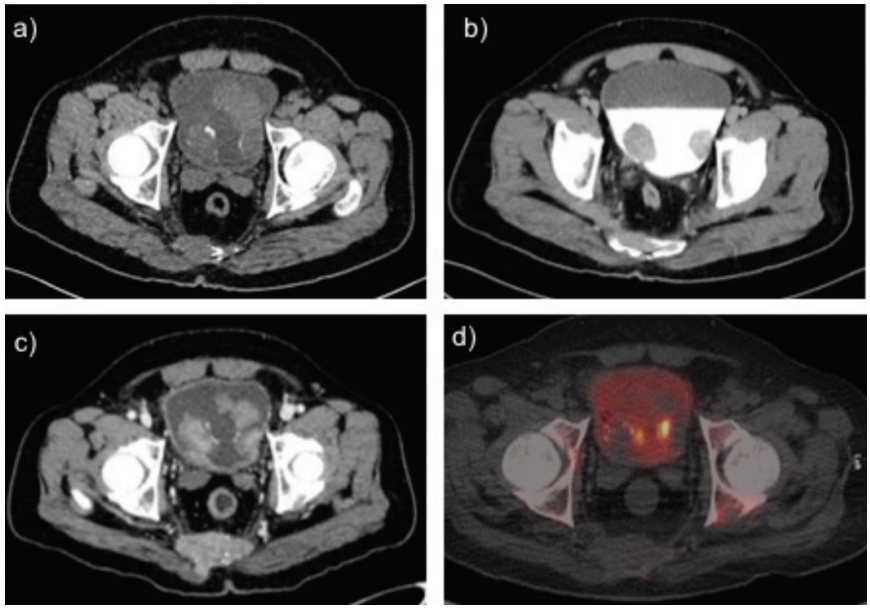

Figure 2. Diagnostic CT a) pre-contrast, b) contrast and, c) delayed portovenous phase images showing focal lesions of varying sizes in the urinary bladder. The largest lesion was at the right uretero-vesicle junction with evidence of extra mural and perivesical fat stranding with marginal interrupted calcification. Another suspicious lesion is seen in the left anterolateral wall. (d) Fused ^{18}F-NaF PET/CT images in soft tissue window show ^{18}F-NaF uptake at the calcification.

Bladder transitional cell carcinoma is the second most common urinary tract malignancy (1). Common sites of metastasis are nodal, skeletal, hepatic, pulmonary, and adrenal glands (2). Among these, the spinal axis where these are usually lytic (3). ^{18}F-NaF is an excellent bone-seeking tracer with predominant skeletal uptake due to quick first-pass extraction, minor plasma protein binding and rapid renal excretion. After one hour of administration, around 10% of this tracer is found in plasma (4). ^{18}F-NaF PET/CT is highly sensitive in characterizing both blastic and lytic lesions. Due to its excellent spatial resolution, this tracer is can also identify increased bone turnover along the thin reactive border around bone lysis (5). Thus, this was a case with depicting lytic bone metastases and extra osseous ^{18}F-NaF uptake in calcified urinary bladder mass (double density sign).

^{18}F-NaF can be localized in extraosseous calcifying lesions. Skeletal primary and metastatic foci can absorb ^{18}F-NaF because of either tumoral calcification or calcifications within necrotic foci (6). In literature, there are examples of extraosseous ^{18}F-NaF uptake for both malignant (brain, cardiac, lymph nodes, liver metastases) and benign etiologies (cardiac amylodosis, meningioma and lung amyloidosis) (7,8,9). The mechanisms of extraosseous ^{18}F-NaF uptake are unclear. Several postulates reveal that the process underlying active calcium turnover demonstrates ^{18}F-NaF uptake. Extraosseous ^{18}F-NaF uptake is often encountered. Thus, the recognition of extra osseous ^{18}F-NaF uptake is essential for precise diagnosis and interpretation.

Ethics

Informed Consent: The institutional review board waived the need to obtain informed consent.

Peer-review: Externally and internally peer-reviewed.

Authorship Contributions

Surgical and Medical Practices: S.U., Concept: S.U., N.A., Design: S.U., N.A., Data Collection or Processing: S.U., N.A., Analysis or Interpretation: S.U., N.A., Literature Search: S.U., Writing: S.U., N.A.

Conflict of Interest: No conflict of interest was declared by the authors.

Financial Disclosure: The authors declared that this study received no financial support.

References

1. Siegel RL, Miller KD, Jemal A. Cancer statistics, 2016. CA Cancer J Clin 2016;66:7-30.
2. Babaian RJ, Johnson DE, Llamas L, Ayala AG. Metastases from transitional cell carcinoma of urinary bladder. Urology 1980;16:142-144.
3. Kirkali Z, Chan T, Manoharan M, Algaba F, Busch C, Cheng L, Kiemeney L, Kriegmair M, Montironi R, Murphy WM, Sesterhenn IA, Tachibana M, Weider J. Bladder cancer: epidemiology, staging and grading, and diagnosis. Urology 2005;66(6 Suppl 1):4-34.
4. Czernin J, Satyamurthy N, Schiepers C. Molecular mechanisms of bone 18F-NaF deposition. J Nucl Med 2010;51:1826-1829.
5. Araz M, Aras G, Küçük ÖN. The role of 18F-NaF PET/CT in metastatic bone disease. J Bone Oncol 2015;4:92-97.
6. Usmani S, Gnanasegaran G, Marafi F, Esmail A, Ahmed N, Van den Wyngaert T. The clinical significance of incidental soft tissue uptake on whole body 18F-sodium fluoride bone PET-CT. Clin Radiol 2019;74:95-110.
7. Korkmaz U, Ustun F. 18F-NaF PET/CT and Extraordinary Involvement: Non-calcific Brain Involvement in a Prostate Cancer Case. Mol Imaging Radionucl Ther 2020;29:41-44.
8. Sheth S, Colletti PM. Atlas of sodium fluoride PET bone scans: atlas of NaF PET bone scans. Clin Nucl Med 2012;37:e110-116.
9. Van Der Gucht A, Galat A, Rosso J, Guellich A, Garot J, Bodez D, et al. [18F]-NaF PET/CT imaging in cardiac amyloidosis. J Nucl Cardiol 2016;23:846-849.

Interesting Image
Mol Imaging Radionucl Ther 2021;30:193-196 DOI:10.4274/mirt.galenos.2020.58661

Radium-223 Treatment in mCRPC Patient with Polycythemia Vera

Polisitemi Vera Tanılı mCRPC Hastasında Radyum-223 Tedavisi

Cristina de Angelis[1], Viviana Frantellizzi[1], Mariano Pontico[2], Maria Silvia de Feo[1], Julia Lazri[1], Giuseppe de Vincentis[1]

[1]Sapienza University of Rome, Department of Radiological Sciences, Oncology and Anatomical Pathology, Rome, Italy
[2]Sapienza University of Rome, Ph.D. Program in Morphogenesis and Tissue Engineering, Department of Medico-surgical Sciences and Biotechnologies, Rome, Italy

Abstract

There have been several studies on the clinical outcomes of Radium-223 treatment in patients with metastatic castration-resistant prostate cancer (mCRPC) who may have an increased risk of hematologic comorbidities. To the best of our knowledge, this is the first study to explore the potential bone marrow adverse effects (AEs) of Radium-223 administered with specific drugs used for hematologic conditions, such as polycythemia vera (PV). We report the case of a patient with mCRPC who was administered a combined treatment of Radium-223 and hydroxyurea for PV, aiming to support clinicians in predicting eventual AEs.

Keywords: Prostate cancer, mCRPC, Radium-223, polycythemia vera, hematogical toxicity

Öz

Hematolojik komorbidite riski artmış metastatik kastrasyona dirençli prostat kanseri (mCRPC) olan hastalarda Radyum-223 tedavisinin klinik sonuçları üzerine çeşitli çalışmalar yapılmıştır. Bilgimiz dahilinde bu çalışma, Radyum-223 ile birlikte polisitemia vera (PV) gibi bir hematolojik hastalık için özel ilaçlar alan bir hastada potansiyel kemik iliği yan etkilerinin (YE) araştırıldığı ilk çalışmadır. Burada, klinisyenleri olası YE'leri öngörmede desteklemesi amaçlanan ve PV ile birlikte mCRPC tanısı için Radyum-223 ve hidroksiüre tedavileri uygulanan bir olgu sunulmuştur.

Anahtar Kelimeler: Prostat kanseri, mCRPC, Radyum-223, polisitemia vera, hematolojik toksisite

Prostate cancer (PCa) represents the second most prevalent cancer in men and the fifth cause of cancer-related mortality worldwide (1). Bone secondary tumor localizations are the most frequent expression of advanced PCa, representing the cause of morbidity and mortality and determining a poor prognosis. Several studies have been provided concerning the clinical outcomes of Radium-223 treatment in patients with metastatic castration-resistant prostate cancer (mCRPC) (2,3). Moreover, patients with mCRPC could suffer from hematologic comorbidities. Notably, to our knowledge, there are no studies involving the use of Radium-223 in patients with mCRPC and preexisting hematological conditions, such as polycythemia vera (PV), a chronic myeloproliferative disorder. Thus, studies that could support clinicians to predict eventual adverse effects (AEs) in these cases are warranted.

Address for Correspondence: Mariano Pontico MD, Sapienza University of Rome, Ph.D. Program in Morphogenesis and Tissue Engineering, Department of Medico-surgical Sciences and Biotechnologies, Rome, Italy
Phone: 0649978590 **E-mail:** mariano.pontico@uniroma1.it ORCID ID: orcid.org/0000-0001-6143-4775
Received: 27.03.2020 **Accepted:** 05.08.2020

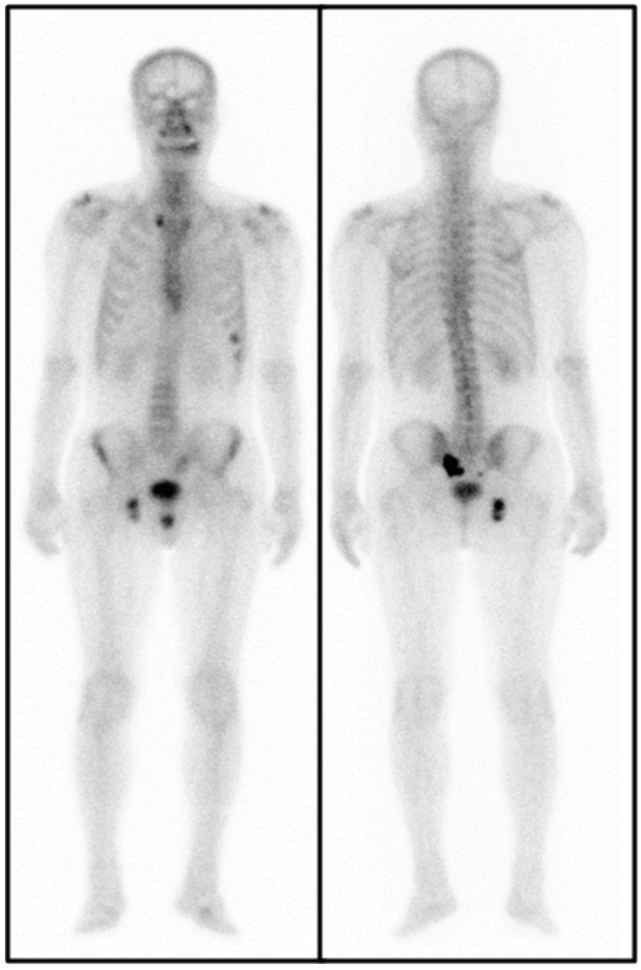

Figure 1. A 71-year-old male diagnosed with PV in 2000 and PCa in 2013 was referred to our hospital. After radical prostatectomy, the Gleason score was 8 (3+5) with pT3b-R1 staging. In 2014, RT on the prostatic region was performed, and subsequently systemic treatment was introduced. Treatment with hydroxyurea for PV (500 mg for 5 days, 1000 mg for 2 days, per week) had also been administered. Radium-223 was administered according with the current EANM guidelines. Before the first administration, a technetium-99m -HDP bone scan was performed, depicting an oligometastatic disease. An interim bone scan was obtained after the third administration and a further one after the sixth at the end of treatment. Follow-up bone scans at 3, 6, and 12 months after the end of Radium-223 treatment was carried out.

Patients with mCRPC with compromised bone marrow reserve due to previous therapies have an increased risk of hematological AEs when enrolled in the Radium-223 treatment (4). Although the occurrence of anemia and neutropenia were not significantly different between placebo and the Radium-223 group in the ALSYMPCA trial (5), the cumulative effects of Radium-223 and other chemotherapies remain unelucidated.

In our case, no AEs of any kind were experienced during treatment. Hemoglobin (Hb) gradually reduced between the first and second cycles, but values remained >13 mg/dL. Consequently, the hematologist decided to lower the hydroxyurea dosage to 500 mg once a day after the second cycle, and Hb values quickly normalized before the third administration. At the time of the first medical examination, the patient reported taking non-steroidal anti-inflammatory drugs (NSAIDs) to control pain as necessary. Notably, after the first administration, the BPI value dropped from 5 to 0, and NSAIDs were not required. One year after the first dose of Radium-223, the patient reported excellent control of bone pain and absence of the need for NSAIDs.

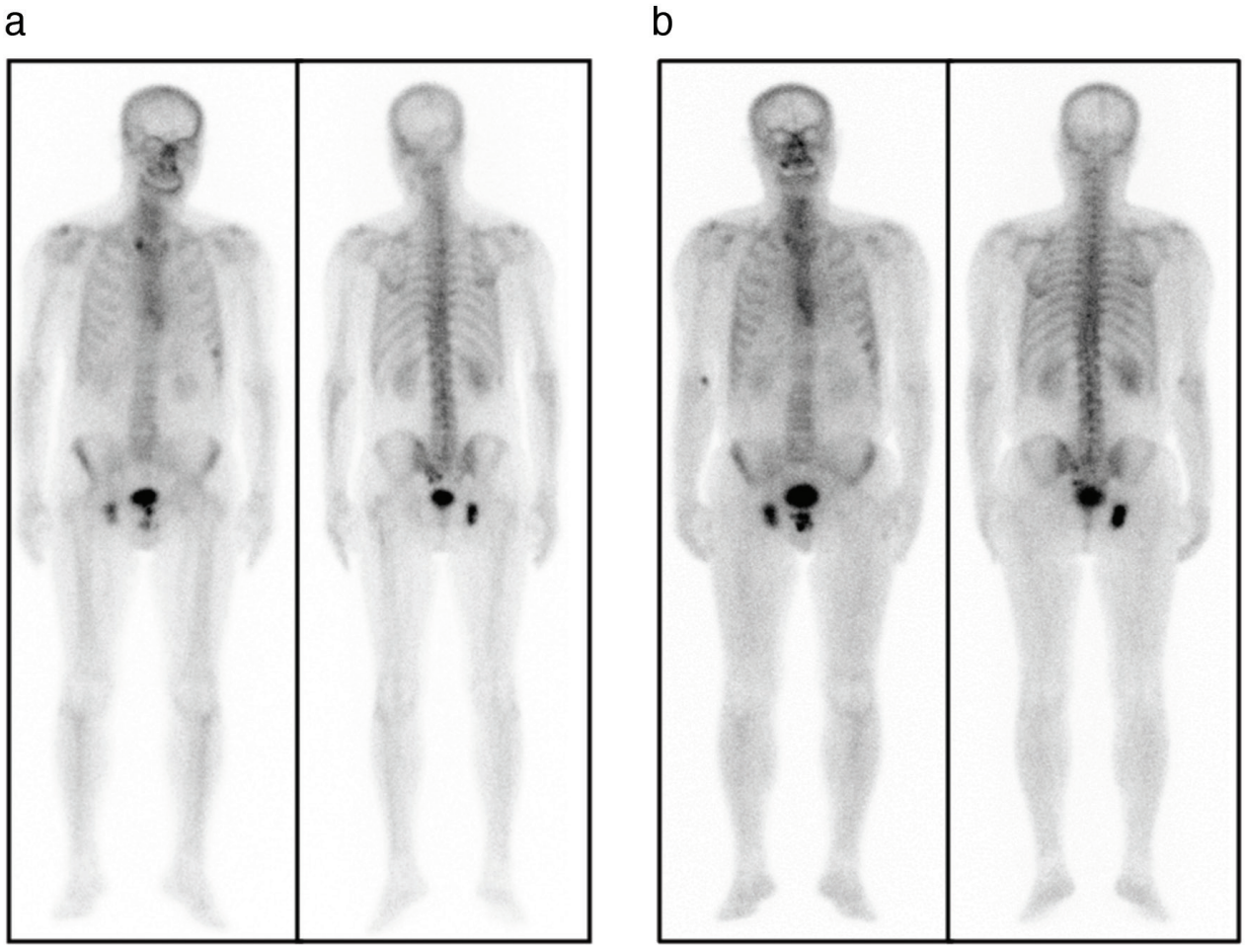

Figure 2. Compared to the pretreatment scan, the bone scan obtained after the conclusion of the Radium-223 treatment (a) revealed a marked regression of the osteotropic radiotracer increased uptake located in the right side of the sacrum, a significant reduction of uptake intensity of the same finding in the contralateral side, and a slighter decrease of uptake in the 7th and 8th left ribs. No differences were observed in the right ischiopubic ramus. Successively, a bone scan obtained 6 months after treatment showed total regression of the pathologic uptake located in the right side of the sacrum and an even more significant uptake intensity decline of the contralateral finding, such as that in the eighth left rib. No differences of radiotracer uptake were noted in the seventh left rib and in the right ischiopubic ramus. The bone scan obtained 1 year after Radium-223 administration (b) corroborated the favorable outcomes highlighted by the 6 months bone scan follow-up, confirming the persistence of osteotropic pathologic uptake in the 7th left rib and in the right ischiopubic ramus with remnant weak increased uptake in the sacrum, suggesting a substantially stable disease. The benefits of Radium-223 in our patient with mCRPC were remarkable; not only did bone scans reveal a regression of skeletal secondary localizations uptake but pain control was also fairly obtained without using NSAIDs.

Several studies are investigating the effectiveness of a combination therapy on patients with mCRPC and its potential cumulative effect on hematologic toxicity. Even though the biological damages of Radium-223 on the bone marrow have been minimized (6,7), defining the hematologic profile of patients with mCRPC is a key step to limit the chance of hematologic AEs. Although rare, the potential AEs of Radium-223 on bone marrow functionality must be considered (8). This has been the main concern when administering this radionuclide to patients with mCRPC who often receive or are still receiving other systemic therapies. Particular attention must be paid when mCRPC coexists with hematologic conditions that require suppression of the excessive functionality of the bone marrow. However, our study has several limitations, such as that PV may not represent the optimal model to assess the potential cytotoxic effects of hydroxyurea because PV is not typically characterized by the occurrence of a cytopenic condition.

This study supports and confirms the existing evidence in the literature about the hematologic safety of Radium-223 that is specifically applied in a patient with impaired bone marrow functionality due to PV. Additionally, Radium-223 appears to be safe and well tolerated even when combined with a cytotoxic agent, such as hydroxyurea.

Ethics

Informed Consent: Informed consent was obtained from the patient.

Peer-review: Externally peer-reviewed.

Authorship Contributions

Surgical and Medical Practices: C.A., J.L., M.S.F., Concept: G.V., V.F., Design: G.V., V.F., M.P., Data Collection or Processing: V.F., C.A., Analysis or Interpretation: G.V., V.F., M.P., Literature Search: C.A., J.L., M.S.F., Writing: C.A., M.P., J.L.

Conflict of Interest: No conflict of interest was declared by the authors.

Financial Disclosure: The authors declared that this study received no financial support.

References

1. Wong MC, Goggins WB, Wang HH, Fung FD, Leung C, Wong SY, Ng CF, Sung JJ. Global Incidence and Mortality for Prostate Cancer: Analysis of Temporal Patterns and Trends in 36 Countries. Eur Urol 2016;70:862-874.
2. Parker C, Nilsson S, Heinrich D, Helle SI, O'Sullivan JM, Fosså SD, Chodacki A, Wiechno P, Logue J, Seke M, Widmark A, Johannessen DC, Hoskin P, Bottomley D, James ND, Solberg A, Syndikus I, Kliment J, Wedel S, Boehmer S, Dall'Oglio M, Franzén L, Coleman R, Vogelzang NJ, O'Bryan-Tear CG, Staudacher K, Garcia-Vargas J, Shan M, Bruland ØS, Sartor O; ALSYMPCA Investigators. Alpha emitter radium-223 and survival in metastatic prostate cancer. N Engl J Med 2013;369:213-223.
3. De Vincentis G, Follacchio GA, Frantellizzi V, Prelaj A, Farcomeni A, Giuli A, Bianco V, Tomao S. 223Ra-dichloride therapy in an elderly bone metastatic castration-resistant prostate cancer patient: a case report presentation and comparison with existing literature. Aging Clin Exp Res 2018;30:677-680.
4. Ricci M, Frantellizzi V, Bulzonetti N, De Vincentis G. Reversibility of castration resistance status after Radium-223 dichloride treatment: clinical evidence and review of the literature. Int J Radiat Biol 2019;95:554-561.
5. De Vincentis G, Monari F, Baldari S, Salgarello M, Frantellizzi V, Salvi E, Reale L, Napolitano S, Conti G, Cortesi E. Narrative medicine in metastatic prostate cancer reveals ways to improve patient awareness & quality of care. Future Oncol 2018;14:2821-2832.
6. Vogelzang NJ, Coleman RE, Michalski JM, Nilsson S, O'Sullivan JM, Parker C, Widmark A, Thuresson M, Xu L, Germino J, Sartor O. Hematologic Safety of Radium-223 Dichloride: Baseline Prognostic Factors Associated With Myelosuppression in the ALSYMPCA Trial. Clin Genitourin Cancer 2017;15:42-52.e8.
7. Saad F, Carles J, Gillessen S, Heidenreich A, Heinrich D, Gratt J, Lévy J, Miller K, Nilsson S, Petrenciuc O, Tucci M, Wirth M, Federhofer J, O'Sullivan JM; Radium-223 International Early Access Program Investigators. Radium-223 and concomitant therapies in patients with metastatic castration-resistant prostate cancer: an international, early access, open-label, single-arm phase 3b trial. Lancet Oncol 2016;17:1306-1316.
8. De Vincentis G, Follacchio GA, Frantellizzi V, Liberatore M, Monteleone F, Cortesi E. Prostate-Specific Antigen Flare Phenomenon During 223Ra-Dichloride Treatment for Bone Metastatic Castration-Resistant Prostate Cancer: A Case Report. Clin Genitourin Cancer 2016;14:e529-e533.

Interesting Image
Mol Imaging Radionucl Ther 2021;30:197-200 DOI:10.4274/mirt.galenos.2021.15013

PET/CT for Early Detection of COVID-19 Pneumonia: Diffuse Fluorodeoxyglucose Uptake in the Lungs without any Additional Changes in a Patient with Breast Cancer

PET/BT'de COVID-19 Erken Bulgusu: Meme Kanserli Hastada Sekel BT Bulguları Zemininde Diffüz Artmış Akciğer Tutulumu

Büşra Özdemir[1], Burak Günay[2], Derya Karabulut[2], Gülay Durmuş Altun[1]

[1]*Trakya University Faculty of Medicine, Deparment of Nuclear Medicine, Edirne, Turkey*
[2]*Trakya University Faculty of Medicine, Deparment of Radiology, Edirne, Turkey*

Abstract

Coronavirus disease-2019 (COVID-19), which causes infections in the upper and lower respiratory tract, became a pandemic shortly after it was first diagnosed in Wuhan city, China. Many people are affected with high mortality rates and severe respiratory distress syndrome. During this pandemic, all physicians paid attention to the findings of COVID-19. Suggestive findings in ^{18}fluorine-fluorodeoxyglucose (^{18}F-FDG) positron emission tomography/computed tomography (PET/CT) were characterized as increased ^{18}F-FDG uptake in bilateral peripheral consolidative areas and ground glass opacities. We aimed to show diffuse FDG uptake in PET images with indefinable lesions in CT as a suspicious finding for early COVID-19.

Keywords: ^{18}F-FDG, COVID-19, PET/CT, SARS-CoV-2

Öz

Koronavirüs hastalığı-2019 (COVID-19) Çin'in Vuhan kentinde ortaya çıktıktan hemen sonra tüm dünyaya yayılmış alt ve üst solunum yolu enfeksiyonlarına yol açan bir virüstür. COVID-19, dünya genelinde birçok hastada asemptomatik hastalıktan respiratuvar distres sendromuna kadar geniş bir klinik spektrum oluşturmaktadır. Bu pandemi döneminde tüm klinisyenler COVID-19'un görüntüleme bulgularını bilmelidir. ^{18}Flor-florodeoksiglukoz (^{18}F-FDG) pozitron emisyon tomografisi/bilgisayarlı tomografide bilateral periferik konsolidasyon ve buzlu cam dansiteli alanlarda artmış ^{18}F-FDG tutulumu COVID-19 hastalarında karakteristiktir. Biz bu olgu örneğinde sekel akciğer dokusu zemininde yeni gelişen karakteristik tomografi bulgusu olmadan akciğerde diffüz artmış ^{18}F-FDG tutulumu ile tanı alan bir hastamızı sunduk.

Anahtar Kelimeler: ^{18}F-FDG, COVID-19, PET/BT, SARS-CoV-2

Address for Correspondence: Büşra Özdemir MD, Trakya University Faculty of Medicine, Deparment of Nuclear Medicine, Edirne, Turkey
Phone: +90 284 235 76 41 **E-mail:** busraozdemir39@gmail.com ORCID ID: orcid.org/0000-0001-8540-0115
Received: 19.12.2020 **Accepted:** 12.05.2021

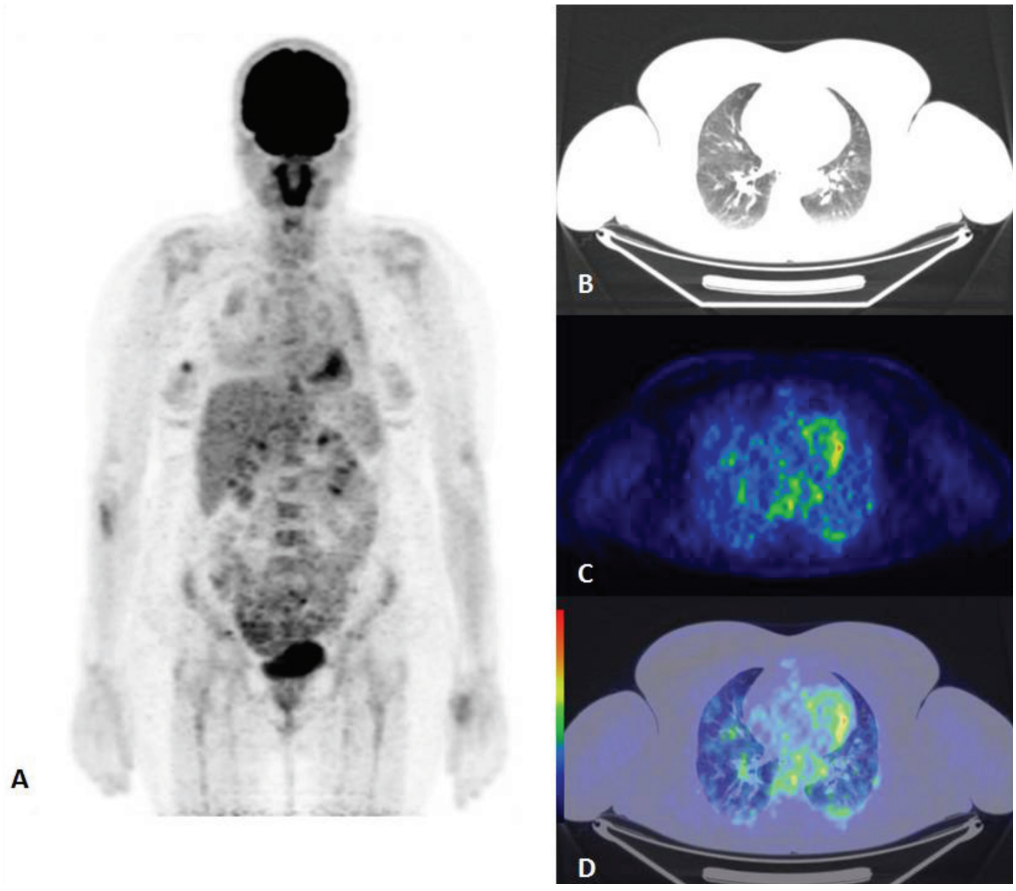

Figure 1. A 49-year-old female was biopsied for breast cancer and underwent positron emission tomography/computed tomography (PET/CT) for the staging and determination of disease extension. The patient was counseled for respiratory symptoms, such as cough, dyspnea, fatigue, and fever. She had no complaints or any known risky contacts. In maximum intensity projection images, (A) there was increased ^{18}fluorine-fluorodeoxyglucose (^{18}F-FDG) uptake in the right retro-areolar region, right axillary lymph node, and bilateral lung fields. After correlative assessment of axial tomography (B), PET (C), and fusion images (D), this diffuse lung uptake was interpreted as suspicious of interstitial pneumonia, which is highly suggestive of Coronavirus disease-2019 (COVID-19) (1,2). The referring physician was contacted, and the patient underwent diagnostic computed tomography (CT) and reverse transcription-polymerase chain reaction (RT-PCR). Although the chest CT scan was undiagnostic, RT-PCR confirmed the COVID-19 infection.

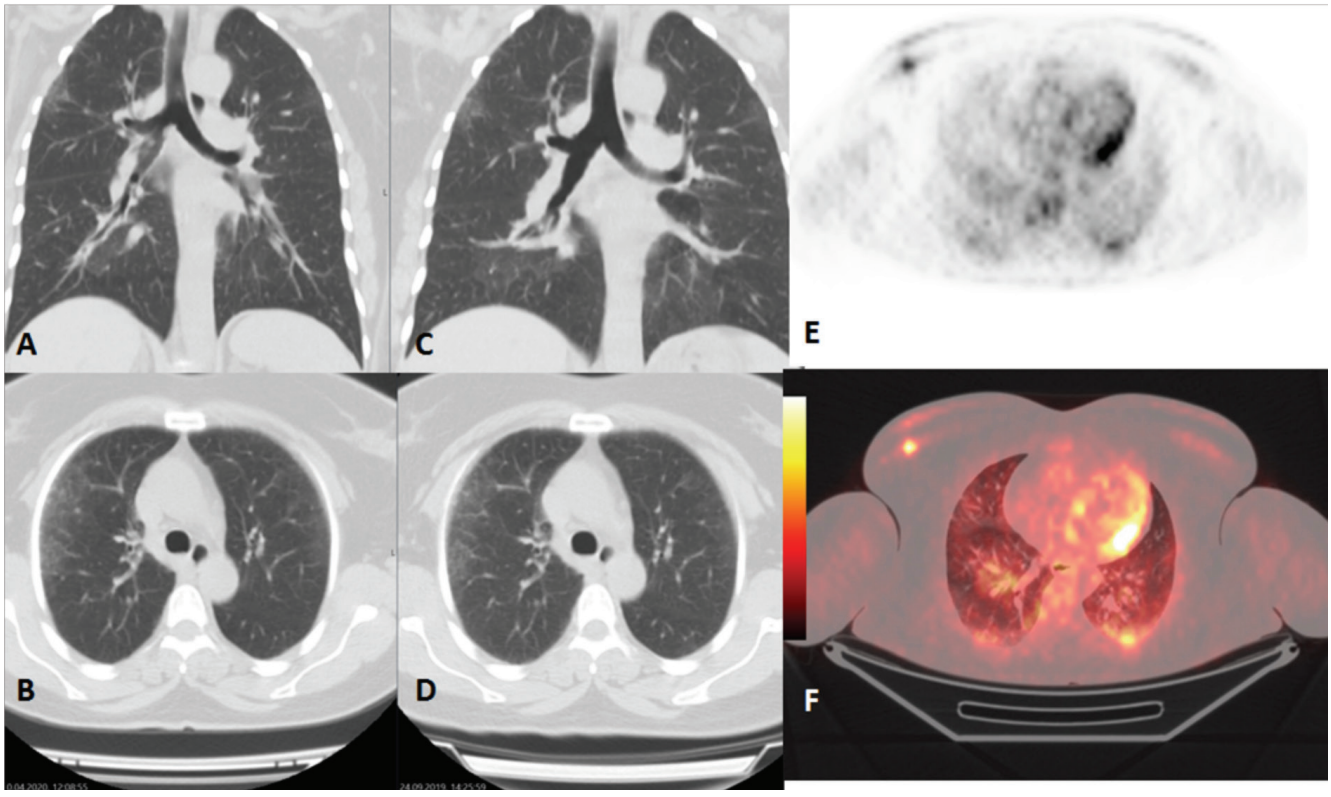

Figure 2. We compared the diagnostic axial and coronal chest CT images (A, B) taken to evaluate suspicion of COVID-19 on April 10, 2020, one day after PET/CT, with diagnostic axial and coronal chest CT (C, D) from September 2019. In both images, there was subpleural ground glass opacities and mild interseptal thickness accompanied by increased reticular density in the anterior segment of the upper lobe of the right lung and anterior segment of the upper lobe of the left lung. This was revealed as asymptomatic sequelae changes due to interstitial parenchymal disease. There were no specific changes that may be related to COVID-19 pneumonia. When we evaluated PET/CT's axial PET and hybrid images (E, F) on April 9, 2020, bilateral diffuse lung uptake without the addition of new CT findings was suggestive of COVID-19 on PCR, confirming COVID-19 positive in an asymptomatic patient. Findings of COVID-19 pneumonia may be summarized as peripheral ground glass opacites and consolidative areas in multiple segments (3). In this case, increased uptake was mainly due to increased glycolysis from leukocyte chemotaxis and accumulation related to bilateral interstitial inflammation (4). PET/CT may detect the earliest signs of interstitial pneumonia with high sensitivity (4). The ability to detect asymptomatic patients and prevent disease spread has recently become the most important aspect of PET/CT in this pandemic era of COVID-19 infection (5).

Ethics

Informed Consent: The patient gave consent to the use of her data for medical purposes and signed the consent form during imaging.

Peer-review: Externally and internally peer-reviewed.

Authorship Contributions

Surgical and Medical Practices: B.Ö., B.G., Concept: B.Ö., D.K., Design: G.D.A., Data Collection or Processing: B.Ö., B.G., Analysis or Interpretation: G.D.A., Literature Search: D.K., G.D.A., Writing: B.Ö., B.G.

Conflict of Interest: No conflict of interest was declared by the authors.

Financial Disclosure: The authors declared that this study received no financial support.

References

1. Qin C, Liu F, Yen TC, Lan X. 18F-FDG PET/CT findings of COVID-19: a series of four highly suspected cases. Eur J Nucl Med Mol Imaging 2020;47:1281-1286.
2. Artigas C, Lemort M, Mestrez F, Gil T, Flamen P. COVID-19 Pneumonia Mimicking Immunotherapy-Induced Pneumonitis on 18F-FDG PET/CT in a Patient Under Treatment With Nivolumab. Clin Nucl Med 2020;45:e381-e382.
3. Zhou Z, Guo D, Li C, Fang Z, Chen L, Yang R, Li X, Zeng W. Coronavirus disease 2019: initial chest CT findings. Eur Radiol 2020;30:4398-4406.
4. Becker W, Meller J. The role of nuclear medicine in infection and inflammation. Lancet Infect Dis 2001;1:326-333.
5. Albano D, Bertagna F, Bertoli M, Bosio G, Lucchini S, Motta F, Panarotto MB, Peli A, Camoni L, Bengel FM, Giubbini R. Incidental Findings Suggestive of COVID-19 in Asymptomatic Patients Undergoing Nuclear Medicine Procedures in a High-Prevalence Region. J Nucl Med 2020;61:632-636.

Interesting Image
Mol Imaging Radionucl Ther 2021;30:201-204 DOI:10.4274/mirt.galenos.2021.69926

A Case with ^{68}Ga-FAPI Positive and ^{18}F-FDG Negative Breast Cancer

^{68}Ga-FAPI Pozitif, ^{18}F-FDG Negatif Meme Kanseri Olgusu

Halil Kömek[1], Cihan Gündoğan[1], Hülya Etem[2], Canan Can[1]

[1]University of Health Sciences Turkey, Gazi Yaşargil Training and Research Hospital, Clinic of Nuclear Medicine, Diyarbakır, Turkey
[2]University of Health Sciences Turkey, Gazi Yaşargil Training and Research Hospital, Clinic of Pathology, Diyarbakır, Turkey

Abstract

A female patient diagnosed of infiltrative breast carcinoma using tru-cut biopsy underwent ^{18}flourine-fluorodeoxyglucose (^{18}F-FDG) positron emission tomography/computed tomography (PET/CT) for staging. The tumor was located in the superior external quadrant of the right breast, and did not exhibit pathological uptake in ^{18}F-FDG PET/CT. Later, gallium-68 (^{68}Ga) fibroblast activation protein-specific inhibitor (FAPI)-04 PET/CT imaging was performed and the primary tumor showed intense radiotracer accumulation. This presumes that ^{68}Ga-FAPI PET/CT imaging is superior to ^{18}F-FDG imaging in detecting the primary tumor in breast cancer, thereby suggesting the replacement of FAPI by ^{18}F-FDG in breast-cancer staging in the future.

Keywords: ^{68}Ga-FAPI, ^{18}F-FDG, PET/CT, breast cancer

Öz

Tru-cut biyopsi sonucu infiltratif meme karsinomu gelen bir kadın hastaya evreleme amacıyla ^{18}fluoride-florodeoksiglikoz (^{18}F-FDG) pozitron emisyon tomografi/bilgisayarlı tomografi (PET/BT) görüntüleme yapıldı. Sağ meme üst dış kadranda yer alan tümör, ^{18}F-FDG PET/BT'de patolojik aktivite tutulumu göstermedi. Daha sonra hastaya galyum-68 (^{68}Ga)-fibroblast aktivasyon protein spesifik inhibitör (FAPI)-04 PET/BT görüntüleme yapıldı ve primer tümör yoğun radyofarmasötik tutulumu gösterdi. Bu olgu ^{68}Ga-FAPI PET/BT görüntülemenin meme kanserinde primer tümörleri tespit etmede ^{18}F-FDG görüntülemeden üstün olabileceğini göstermiştir ve gelecekte meme kanseri evrelemesinde ^{18}F-FDG'nin yerini FAPI'nın alabileceğini düşündürmektedir.

Anahtar kelimeler: ^{68}Ga-FAPI, ^{18}F-FDG, PET/BT, meme kanseri

Address for Correspondence: Cihan Gündoğan MD, University of Health Sciences Turkey, Gazi Yaşargil Training and Research Hospital, Clinic of Nuclear Medicine, Diyarbakır, Turkey
Phone: +90 530 145 75 15 **E-mail:** cihangd@hotmail.com ORCID ID: orcid.org/0000-0001-5700-6292
Received: 18.05.2021 **Accepted:** 08.07.2021

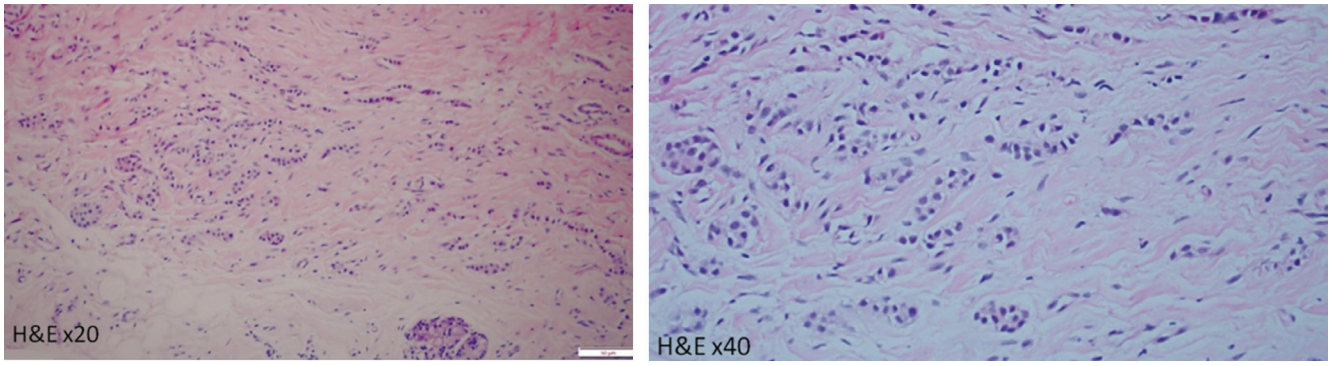

Figure 1. A tru-cut biopsy performed on a 48-year-old woman, whose breast ultrasound revealed a Breast Imaging Reporting and Data System-4B lesion measuring 20×9 mm in the right breast at the 10 o'clock position. The histologic diagnosis was infiltrative breast carcinoma and tumor cells were in the form of single-cell infiltration in focal areas (hematoxylin and eosin ×20 and ×40) without myoepithelium in the collagenous stroma (estrogen receptor is strongly positive in 95% of the cells, progesterone moderately positive in 5% of the cells, and CerbB2 is negative).

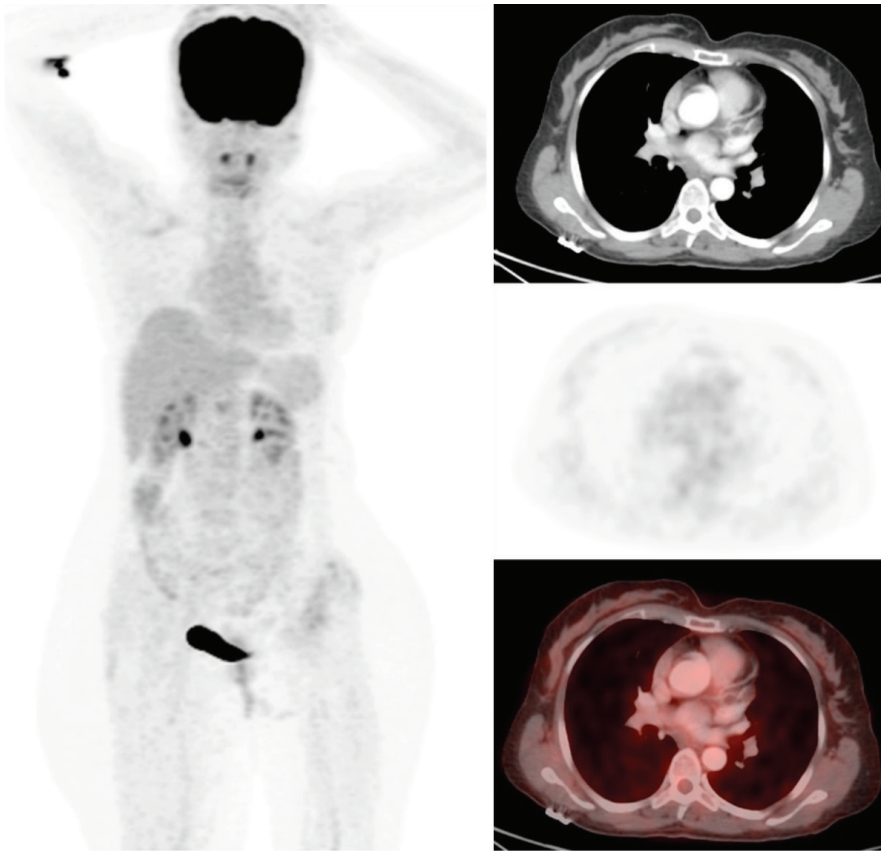

Figure 2. ^{18}Flourine-fluorodeoxyglucose (^{18}F-FDG) positron emission tomography/computed tomography (PET/CT) performed for breast-cancer staging. However, the primary tumor in the superior external quadrant of the right breast did not exhibit pathological uptake in the maximum intensity projection (MIP) and axial CT/PET-fusion images.

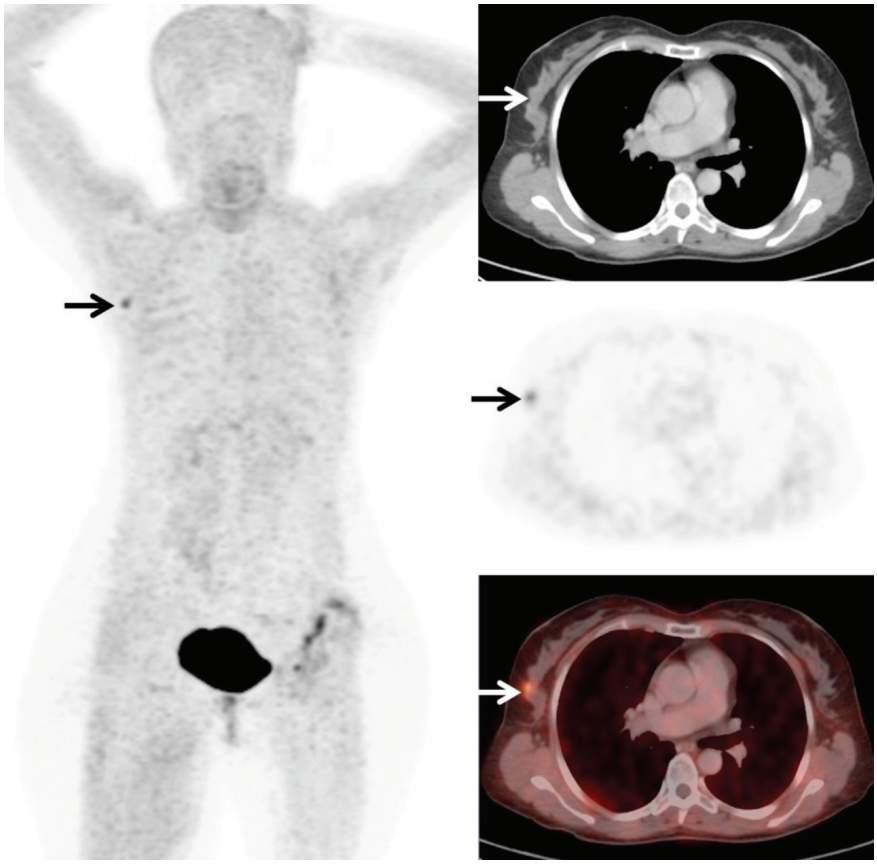

Figure 3. Gallium-68 (^{68}Ga)-fibroblast activation protein-specific inhibitor (FAPI)-04 PET/CT revealing intense radiotracer accumulation in the primary tumor distinguishing it from the MIP (a) image. The axial view of ^{68}Ga-FAPI-04 PET/CT (CT, PET, and fusion images, respectively) demonstrated intense radiotracer uptake in a lesion in the superior external quadrant of the right breast, of about 1.5 cm in size with a maximum standardized uptake value (SUV_{max}) of 5.3 (arrows). ^{68}Ga-FAPI is a recently introduced imaging agent targeting fibroblast activation protein that is highly expressed in various tumors (1,2). Recent case reports reveal that the mean SUV_{max} of breast cancers and metastases were found to be high (3,4,5). A recent study showed that ^{68}Ga-FAPI-04 PET/CT is superior to ^{18}F-FDG PET/CT in detecting primary tumors in patients with breast cancer by demonstrating its high sensitivity, high SUV_{max}, and high tumor-to-background ratio (6). ^{68}Ga-FAPI-04 PET/CT is also superior to ^{18}F-FDG PET/CT in detecting lymph node, hepatic, bone, and cerebral metastases owing to its lower background activity and higher uptake in subcentimetric lesions (6). Thus, our case depicts that ^{68}Ga-FAPI-04 PET/CT should be considered in cases with ^{18}F-FDG-negative breast cancer.

Ethics

Informed Consent: Written informed consent was obtained from the patient.

Peer-review: Externally peer-reviewed.

Authorship Contributions

Surgical and Medical Practices: H.K., C.G., H.E., C.C., Concept: H.K., C.G., H.E., C.C., Design: H.K., C.G., H.E., C.C., Data Collection or Processing: H.K., C.G., H.E., C.C., Analysis or Interpretation: H.K., C.G., H.E., C.C., Literature Search: H.K., C.G., H.E., C.C., Writing: H.K., C.G., H.E., C.C.

Conflict of Interest: No conflict of interest was declared by the authors.

Financial Disclosure: The authors declared that this study received no financial support.

References

1. Kratochwil C, Flechsig P, Lindner T, Abderrahim L, Altmann A, Mier W, Adeberg S, Rathke H, Röhrich M, Winter H, Plinkert PK, Marme F, Lang M, Kauczor HU, Jäger D, Debus J, Haberkorn U, Giesel FL. 68Ga-FAPI PET/CT: Tracer Uptake in 28 Different Kinds of Cancer. J Nucl Med 2019;60:801-805.
2. Chen H, Pang Y, Wu J, Zhao L, Hao B, Wu J, Wei J, Wu S, Zhao L, Luo Z, Lin X, Xie C, Sun L, Lin Q, Wu H. Comparison of [68Ga]Ga-DOTA-FAPI-04 and [18F] FDG PET/CT for the diagnosis of primary and metastatic lesions in patients with various types of cancer. Eur J Nucl Med Mol Imaging 2020;47:1820-1832.
3. Pang Y, Zhao L, Chen H. 68Ga-FAPI Outperforms 18F-FDG PET/CT in Identifying Bone Metastasis and Peritoneal Carcinomatosis in a Patient With Metastatic Breast Cancer. Clin Nucl Med 2020;45:913-915.
4. Can C, Gündoğan C, Güzel Y, Kaplan İ, Kömek H. 68Ga-FAPI Uptake of Thyroiditis in a Patient With Breast Cancer. Clin Nucl Med 2021;46:683-685.
5. Gündoğan C, Güzel Y, Can C, Alabalik U, Kömek H. False-Positive 68Ga-Fibroblast Activation Protein-Specific Inhibitor Uptake of Benign Lymphoid Tissue in a Patient With Breast Cancer. Clin Nucl Med 2021;46:e433-e435.
6. Kömek H, Can C, Güzel Y, Oruç Z, Gündoğan C, Yildirim ÖA, Kaplan İ, Erdur E, Yıldırım MS, Çakabay B. 68Ga-FAPI-04 PET/CT, a new step in breast cancer imaging: a comparative pilot study with the 18F-FDG PET/CT. Ann Nucl Med 2021;35:744-752.

2021 Referee Index - 2021 Hakem Dizini

A. Özgür Karaçalıoğlu
Ali Sarıkaya
Ayşe Mavi
Ayşegül Akgün
Berna Okudan Tekin
Bilal Kovan
Bilge Volkan Salancı
Billur Çalışkan
Bircan Sönmez
Bülent Turgut
Cengiz Taşçı
Corinna Altini
Csaba Juhasz
Cüneyt Türkmen
Doğangün Yüksel
Elgin Özkan
Elif Özdemir
Emel Ceylan Günay
Emre Demirci
Emre Entok
Fatma Suna Kıraç
Feyza Şen
Fikriye Gül Gümüşer
Filiz Özülker
Funda Üstün
Gonca G. Bural
Gonca Kara Gedik
Gözde Dağlıöz Görür
Gülin Vural Uçmak
Hakan Demir
Hanife Aslı Ayan Eke
Hatice Sınav Uslu
Hülya Yalçın
Irena Dimitrova Kostadinova
İlknur Ak Sivrikoz
İnanç Karapolat
Mahmut Yüksel
Maria Lyra Georgosopoulou
Mehmet Reyhan
Meliha Korkmaz
Meryem Kaya
Mine Araz
Mustafa Kula
Mustafa Yıldız
Nedim Cüneyt Murat Gülaldı
Nilüfer Yıldırım
Nurhan Ergül
Nuri Arslan
Özlem Özmen
Pınar Özgen Kırtalı
Rabia Lebriz Uslu Beşli
Sait M. Sağer
Salih Özguven
Salih Sinan Gültekin
Semra Özdemir
Serdar Savaş Gül
Serkan İşgören
Sevin Coşar Ayaz
Seyhan Karaçavuş
Tamer Özülker
Taner Erselcan
Tanju Yusuf Erdil
Tarık Şengöz
Türkay Toklu
Ümit Özgür Akdemir
Zehra Özcan
Zekiye Hasbek
Zeynep Burak

2021 Author Index - 2021 Yazar Dizini

Abdullatif Amini....50, 107
Ali Fuat Yapar....119
Ali Gholamrezanezhad....50, 107
Ayperi Öztürk....101
Ayşe Uğur....34
Ayşegül Akgün....122
Ayşegül Aksu....144
Bahri Akdeniz....169
Bedrettin Yıldızeli....28
Bihter Şentürk....169
Bora Torus....86
Burak Günay....197
Bülent Mutlu....28
Büşra Özdemir....8, 197
Canan Can....201
Catalina Melo Arango....110
Cihan Gündoğan....79, 201
Coşkun Çakır....63
Cristina de Angelis....193
Derya Karabulut....197
Doğangün Yüksel....34
Ebru Tatcı....101
Ersoy Doğan....177
Esmail Jafari....50, 107
Esra Arslan....63, 126
Evrim Erdemoğlu....93
Fadime Didem Can Trabulus....63
Fatma Sılan....158
Feyza Şen....28, 39
Firoozeh Dehdar....50
Fulya Koç Öztürk....158
Funda Demirağ....101
Gabriela Mateva....1
Gad Abikhzer....113
Gamze Çapa Kaya....144
Giuseppe De Vincentis....60, 193
Göksu Yavuz Abdioğlu....47
Gülay Durmuş Altun....8, 197
Güneş Sağer....57
Habibollah Dadgar....107
Hakan Korkmaz....86
Halil Kömek....201
Halil Turgut Turoğlu....28, 39, 177, 187
Hasan Önner....129
Hatice Özer....150
Hojjat Ahmadzadehfar....107
Hülya Etem....201
Iraj Nabipour....107
Irena Kostadinova....1
Iván Fabricio Vega Gonzalez....110
İpek Tamsel....122
İsmail Çırpan....158
İsmail Zihni....93
Jaruwan Onwanna....69
Javier Novales-Diaz....113
Julia Lazri....193
Kerim Sönmezoğlu....57
Kevser Öksüzoğlu....28, 39
Kitiwat Khamwan....69
Laura Cosma....60
Lebriz Uslu....57
Lina López Vélez....110
Majid Assadi....50, 67, 107
Marc Hickeson....113
Maria Silvia de Feo....193
Mariano Pontico....60, 193
Marylin Acuña Hernandez....110
Maythinee Chantadisai....69
Mehmed Yanartaş....28
Mehmet Argın....122
Mehmet Erdoğan....86, 93
Mehmet Reyhan....119
Mehmet Semih Çakır....79
Mehmet Yılmaz Akgün....158
Merve Cin....63
Meryem İlkay Eren Karanis....129
Metin Çiriş....86
Mohsen Qutbi....54
Muhammet Ali Ayvaz....47
Muhammet Sait Sağer....57
Murat Elli....18
Mustafa Avcı....86
Mustafa Erol....129
Mustafa Yıldız....86
Nada Almenieir....113
Nazlı Pınar Karahan Şen....169

2021 Author Index - 2021 Yazar Dizini

Nebil Bal 119
Nermin Karahan 93
Neşe Torun 119
Nilgün Aracı 158
Nilüfer Bıçakçı 18
Nuh Filizoğlu 39
Nurhan Ergül 79
Nuri Karabay 177
Ogün Bülbül 177
Olga Yaylalı 34
Özgül Ekmekçioğlu 137
Özgür Kılıçkesmez 79
Özhan Özdoğan 177
Özlem Elmas 117
Özlem Özmen 101
Öztürk Özdemir 158
Rabiye Uslu Erdemir 117
Recep Bekis 169
Remzi Adnan Akdoğan 47
Reza Nemati 107
Rıza Umar Gürsu 79
Sabahat İnanır 28, 39, 187
Salih Özgüven 28, 39, 187
Seçkin Bilgiç 57
Selin Kesim 28, 39, 187
Selin Soyluoğlu 8
Sema Rakıcı 47
Semra Özdemir 158
Serkan Akın 47
Serpil Taş 28
Sertaç Asa 57
Seval Erhamamcı 119
Sevim Süreyya Şengül 86, 93
Seyed Javad Rekabpour 107
Seyit Ahmet Ertürk 150
Sibel Göksel 47
Stoyan Handzhiev 1
Süheyla Ekemen 126
Sülen Sarıoğlu 177
Şerife Mehtap Boylubay 86
Tamer Aksoy 63, 79, 126
Tanju Yusuf Erdil 28, 39, 187
Tevfik Fikret Çermik 63, 79, 126
Tunç Öneş 28, 39
Ülkü Korkmaz 8
Vilma Derbekyan 113
Viviana Frantellizzi 60, 193
Wirunpatch Buratachwatanasiri 69
Yothin Rakvongthai 69
Yuda Chongpison 69
Zekiye Hasbek 150
Zümrüt Arda Kaymak 93

2021 Subject Index / 2021 Konu Dizini

^{18}F-FDG PET/^{18}F-FDG PET 57
^{18}F-FDG PET/CT scans/^{18}F-FDG PET/BT taramaları 86
^{18}F-FDG PET/CT/^{18}F-FDG PET/BT 18, 47, 93, 101, 107, 117, 119, 126, 137, 158
^{18}F-FDG/^{18}F-FDG 63, 79, 150, 197, 201
^{18}F-FDOPA/^{18}F-FDOPA 69
^{18}F-flourodeoxyglucose positron emission tomography/computerized tomography/^{18}F-florodeoksiglikoz pozitron emisyon tomografi/bilgisayarlı tomografi..... 122
^{18}fluoride-fluorodeoxyglucose/^{18}florür-florodeoksiglukoz... 129
6-minute walk distance/6 dakikalık yürüme testi 28
^{68}Ga-DOTA-TATE/^{68}Ga-DOTA-TATE 39
^{68}Ga-DOTATATE PET/MRI/^{68}Ga-DOTATATE PET/MRG..... 107
^{68}Ga-FAPI/^{68}Ga-FAPI..... 201
^{68}Ga-PSMA/^{68}Ga-PSMA 63, 79
^{68}Ge/^{68}Ga generator/^{68}Ge/^{68}Ga jeneratör 34
Abscess/Apse 60
Abscessualized cancer/Apseli kanser..... 60
AFP/AFP 79
Artifact/Artefakt..... 54
Atypical pulmonary carcinoid tumor/Atipik pulmoner karsinoid tümör 101
Benign bone lesions/İyi Huylu kemik lezyonları..... 113
Bisphosphonate/Bisfosfonat..... 122
Bone scan/Kemik sintigrafisi 122
Bone SPECT/CT/Kemik SPECT/BT..... 187
BRCA1-2 mutation/BRCA1-2 mutasyonu..... 158
Breast cancer/Meme kanseri..... 129, 158, 201
Breast carcinoma/Meme karsinomu..... 117
Breast/Meme..... 54
Cancer of the head and neck/Baş boyun kanseri 177
CEUS/CEUS 1
Chemical impurity/Kimyasal safsızlık 34
Childhood malignancy/Çocukluk çağı maligniteleri..... 18
Childhood/Çocukluk çağı..... 119
Chronic thromboembolic pulmonary hypertension/Kronik tromboembolik pulmoner hipertansiyon 28
Colorectal cancer/Kolorektal kanser..... 93
Congenital melanocytic nevus/Kongenital melanositik nevüs ..119
Contrast-enhanced echocardiography/Kontrastlı ekokardiyografi..... 67
Coronary angiography/Koroner anjiyografi..... 169
COVID-19/ COVID-19..... 197
Cutaneous melanoma/Kutanöz melanoma 119
Diffusion/Difüzyon..... 177
Early Parkinson's disease detection/Erken Parkinson hastalığı tespiti 69
Fluorodeoxyglucose ^{18}F/Florodeoksiglukoz ^{18}F 110
FUO/FUO..... 60
Gallium-68/Galyum-68..... 34
Gastric cancer/Mide kanseri..... 150
Gastric carcinoma/Mide kanseri..... 63
Gastric metastasis/Mide metastazı..... 47
Gastrointestinal hemorrhage/Gastrointestinal kanama..... 8
GCA/DHA..... 57
GMP/GMP..... 34
Hematogical toxicity/Hematolojik toksisite 193
Hepatobiliary scan/Hepatobiliyer tarama..... 54
Hepatocellular cancer/Hepatosellüler kanser 79
Hepatopulmonary syndrome/Hepatopulmoner sendrom.... 67
HER-2/HER-2..... 150
Hybrid imaging/Hibrit görüntüleme..... 60
Hypoxia-inducible factor-1α/Hipoksi ile indüklenebilir faktör-1α 93
Incidental thyroid nodules/Tesadüfi tiroid nodülleri 86
Langerhans' cell histiocytosis/Langerhans hücreli histiyositoz ...187
Lean body mass/Yağsız vücut kütlesi 144
Li-Fraumeni syndrome/Li-Fraumeni sendromu..... 110
Liver/Karaciğer..... 54
Long bone/Uzun kemik 122
lung perfusion scintigraphy/akciğer perfüzyon sintigrafisi... 67
Magnetic resonance imaging/Manyetik rezonans görüntüleme..... 122
mCRPC/mCRPC..... 193
Mean pulmonary arterial pressure/Ortalama pulmoner arter basıncı 28
Melena/Melena 47
Metabolic tumor volume/Metabolik tümör hacmi 86, 129
Metastasis/Metastaz..... 117
Metastatic liver lesions/Metastatik karaciğer lezyonları..... 1
MTV/MTV 93

2021 Subject Index / 2021 Konu Dizini

Myocardial perfusion imaging/Miyokard perfüzyon görüntüleme 169
Myocarditis/Miyokardit 50
NaF/NaF 113
Neuroendocrine tumor/Nöroendokrin tümör 107
Neuroendocrine tumors/Nöroendokrin tümörler 39
Normal subjects/Normal olgular 39
Osteonecrosis/Osteonekroz 122
Permeability/Permeabilite 177
PET/CT/PET/BT 1, 39, 63, 79, 150, 197, 201
Pharmacokinetic model/Farmakokinetik model 69
Polycythemia vera/Polisitemia vera 193
Positron emission tomography/computed tomography/Pozitron emisyon tomografisi/bilgisayarlı tomografi 129
Positron emission tomography/Pozitron emisyon tomografisi 110, 177
Primary liver tumors/Primer karaciğer tümörleri 1
Prostate cancer/Prostat kanseri 193
Prostate carcinoma/Prostat kanseri 63
Prostate specific membrane antigen/Prostat spesifik membran antijeni 144
PRRT/PRRT 107
PSMA PET/PSMA PET 57
Pulmonary carcinoid tumor/Pulmoner karsinoid tümör 101
Pulmonary hamartoma/Pulmoner hamartom 101
Pulmonary vascular resistance/Pulmoner vasküler direnç 28
Quantitative analysis/Kantitatif analiz 69
Radiofrequency ablation/Radyofrekans ablasyon 1
Radium-223/Radyum-223 193
Red blood cell scintigraphy/İşaretli eritrosit sintigrafisi 8
Response/Tedaviye yanıt 18
Restaging/Yeniden evreleme 18
Right-to-left shunt/Sağdan sola şant 67
SARS-CoV-2/SARS-CoV-2 197
Single photon emission computed tomography/computed tomography/Tek foton emisyonlu bilgisayarlı tomografi/bilgisayarlı tomografi 8
Small-angle Compton scatter/Küçük açılı Compton scatter 54
Sodium-fluoride PET/Sodyum-florür PET 113
Somatostatin receptor scintigraphy/Somatostatin reseptör sintigrafisi 50
Somatostatin receptors/Somatostatin reseptörleri 39
SPECT/CT/SPECT/BT 60, 169
SPECT/SPECT 50
Squamous cell carcinoma/Yassı hücreli kanser 177
Staging/Evreleme 18
Statistical parametric mapping/İstatistiksel parametrik haritalama 69
Striped muscle/Çizgili kas 117
SUL/SUL 144
SUV/SUV 144
SUV_{max}/SUV_{maks} 137, 158
Systemic sarcoidosis/Sistemik sarkoidoz 126
Tc-99m octreotide/Tc-99m oktreotid 50
Tc-99m-HMPAO-labeled leukocytes/Tc-99m-HMPAO işaretli lökositler 60
Technetium-99m-macroaggregated albumin/Teknetyum-99m-makrokümelenmiş albümin 67
Technetium-99m-methylene diphosphonate bone scintigraphy/Teknesyum-99m-metilen difosfonat kemik sintigrafisi 187
Testicular choriocarcinoma/Testiküler koryokarsinom 47
testis carcinoma/Testis karsinomu 126
Thyroid cancer/Tiroid kanseri 137
TLG/TLG 93
Total lesion glycolysis/Toplam lezyon glikoliz 86, 129
Vasculitis/Vaskülit 57
Ventilation/perfusion scintigraphy/Ventilasyon/perfüzyon sintigrafisi 28